Photocopy and Use Authorization

In presenting this thesis in partial fulfillment of the requirements for an advanced degree at Idaho State University, I agree that the Library shall make it freely available for inspection. I further state that permission for extensive copying of my thesis for scholarly purposes may be granted by the Dean of Graduate Studies, Dean of my academic division, or by the University Librarian. It is understood that any copying or publication of this thesis for financial gain shall not be allowed without my written permission.

Signature:_____________________________

Date:________________________________

Alluvial fan morphology, chronology, and faulting along the southern Beaverhead Range, Idaho: a record of late Pleistocene faulting and climate variation

by

Emma S. Collins

A thesis

submitted in partial fulfillment

of the requirements for the degree of

Master of Science in the Department of Geosciences

Idaho State University

Summer 2021

To the Graduate Faculty:

The members of the committee appointed to examine the thesis of EMMA S. COLLINS find it satisfactory and recommend that it be accepted.

Dr. Glenn D. Thackray,
Major Advisor

Dr. David W. Rodgers,
Committee Member

Dr. Tammy Rittenour,
Committee Member

Dr. Susan Swetnam,
Graduate Faculty Representative

Acknowledgements

First and foremost, thank you to the ISU Geosciences community. These past two years have been a memorable one and it wouldn't have happened without the support from the faculty and students. This community has made graduate school a very memorable experience.

Thank you to the members of my thesis committee for giving me feedback and patience. Thank you, Glenn Thackray, for giving me encouragement and guidance for writing. Thank you, David Rodgers, for structural advice and Tammy Rittenour for giving me feedback on mapping alluvial fans. Thank you, Susan Swetnam, for taking the time to read through my thesis and giving me appropriate feedback.

Thank you to the optically stimulated luminescence lab at Utah State University who processed my samples despite a pandemic. Thank you to the team at the University of Vermont cosmogenic radionuclide lab for processing my data as well. All of this work was done under COVID-19 stress and I am extremely grateful to have the ability to have all of my ages reported.

Thank you to the many folks who helped me with my research. Thank you Donna Delparte for allowing me to fly drones within my field area. Thank you to my field assistant, Sarah Gonzalez, for tallying my caliche rinds.

Thank you to all of the family and friends that have supported me in this journey.

Table of Contents

List of Figures

List of Tables

Alluvial fan morphology, chronology, and faulting along the southern Beaverhead Range, Idaho: a record of late Pleistocene faulting and climate variation

Thesis Abstract – Idaho State University (2021)

The Beaverhead fault cuts Late Pleistocene alluvial fans on the western flank of the Beaverhead Mountains. The two southernmost fault segments, Blue Dome and Nicholia, are the focus of this study. Geomorphic mapping used 0.5 m resolution LiDAR and field investigation to delineate five fan units (Qaf1-Qaf5). Twenty-five optically stimulated luminescence (OSL) ages on fan gravels are 16 –113 ka. Regional alluvial fan surfaces formed under cooler and/or wetter late Pleistocene climates, and the fan ages suggest multiple periods of cooler and/or wetter climate during the last glaciation. Fault scarps cut Qaf2 – Qaf5 alluvial fans in the Nicholia segment, but fault scarps are absent along the Blue Dome segment. OxCal modeling using fan ages and rupture patterns constrains the most recent fault ruptures on the Nicholia segment to 32 +/- 7.3 ka and 77 +/- 6.8 ka, and the most recent Blue Dome rupture appears to pre-date 110 ka.

Key Words: Alluvial fans, rupture, earthquake, Beaverhead Mountains, fault, optically stimulated luminescence

Chapter I: Introduction

1.0 Introduction

Alluvial fans are range-front landforms that are common in semi-arid climates in the Basin and Range province. Formed by the accumulation of sediments derived from the adjacent mountains, alluvial fans potentially contain a detailed record of climate variations over time scales of >10,000 years. In addition, alluvial fans can potentially record past faulting events that created fault scarps across their surfaces. By dating the deposition of the alluvial fans, we can therefore constrain climatic factors in their growth and reconstruct the faulting history reflected in the fault scarps.

Techniques for measuring the ages of alluvial fan deposits have advanced within the past decade. Previous attempts to estimate the ages of alluvial fans have used soil development (Pierce and Scott, 1982), radiocarbon ages when applicable, and U-series ages from pedogenic carbonates (Sharp et al., 2003). Due to advances in optically stimulated luminescence (OSL) dating in coarse-grained alluvial fans, reconstructing alluvial fan chronology has become more accurate and widespread (Kenworthy et al., 2014). Using OSL ages to date alluvial fans has advantages over other methods. Radiocarbon dating works well when there is organic material to date but is generally lacking in semi-arid alluvial fan settings. Alluvial fans tend to lack boulders for cosmogenic radio nuclide (CRN) dating. The other benefit of OSL dating on alluvial fans is that it dates the deposition of alluvial fan gravel rather than giving a minimum age that CRN ages, U-series ages on pedogenic carbonate, and soil-based methods would provide, or the maximum age implied by radiocarbon dating of detrital organic material incorporated into fan gravels.

The Basin and Range north of the eastern Snake River plain (ESRP) includes three ranges, the Lost River, Lemhi, and Beaverhead ranges (Figure 1.1), and their intervening valleys. Along the western edge of each range, a west-dipping normal fault is present and appears to be active since fault scarps generally cut alluvial fans. This thesis will focus on alluvial fans at the southern end of the Beaverhead Range, in particular fans in the Birch Creek valley mantling the Nicholia and Blue Dome fault segments (red on Figure 1.1). Studying the morphology and distribution of these fans, coupled with fault scarp mapping and OSL geochronology, will provide a broader context to alluvial fan processes in east-central Idaho. We will correlate these OSL ages to previous paleoclimate records and show the main drivers of alluvial fan aggradation. By mapping and dating alluvial fans and fault scarps cutting them, we can also constrain the most recent and penultimate faulting events.

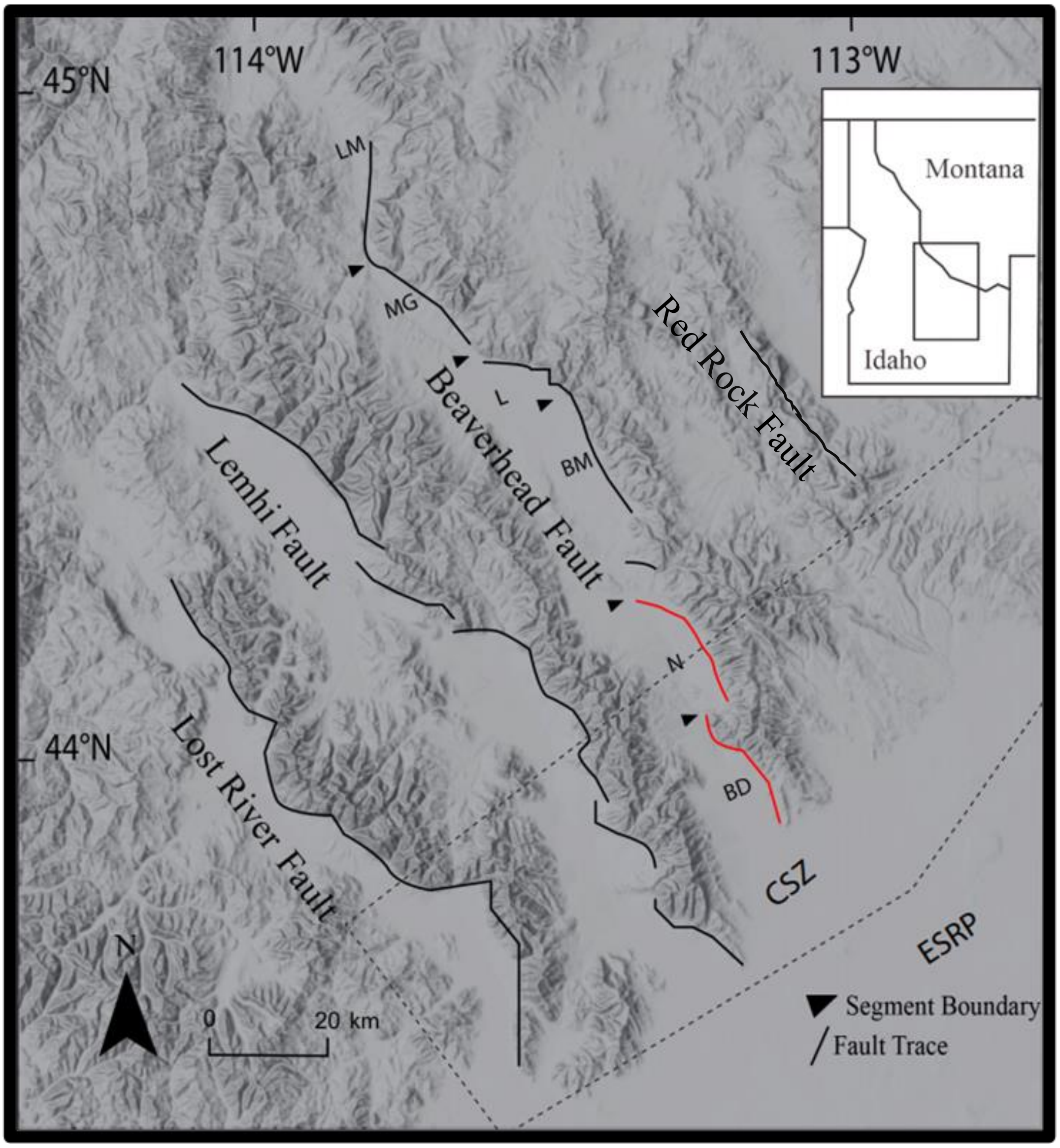

Figure 1.1: General area of study in eastern Idaho. Beaverhead, Lemhi, and Lost River ranges are shown perpendicular to the Snake River Plain. Red line shows the trace of the Beaverhead fault. Segments on the Beaverhead fault are: BD, Blue Dome; N, Nicholia; BM, Baldy Mountain; L, Leadore; MG, Mollie Gulch; LM, Lemhi. Modified from Haller, 1988.

1.1 Regional Stratigraphy and Tectonics

1.1.1 Bedrock Stratigraphic sequence

The southern Beaverhead Range exposes Precambrian and Paleozoic sedimentary units (Figure 1.2) (Garmezy, 1981; Skipp, 1985; Lewis etal., 2012). The western, normal-faulted flank of the southern Beaverhead Range exposes rocks from the Wilbert Formation (Neoproterozoic, Ediacaran)as well as Ordovician, Devonian, and Mississippian formations (Garmezy, 1981; Skipp and Link, 1992; Pearson and Link, 2017). For this project, we will focus on the bedrock that is located in the footwalls of the Blue Dome and Nicholia segments. This bedrock is composed of the Paleozoic units shown in Figure 1.2.

The bedrock on the western flank of the Beaverhead Mountains along the Blue Dome segment is composed primarily of Mississippian limestone (Garmezy, 1981; Skipp, 1985).One of these limestone units is the Middle Canyon Formation. This formation strikes approximately north-south on the western flank of the Beaverhead Mountains.Another Mississippian limestone unit is the Scott Peak Formation, which overlies the Middle Canyon Formation.

The footwall of the Nicholia segment includes the same formations as the Blue Dome segment, as well as the underlying Kinnikinic, Jefferson, and McGowan Creek formations. The Kinnikinic Formation (Middle Ordovician) is exposed in the southern footwall portion of the Nicholia fault segment and is composed of fine to medium grained orthoquartzite (Garmezy, 1981). This unit is overlain by the Jefferson Formation (mid-Devonian) above an unconformity. The Jefferson Formation is comprised of dolomite and sandstones. The McGowan Creek Formation (early Mississippian) overlies the Jefferson Formation with a gradational contact. These units as well as the Middle Canyon and Scott Peak formations are located in the footwall of the northern portion of the segment.

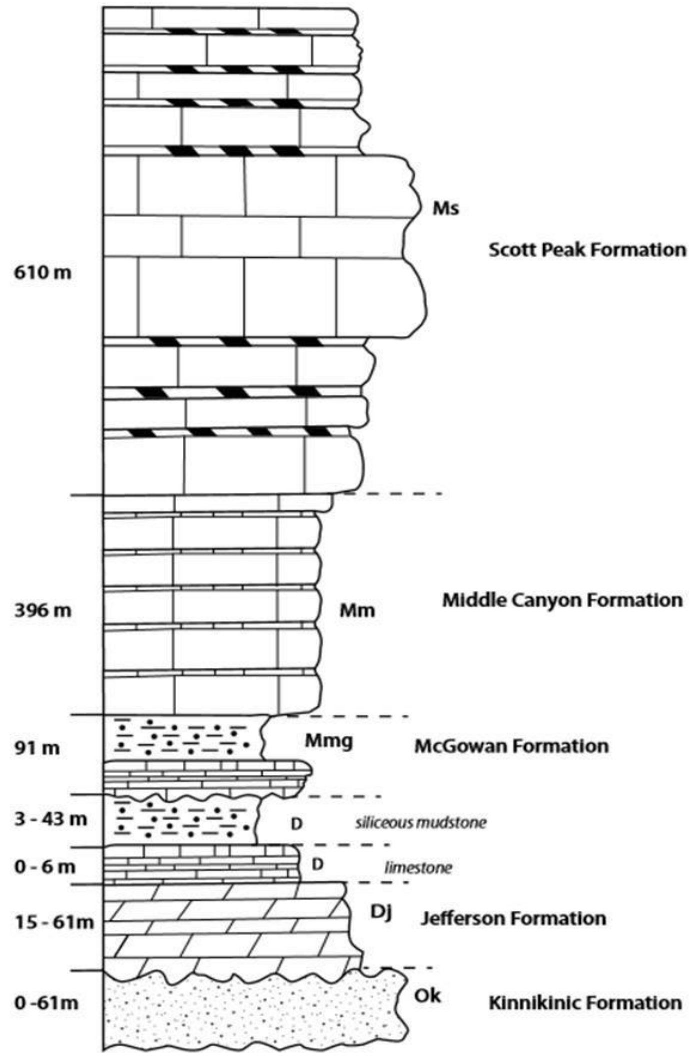

Figure 1.2: General stratigraphic column of the bedrock on the westernflank of the southern Beaverhead range. Modified from Garmezy, 1981.

1.1.2 Neogene- Recent Hot Spot Migration

Crustal extension in east-central Idaho coincided roughly with age-progressing volcanism of the Snake River Plain-Yellowstone volcanic system, often called the "Yellowstone hotspot" (Figure 1.3; Armstrong et al., 1975; Suppe et al., 1975; Anders et al., 1989; Pierce and Morgan, 1992 and 2009). The origin of the "Yellowstone hotspot" is still debated, whether it originated from a deep mantle plume or as a result of processes related to plate subduction and/or extension (Pierce and Morgan, 1992, 2009; Zhou, 2018; Zhou et al., 2017). For the purpose of this thesis the term "Yellowstone hotspot" will be used to describe volcanic patterns and does not reflect the origin of the volcanic activity. The Yellowstone hotspot initiated ~17 Ma near the Nevada-Oregon-Idaho border and has affected the greater Yellowstone region since around 2 Ma (Pierce and Morgan, 1992 and 2009). Volcanism towards the southern portion of Lemhi and Beaverhead ranges are around 6 Ma (Hackett and Morgan, 1988; Pierce and Morgan, 1992 and 2009).

The crystallization of magmatic reservoirs from the Yellowstone volcanism created a residual, higher density load, with a thickness of 17 - 25 km in the upper crust. The densification of the crust caused the eastern Snake River Plain to subside and to flex the crust on the margins (McQuarrie and Rodgers, 1998; Peng and Humphreys, 1998; Zentner, 1989). Thermal decay following NE migration of the Yellowstone volcanism also played a role in the subsidence (Brott et al., 1981; Pierce and Morgan, 1992).

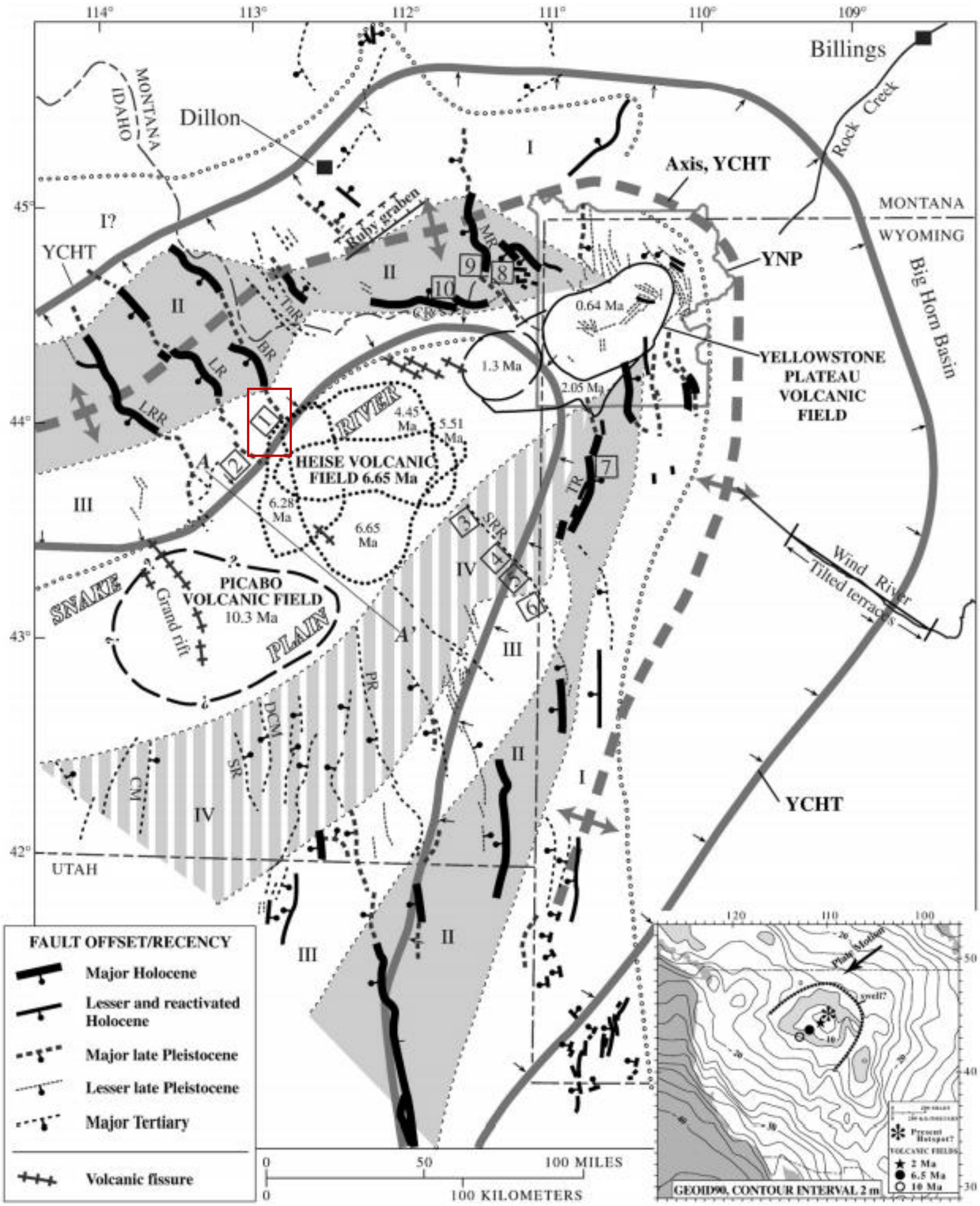

Figure 1.3: The location and timing of the hotspot track is defined by a progression of three volcanic fields with inception ages. The volcanic fields are Picabo 10.21 Ma; Heise 6.62 Ma; and Yellowstone Plateau (2.05 Ma). Red box is the location of the field study. From Pierce and Morgan, 2009.

1.1.3 Neogene – Recent Basin and Range

Extension across the Yellowstone hotspot region influenced the current Basin and Range topography, defined as a series of uplifted blocks with alternating half-graben basins. The estimated initiation age of uplift of the Beaverhead Range is around 10.3 Ma with onset of uplift in the Birch Creek area between 5.4 – 1.6 Ma (Anders and Schlische, 1994; Rodgerset al., 1990).

Located north of the eastern Snake River Plain and described by Payne et al. (2013), the Centennial Shear Zone is defined as the accommodation zone between the volcanic eastern Snake River Plain and the Basin and Range and Centennial tectonic block. Payne et al. (2008; 2012) relied on GPS monitoring and analysis to show the differing surface velocities along the northwestern edge of the ESRP and thereby infer the CSZ. As part of this thesis research, evidence of ESRP-parallel faulting in the southern portion of the Blue Dome segment has been investigated in reconnaissance fashion via LiDAR analysis.

1.1.4 Present day alluvial fans and fault scarps along the Beaverhead Range

The west-dipping Beaverhead fault is located along the western edge of the Beaverhead Range. The maximum cumulative throw of the Beaverhead fault is estimated to be 4 – 6 km (Densmore et al., 2005). Shown in Figure 1.1, the middle fault segments (Leadore and Mollie Gulch) have been active in the Holocene, as evidenced by the presence of fault scarps cutting late Pleistocene alluvial fans (Haller, 1988; Crone and Haller, 1991). The northern and southern segments of the Beaverhead fault (Blue Dome and Lemhi segments) have notably lower frequency seismic activity. This seismic pattern is reflected in the segments on the Lemhi and Lost River faults as well (Haller, 1988; Crone and Haller, 1991; Pierce and Morgan, 1992).

1.2 Alluvial Fan processes and chronology in east central Idaho

Alluvial fans are landforms that form at the mouths of canyons along mountain ranges, notably in semi-arid landscapes in western North America. These geomorphic features are fan shaped and formed from locally derived sediments from their respective catchments. The size of alluvial fans varies from kilometers to tens of kilometers in width. Alluvial fans can be formed by sheet flow, where shallow water is not confined to a channel but rather spread out over the surface, or by migrating, focused channels. Debris flows can also form fans as well. These sediments are normally coarse grained and poorly sorted.

A 1:250,000 scale geological surficial map by Scott (1982) shows three distinct alluvial fan units along the Beaverhead fault, designated as afc, af2, and af3. Unit afc is described from soil evidence as a Holocene to Upper-Middle Pleistocene deposit, af2is an Upper Pleistocene deposit, and af3 is a Middle to Lower Pleistocene deposit. He inferredthat Holocene deposits are finer grained while Pleistocene gravel deposits are coarser. He used soil profiles to estimate landform ages.

Along the Blue Dome segment, af2 is the fan unit that extends directly from the canyon mouths, and af3 is the fan lying topographically above af2. Along the Blue Dome segment, Scott (1982) mapped Holocene to Upper – middle Pleistocene alluvium along the range front in small areas in between alluvial fans.

The Nicholia segment shows a similar pattern. The same three map units—afc, af2, and af3—are mapped in the same pattern where af2 units are the alluvial fans lying directly at the canyon mouth and af3 is topographically higher. Mapped afc units are the range-front alluvium and colluvium deposits aswell and are notably of less extent than af2 and af3 deposits. The biggest difference between the mapped Blue Dome and Nicholia range front geomorphology is that in the northern Nicholia segment, there is a mapped glacial outwash fan of inferred Pinedale age (gpo).

Pierce and Scott (1982) used soil profile data to infer that the youngest alluvial fan deposits in east central Idaho are 70-11 k.y. old. Pierce and Scott (1982) correlated these alluvial fans with other landforms such as terraces and moraines. They hypothesized that alluvial fans grew during glacial intervals, because the cooler Pleistocene temperatures would allow for an increase of annual discharge and increased sediment supply from hillslopes and in glacial systems. Due to decreased evaporation and increased snowfall, water flow persists later in the season and increases the transport capacity. This runoff wouldn't infiltrate into the ground due to effective permafrost in higher altitudes. A more rapid discharge of snowmelt would occur due to snow melting later in each year. This provides a short and intense discharge that would erode and transport sediment within the basin.

In the Pierce and Scott (1982) model, late-Pleistocene alluvial fans would contain coarser gravels than Holocene fans. Glaciers would enhance sediment production due to glacial erosion and in unglaciated valleys, snowpack would melt later and increase erosion along hillslopes. However, They noted that the presence of a glacier is not the primary control of sediment production. Pierce and Scott (1982) thought that the frost erosion of bedrock that would have occurred under cooler climates created more colluvial deposits that would then be transported downstream. They also hypothesized that cooler climates would also increase the effective moisture within the soil and therefore would reduce soil erosion. This would decrease the rate that fine grained sediment was eroded. The increased discharge and supply of more coarse-grained gravel would build the late-Pleistocene alluvial fans observed in central and southeastern Idaho.

Haller (1988) used soil development, alluvial fan morphology, and surface morphology to estimate alluvial fan ages. She estimated that, along the Blue Dome and Nicholia segments, the youngest alluvial fans, extending directly from the canyon mouths, are most likely early Holocene in age. Older fan ages were estimated to be late Pleistocene.

Kenworthy et al. (2014) refined the work of Pierce and Scott (1982) by using optically stimulated luminescence (OSL) to date the range-front alluvial fans in the central Lost River Range. They found fan age groupings of 10 - 20 ka, 20 - 35 ka, 35 - 60 ka, and 90 - 120 ka for their fan units Qa1 - Qa4. There are moraines present on a portion of the range front, inferred to correlate with the 20 -35 ka and 90 - 120 ka alluvial fans. This suggests that alluvial fans aggrade during late Pleistocene cold intervals, regardless of the presence of glaciers, supporting the hypothesis of Pierce and Scott (1982). Finally, Kenworthy (2010) also noted that alluvial fan ages did not differ between fault segments that have differing slip rates and that the slip-rate is not a major control of alluvial fan aggradation.

Despite all of this work in east central Idaho, no OSL, radiocarbon, or CRN ages have previously been obtained along the Blue Dome and Nicholia segments to determine the ages of alluvial fans.

1.3 Fault Mapping

1.3.1 Normal Fault Mapping

Normal fault mapping in east central Idaho was done previously by Haller (1988), Crone and Haller (1991), Skipp (1985), and others. Haller (1988) identified segment boundaries along the Lost River, Lemhi, Beaverhead faults. She used four criteria to define segment boundaries: a major en échelon step in the continuity of fault scarps; changes in fault scarp morphology; bedrock morphology along the range front; and change in topographic relief between the range and associated basin indicating that the fault throw differs along each area. Haller (1988) divided each of the faults into six segments and determined a consistent slip pattern: the middle segments of the faults show higher slip rates than the segments towards the ends of the faults.

1.3.2 Nicholia and Blue Dome Segments

Previous fault mapping on the Nicholia and the Blue Dome segments was done by Haller (1988). The boundary between the two segments is defined by the change in bedrock topography (Figure 1.1) creating a right-stepping en-echelon pattern. The Blue Dome segment is 25 km long (Haller, 1988). The segment has a maximum topographic relief of 1,300 m. Haller (1988) inferred that the Blue Dome segment has not been active in the past 100 ka, based on the range front morphology and application of criteria from Bull (1987), so the existence and age of faulting along the Blue Dome segment is unclear.

The Nicholia fault segment is 42 km long according to Haller (1988) (Figure 1.1). The maximum topographic relief is around 1,485 m from the highest point to the adjacent valley (Haller, 1988). In contrast to the Blue Dome segment, the Nicholia segment does have a documented Late Pleistocene faulting history. Most alluvial fans on the Nicholia segment are carbonate-rich with basal-carbonate coatings (<1mm) on clasts which are indicative of pedogenic calcic horizon development. The time it takes for these calcic-coatings to develop suggest that alluvial fans are Pinedale in age (<30 ka) (Haller, 1988). Nicholia fault scarps are mostly continuous across these alluvial fans, except they don't appear across the youngest alluvial fan sequence. These relations, as well as the age of soil development, suggest the last rupture on the Nicholia segment was around 15 ka (Haller, 1988).

1.4 Methods

1.4.1 Mapping

1.4.1.1 LiDAR

Geomorphic mapping was done using 0.5 m LiDAR in ArcGIS Pro at the scale of 1:15,000. Alluvial fan relative age relationships were determined through geomorphic relationships on LiDAR-derived images. The lowest fan is designated Qaf1 and progressively higher fans are classified as Qaf2 – Qaf5. The alluvial fan mapping was done using ArcGIS Pro 10.4 software and ArcMap 10.4.

1.4.1.2 Field observations

Field work was conducted to evaluate the LiDAR based mapping. This was done by walking and driving alluvial fans and checking to make sure surfaces correlate based on elevation and slope. Field work was done along the Beaverhead range front near the Blue Dome and Nicholia fault segments as well as digging a total of 25 sampling trenches (12 for the Nicholia and 13 for the Blue Dome). The trenches were used to study the soil development and sediment stratigraphy as well as collect OSL samples (Section 2.2). Alluvial fans south of Bare Canyon in the Blue Dome segment were the focus of the field observations, given their complex relationships and relevance to paleo-seismologic evaluations. Field observations also refined LiDAR mapping done in the Cliff and Scott canyons in the Nicholia segment.

1.4.1.3 Correlations via Pedogenic Carbonate Thickness Variations

The thickness of pedogenic carbonate coatings on gravel clasts can help determine the estimated age of soil. The gravel clasts in older soils generally have thicker accumulation of pedogenic carbonate (Kenworthy, 2004; Vincent et al., 1994; Birkeland; 1998). Carbonate clast thickness was measured in the soil horizon with the greatest accumulatedcarbonate. These soil horizons averaged 30 cm depth below the land surface underlying the A – ABk horizons. The carbonate horizons are typically Bk1-3 horizons, the zoneof maximum carbonate accumulation (ZMA). Over time, it is thought that the thickness of the ZMA and the thickness of pedogenic carbonate rinds increases (Birkeland; 1998). At each site, 50 gravel clasts were collected randomly from the ZMA. Clast dimensions were not recorded, on the basis of findings by Vincent et al. (1994), who concluded that clast size does not correlate to pedogenic thickness. Most of the clasts were limestone or dolomite. The measurements of the pedogenic carbonate clasts were done on the thickest portion of the rind. The mean rind thickness of each sample site was then calculated and means were calculated for each site. The mean pedogenic rind thicknesses for the associated fan units allowed me to distinguish map units done and estimate alluvial fan age from LiDAR and field observations.

1.4.1.4 Structure from Motion Topographic Analysis

To further evaluate the presence or absence of degraded fault scarps along the Blue Dome segment; two drones were flown over the northern portion of the segment: a Phantom Pro 4 quadcopter and Trinity F90 fixed-wing. The images were used to create an orthomosaic and DEM outputs of the area. This allows finer topographic detail of the area where a fault scarp might mark the landscape. We collected data over Long and Bare canyons because there is a visible sequence of alluvial fans of distinct ages.

Phantom Pro 4 V2

A Phantom Pro 4 was flown over alluvial fans at the mouth of Long Canyon with a still camera attached to the base. Our total flight path is shown in Figure 1.4 in which the drone was around 80 m above the ground surface and the photos had around 75% overlap. The photos were uploaded into AgiSoft Metashape. A dense cloud was created with an aggressive measure and a high-quality output. The orthomosaic and DEM exports were then used in ArcMap 10.4 to look for evidence of a fault scarp.

Trinity F90

The fixed wing Trinity F90 was flown over portions of the mouth of Bare Canyon shown in Figure 1.5. Ground control points were not placed in this area and thus there are errors for imagealignment. The Trinity F90 has attached an RGB sensor that takes higher resolution photos than the Phantom Pro 4. The flight plan included an approximately 10% overlap with the Phantom Pro 4 image acquisition.

Image Processing

The DEM and orthomosaic images were created in Agisoft and then exported to ArcMap 10.7 to do a fault scarp analysis. The orthomosaic image was analyzed for evidence sagebrush clustering that might indicate a fault trace, since it is common for sagebrush and other foliage to cluster in depressions where water is more likely to pool. Topographic profiles were created along the alluvial fans to see if there was evidence of a subtle fault scarp. At least two profiles were drawn along each fan surface and their profiles were analyzed for evidence of a degraded fault scarp

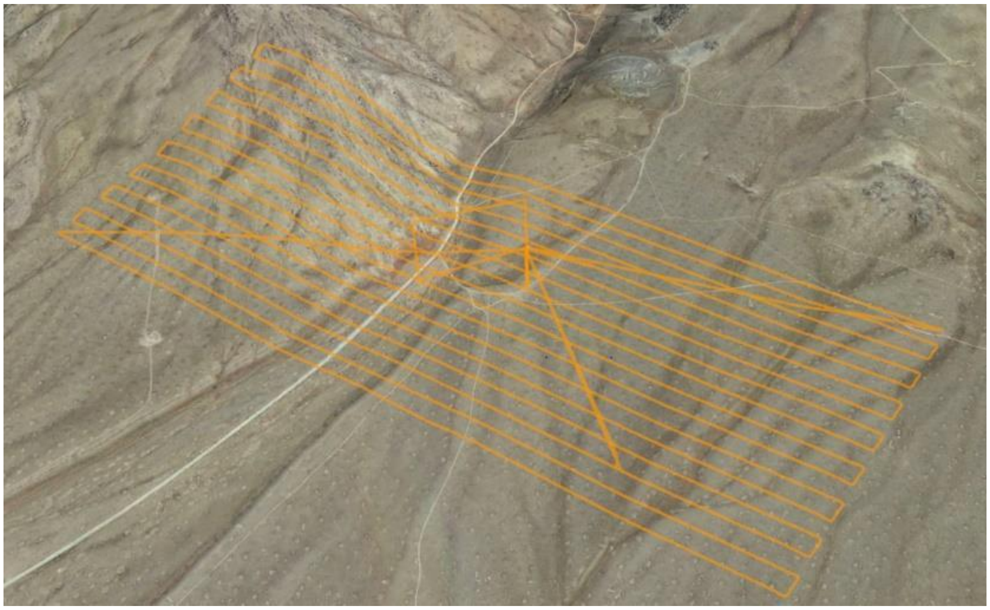

Figure 1.4: Flight path of the Phantom Pro 4. Four separate flightsoccurred to complete the path of the image.

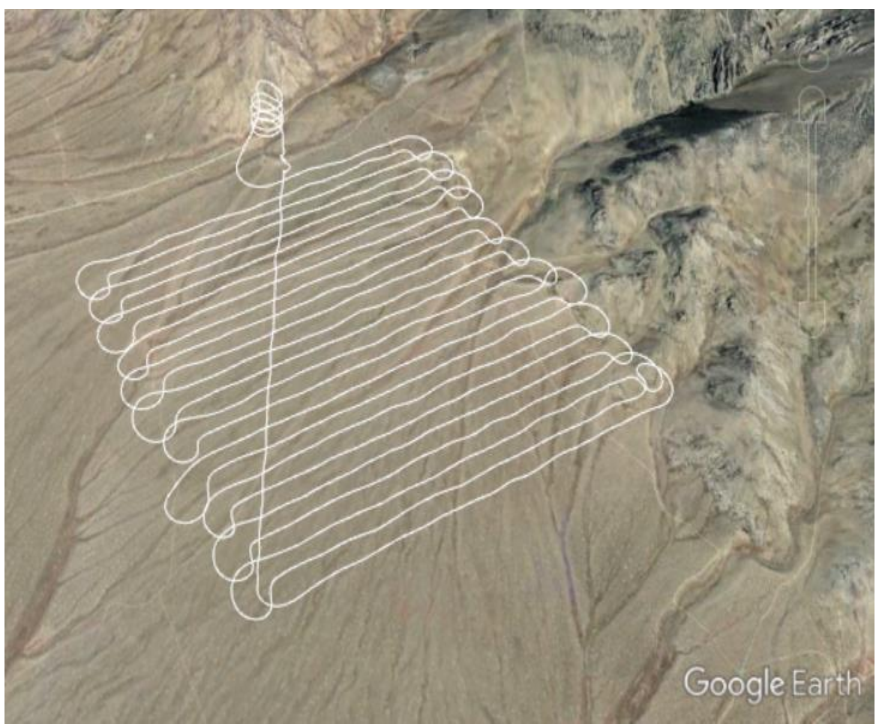

Figure 1.5: Flight path of the Trinity F90 showing the collected imagery forBare Canyon and a little of the alluvial fans near Long Canyon.

1.4.2 Hypsometry Analysis

Hypsometry is the graphical representation of elevation changes in percentage over a given area. By studying the elevation of the drainage basins incised into the rugged mountains, we can compare them to glacial equal-line altitude (ELA's) and see whether snowpack or glaciers were the main influence for the driving force of aggradation. Two sets of 1 arc second (30 m) public GeoTIFF sets were obtained from the USGS National Map Viewer for this study, because the INL LiDAR did not reach up towards the bedrock ridges in the Nicholia segment. Figures 1.6 and 1.7 show the locations of the selected canyons and their respective alluvial fans for the Nicholia and Blue Dome segment respectively. By comparing the area of the basin to the area of the respective alluvial fans we can also see if there is a correlation that an increase of basin area would also increase the size of the alluvial fans.

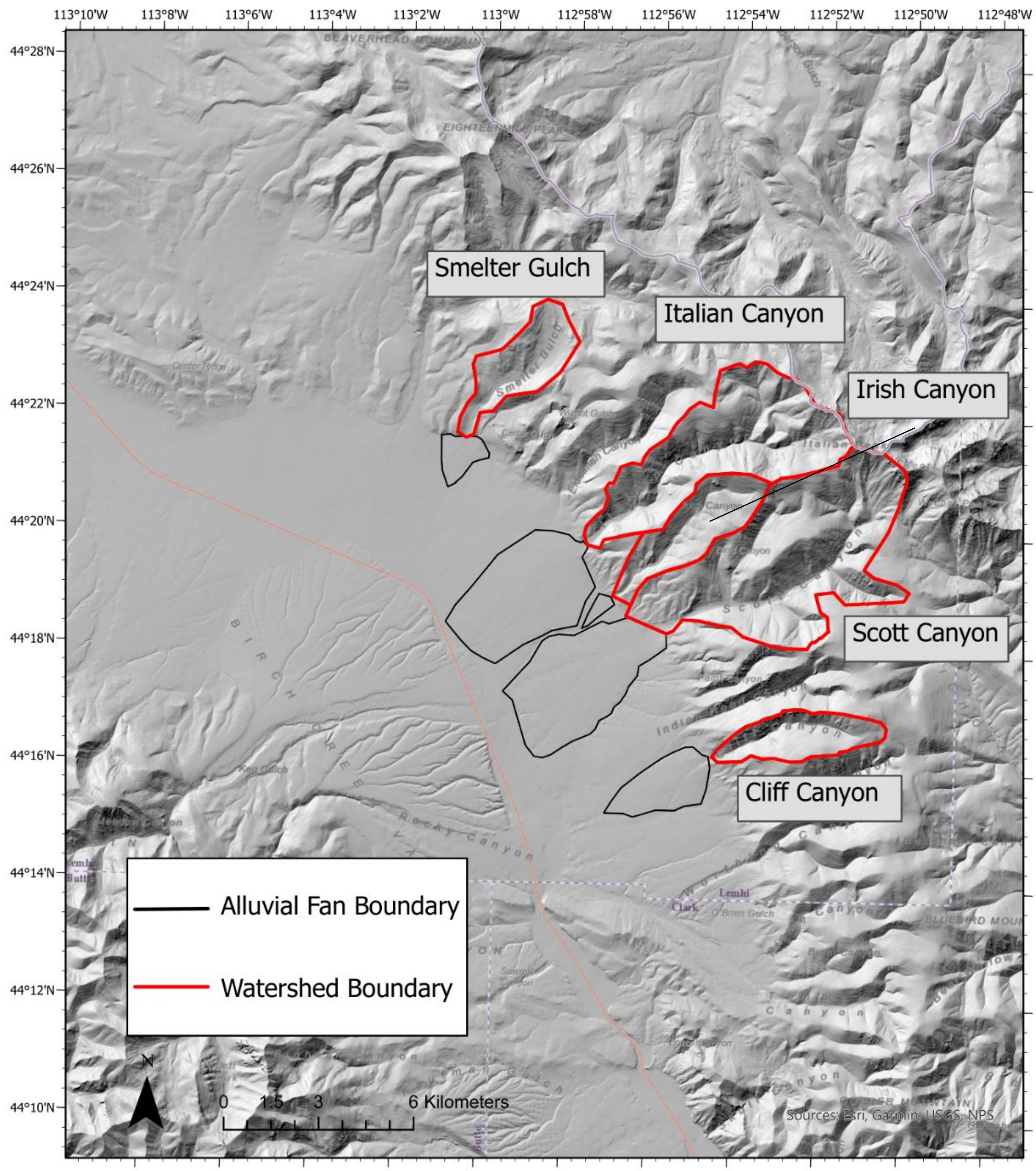

Figure 1.6: Map of the Nicholia segment showing the drainage basins (in red) and the alluvial fan area (in black). Five canyonswere selected: Cliff, Scott, Irish, Italian, and Smelter canyons

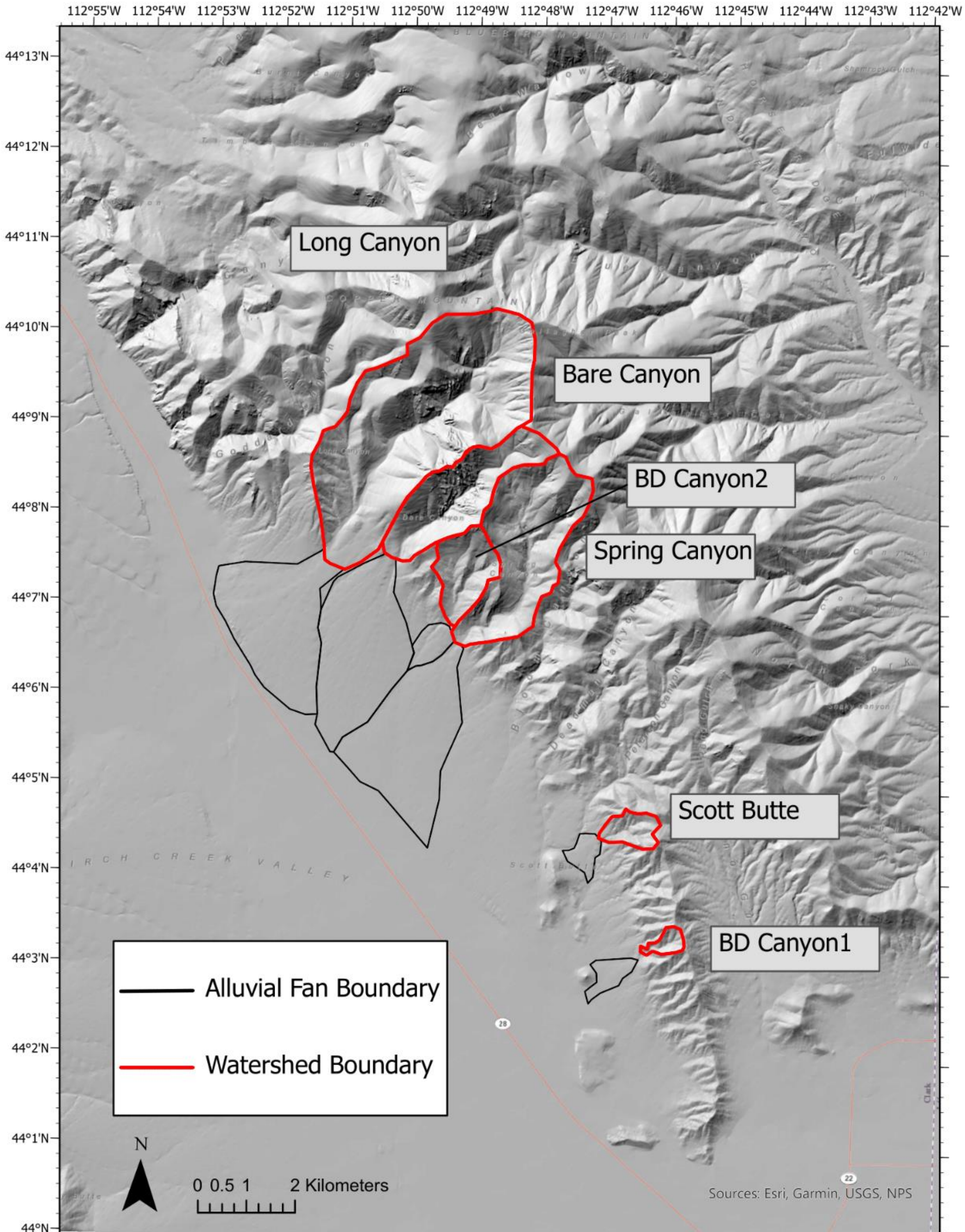

Figure 1.7: Map of the Blue Dome segment showing where the canyons and alluvial fans were selected**.** . Six canyonswere selected for this analysis, Long, Bare, Spring, and Scott Butte. Two additional canyons, BD Canyon 1 and BD Canyon 2 were also included.

1.4.3 Fault scarp analysis

Topographic profiles were extracted from lidar data along lines perpendicular to the strike of the fault scarps. Fault scarp vertical separation was determined by taking the slope of the hanging wall and footwall and then subtracting the elevations of the slopeof the hanging wall and footwall to get the height of the scarp that is vertical to the slope. The equation below describes how to measure the vertical separation between the two slopes.

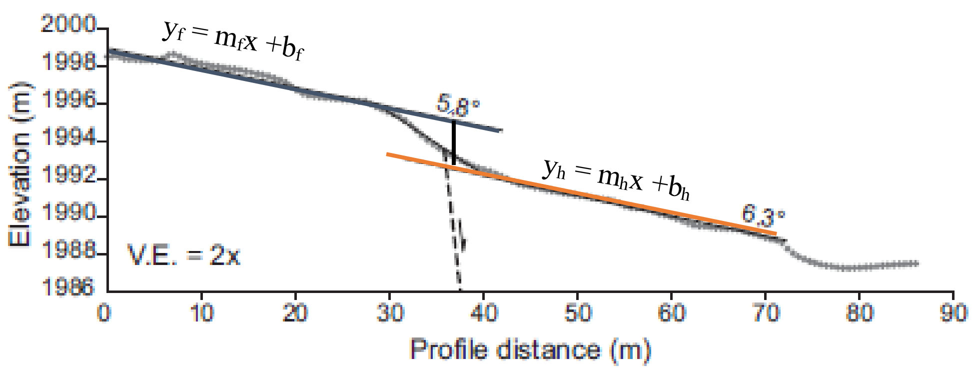

Figure 1.8: Topographic profile along with linear regressions of a normal fault scarp. Vertical separation (black) is measured halfway up on the fault scarp. The slopes of the hanging wall (orange) and footwall (blue) were used. Modified from Amos et al. (2010).

$$v(x) = x(m_h - m_f) + b_h - b_f$$

where m_h and m_f are the slopes of the hanging wall and footwall respectively (Figure 1.8). The variables b_h and b_f are the y intercepts of the calculated slopes while x is the distance along the profile. The variable x in this equation will always be the midpoint of the scarp. The method is described in Thompson et al. (2002). Fault profiles were drawn in ArcMap 10.4 using the 3D analysist tool and then exported into Excel for analysis. This was done for a series of alluvial fans to determine the relationship between fault scarp height and the age of the fan and to determine fault rupture timing.

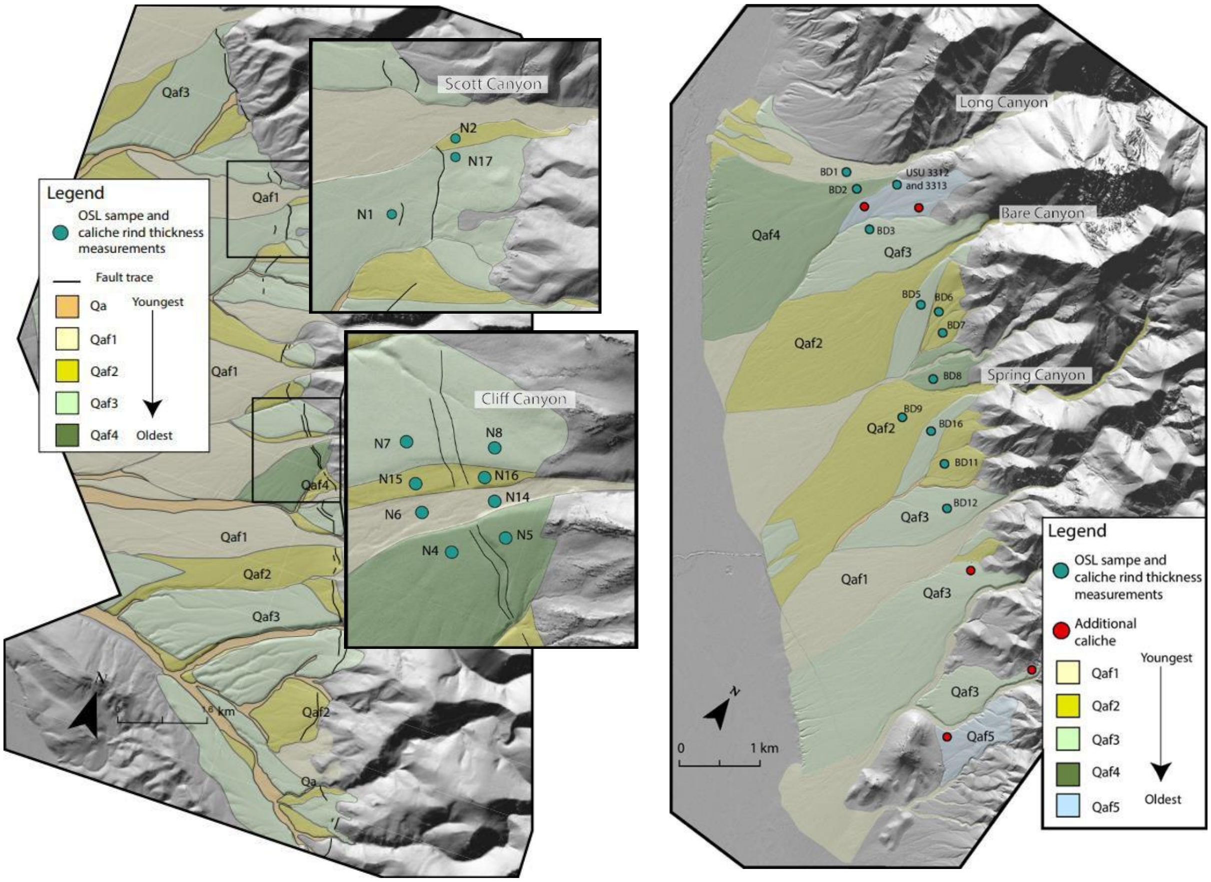

Figure 1.9: Landform and fault scarp map of the Nicholia segment. Optical stimulated luminescence sample sites shown in the teal dotsin the Scott and Cliff canyons. Qa is the current alluvial deposit while ages increase from Qaf1 to Qaf4. b. Landform and fault scarp map of the Blue Dome segment, showing shows the alluvial fan and optical stimulated luminescence sampling in the Blue Dome segment.

1.4.4 Optically Stimulated Luminescence dating

Optically stimulated luminescence (OSL) dating is a dating technique that dates the last time sediment has been exposed to sunlight. OSL dating uses quartz and feldspar grains that are exposed to ionizing radiation following burial and trap elections into the upper orbitals in the atoms. When exposed to sunlight, the accumulated signal is reset. For this project we used quartz grains to calculate the OSL age. The ages are calculated by measuring the equivalent dose and dose rate. Equivalent dose is the accumulated natural irradiation of the sample once the quartz is buried, and the dose rate is the rate at which the sample is irradiated. By dividing the equivalent dose (De) by the dose rate we can calculate the OSL age.

1.4.4.1 Optically Stimulated sample strategy

The OSL sample locations are shown in Figure 1.9a and b for the Nicholia and Blue Dome segments respectively. Twelve OSL samples were collected from the Nicholia segment and thirteen from the Blue Dome segment. Because the Blue Dome segment lacks documented fault scarps cutting alluvial fans, OSL samples and soil data were collected from a variety of fans across the range front. OSL samples were collected primarily from Long, Bare, and Spring canyons because of ease of access to the area and because there are multiple alluvial fans to date at each of the canyons. Sampling across the range front in the Blue Dome segment allowed the alluvial fan chronology to be constrained in better detail. In contrast, the Nicholia segment does have a fault scarp present along the range front. The youngest alluvial fan surface in the Nicholia segment is unfaulted while all four older fan units are cut by fault scarps. Two canyons were chosen to sample the alluvial fans: Scott and Cliff canyons. Cliff Canyon has the best sequence of faulted and unfaulted fans. Four fans were mapped at Cliff Canyon and OSL samples were collected on both the footwall and hanging wall of the fault. This ensures stronger age constraint on the fans. By dating the unfaulted and faulted fans, the last rupture of the Nicholia segment can be constrained.

1.4.4.2 Optically Stimulated Luminescence sample processing

The OSL samples were collected from trenches created by a back hoe with the exception of USU 3312 and 3313, which were collected in a hand-dug trench. The trenches were dug perpendicular to the slope direction of alluvial fans in order to observe the sediments in the downgradient direction. Samples were extracted from underneath a light-proof tarp while using low-red lighting. Approximately 0.01 – 0.03 m^3 of sandy gravel alluvium was collected into a double-bagged garbage bag to ensure that no light interfered with the sample. Water concentration and dose-rate samples were collected adjacent to the sample.

Samples were processed under amber light within the Utah State University Luminescence Lab. The lab uses single-aliquot regenerative-dose (SAR) procedures (Murray and Wintle, 2000) to calculate the equivalent dose (De) of the sample. Dose rates were calculated by irradiating the sample at five doses: below, at, and above the De. A zero and repeated dose were also measured to check for recuperation of the signal. The De is then calculated using either the Central Age Model or the Minimum Age Model by Galbraith and Roberts (2012). Dose rate calculations are dependent on water content, cosmic radiation contribution and sediment chemistry (U, Th, K and Rb). Dose-rate calculations were determined by measuring the amounts of U, Th, K and Rb by using an ICP-MS and ICP-AES and conversion factors from Guérin et al. (2011). Cosmic radiation was calculated by incorporating sample depth, elevation and latitude and longitude of the sample location.

1.4.5 Cosmogenic radionuclide dating

Cosmogenic nuclides are radioactive isotopes produced when cosmic radiation interacts within an *in-situ* atom, causing creation of rare isotopes via spallation. These nuclides accumulate in exposed rock surfaces. The abundance of these nuclides will give an estimate of the exposure age of the mineral when a widely accepted isotopic production rate is applied (Gosse and Phillips, 2001; Cockburn and Summerfield, 2004). For this project, beryllium-10 isotopes were measured on samples of Kinnikinic Formation quartzite boulders exposed in the fault scarp and on a corresponding alluvial fan surface at Pierce Canyon, in the southern end of the Nicholia segment. CRN dating has primarily been used to date boulders along moraines to constrain glacial sequences. It has also been used to date boulders along alluvial fans (Owen et al., 2014). Using CRN to date alluvial fans should produce a younger age than OSL, as boulders are likely to be exposed at the end of an alluvial fan deposition.

1.4.5.1 Cosmogenic sample strategy

Boulders >1 m diameter were sampled on the Pierce Canyon alluvial fan surface shown in Figure 1.10. Eight boulders were sampled, four on the alluvial fan surface, BHPC-01 through -04,and four exposed in a fault scarp. Samples BHPC-05 through BH-08 were collected on a transectup the fault scarp, with the hypothesis that the fault scarp would progressively expose boulders higher on the degraded scarp. These boulders had percussion marks and scratches on the surface indicating that they have been re-worked and conceivably had their ^{10}Be signal reset. Approximately 2.5 cm of rock were removed from the tops of boulders by using an angle grinder and chisels. Shielding, elevation and latitude and longitude calculations were done at each boulder site.

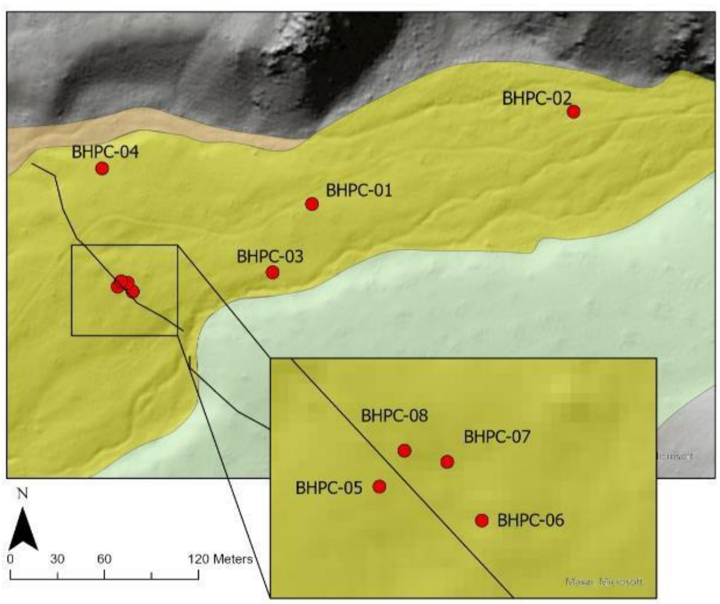

Figure 1.10: Locations of the boulders sampled along Pierce Canyon. Four boulders (BHPC-01 – 04) are located along the alluvial fan surface while BHPC 05 – 08 are located along the fault scar

1.4.5.2 Cosmogenic sample processing

Samples were reduced to 2.5 cm and ground to 410 -710 um at the Idaho State University rock grinding lab. The ground-samples were then sent to the University of Vermont Community Cosmogenic Facility for quartz purification and beryllium extraction. The quartz was purified using HCL, HF, and HNO_3. Samples produced about 20 grams of purified quartz. For more details in UVM CCF procedures, see Corbett et al., (2016). The samples were then analyzed for ^{10}Be content at the Center for Accelerator Mass Spectrometry at Lawrence Livermore National Laboratory. The ages were then calculated using the online calculators formerly known as CRONUS (version 3, Balco et al., 2008).

1.4.5.3 OxCal

OxCal is a modeling software program that determines the chronology of a fault rupture event based on minimum and maximum limiting ages. For the Nicholia segment, OxCal was used to constrain timing of the most recent two events. The model used the 1σ error on the OSL ages. OSL ages. By studying the cross-cutting relationships between the fault scarps and the OSL dated alluvial fan ages, we can create phases in the model where the boundaries selected are the inputted OSL ages. Program parameters and outputs were done by Susan Olig (personal communication, 2021).

References:

Anders, M.H., Geissman, J.W., Piety, L.A., Sullivan, J.T., 1989, Parabolic distribution of circum-eastern Snake River Plain seismicity and latest Quaternary faulting: migratory pattern and association with the Yellowstone hot spot: Journal of Geophysical Research, v. 94, p. 1589-1621.

Anders, M.H., and Schlische R.W., 1994, Overlapping Faults, Intrabasin Highs, and the Growth of Normal Faults: Journal of Geology, v. 102, p. 165-180.

Armstrong, R. I., Leeman, W. P., and Malde, H. E., 1975, K-Ar dating, Quaternary and Neogene volcanic rocks of the Snake River Plain, Idaho: America Journal of Science, v. 275, p. 225 -251.

Balco, G., Stone, J.O., Lifton, N.A., and Dunai, T.J., 2008, A simple, internally consistent, and easily accessible means of calculating surface exposure ages or erosion rates from 10Be and 26Al measurements: Quaternary Geochronology, v. 3, p. 174–195, doi: 10.1016 /j.quageo.2007.12001.

Bronk R. C.,2009. Bayesian analysis of radiocarbon dates: Radiocarbon, v. 11, p. 337–360.

Bull, W.B., 1987, Relative rates of long-term uplift of mountain fronts, in Crone, A. M., and Omdahl, E. M., eds., Directions in Paleoseismology: U.S. Geological Survey Open-File Report 87- 673, p. 192-202.

Chadwick, J.D., Rodgers, D.W., and Payne, S.P., 2007, Contemporary tectonic motion of the eastern Snake River Plain, Idaho: A global positioning system study, 1995–2004: Tectonics, v. 26, p. 1 – 7. TC6005, doi:10.1029/2005TC001914

Cockburn, H.A.P., Summerfield, M.A., 2004. Geomorphological applications of cosmo-genic isotope analysis: Progress in physical Geography v. 28, p. 1–42.

Corbett, L., Bierman, P., and Rood, D., 2016, An approach for optimizing in situ cosmogenic 10Be sample preparation: Quaternary Geology, v. 33, p. 24-34.

Crone, A. J., and Haller, K. M., 1991, Segmentation and the coseismic behavior of Basin and Range normal faults: examples from east-central Idaho and southwestern Montana, U.S.A: Journal of Structural Geology, v. 13, p. 151 – 164.

Densmore, A.L., Dawers, N.H., Gupta, S., and Guidon, R., 2005, What sets topographic relief in extensional footwalls?: Geology, v. 33, no. 6, p. 453-456.

Galbraith, R.F., Roberts, R.G., 2012. Statistical aspects of equivalent dose and error calculation and display in OSL dating: An Overview and some recommendations: Quaternary Geochronology, v. 11, p. 1-27.

Garmezy, L., 1981, Geology and tectonic evolution of the southern Beaverhead Range, east-central Idaho [M.S. thesis]: University Park, The Pennsylvania State University, 155 p.

Gosse, J.C., Phillips, F.M., 2001. Terrestrial in situ cosmogenic nuclides: theory and application: Quaternary Science Reviews v. 20 p. 1,475–1,560. Guérin, G., Mercier, N., Adamiec, G., 2011. Dose-rate conversion factors: update: Ancient TL v.29, p. 5-8.

Hackett, W.R., and Morgan, L.A., 1988, Explosive basaltic and rhyolitic volcanism of the eastern Snake River Plain, Idaho, *in* Link, P.K. and Hackett, W. R. eds, Guidebook to the geology of central and southern Idaho: Idaho Geological Survey Bulletin v. 27 p. 283-301

Haller, K.M., 1988, Segmentation of the Lemhi and Beaverhead faults, east-central Idaho, and Red Rock fault, southwest Montana, during the late Quaternary [M.S. thesis]: Boulder, University of Colorado, 141 p.

Kenworthy, M.K., Rittenour, T.M., Pierce, J.L., Sutfin, N.A., and Sharp, W.D., Luminescence dating without sand lenses: An application of OSL to coarse-grained alluvial fan deposits of the Lost River Range, Idaho, USA: Quaternary Geochronology, v. 23, p. 9-25.

Lewis, R.S., Link, P.K., Standford, L.R., and Long, S.L., 2012, Geological Map of Idaho: Idaho Geological Survey, scale 1:750,000

Link, P.K., and Janecke, S.U., 1999, Geology of east-central Idaho: Geologic roadlogs for the Big and Little Lost River, Lemhi, and Salmon River valleys, in Hughes, S.S., and Thackray, G.D. eds., Guidebook to the Geology of Eastern Idaho: Idaho Museum of Natural History, Pocatello, Idaho, p. 295 -334.

Murray, A.S., Wintle, A.G., 2000. Luminescence dating of quartz using an improved single aliquot regenerative-dose protocol: Radiation Measurements v. 32, p. 57-73.

Owen, L.A., Clemmens, S.J., Finkel, R.C., and Gray, H., 2014, Late Quaternary alluvial fans at the eastern end of the San Bernardino Mountains, Southern California: Quaternary Science Reviews, v. 87, p. 114-134.

Payne, S. J., R. McCaffrey, and R. W. King, 2008, Strain rates and contem-porary deformation in the Snake River Plain and surrounding Basin and Range from GPS and seismicity: Geology, v. 36, p. 647–650

Payne, S.J., McCaffrey, R., King, R.W., and Kattenhorn, S.A., 2012, A new interpretation of deformation rates in the Snake River Plain and adjacent Basin and Range regions from GPS measurements: Geophysical Journal International, v. 189, p. 101–122, doi:10.1111 /j.1365-246X.2012.05370.x.

Pearson, D.M., and Link, P.K., 2017, Field guide to the Lemhi Arch and Mesozoic-Early

Cenozoic faults and folds in east-central Idaho: Beaverhead Mountains in Cox, B., Hargrave, P.K., and McDonald, K., eds. Geology of the Leadore Area and Other Papers: The Tobacco Root Geological Society, Inc., 42nd Annual Field Conference, Guidebook, p. 101 – 111.

Pierce, K.L., and Morgan, L.A., 1992, The track of the Yellowstone hot spot: Volcanism, faulting, and uplift, in Link, P.K., Kuntz, M.A., and Platt, L.B., eds., Regional Geology of Eastern Idaho and Western Wyoming: Geological Society of America Memoir 179.

Pierce, K.L., and Morgan, L.A., 2009, Is the track of the YHS driven by a deep mantle plume?—Review of volcanism, faulting and uplift in light of new data: Journal of Volcanology and Geothermal Research, v. 188, p. 1–25, https://doi.org/10.1016/j.jvolgeores.2009.07.009.

Pierce, K.L., and Scott, W.E., 1982, Pleistocene episodes of alluvial-gravel deposition, southern Idaho, in Bonnichsen, B., and Breckenridge, R.M., eds., Cenozoic Geology of Idaho: Idaho Bureau of Mines and Geology Bulletin, v. 26, p. 685-702.

Scott, W.E., 1982, Surficial geologic map of the eastern Snake River plain and adjacent areas, 111 degree x 115 degree W., Idaho and Wyoming: U.S. Geological Survey, scale 1:250,000, 2 sheets.

Skipp, B., 1985, Contraction and extension faults in the southern Beaverhead Mountains, Idaho and Montana: U.S. Geological Survey Open-File Report 85-545, 170 p.

Suppe, J., Powell, C., and Berry, R., 1975, Regional topography, seismicity, Quaternary volcanism, and the present-day tectonics of the western United States: American Journal of Science, v. 275-A, p. 397-436.

Thompson, S. C., Weldon, R. J., Rubin, C. M., Abdrakhmatov, K., Molnar, P., and Berger, G. W., 2002, Late Quaternary slip rates across the central Tien Shan, Kyrgyzstan, central Asia

Ramsey, B. C., 2009, Bayesian analysis of radiocarbon dates. Radiocarbon, v. 51, p. 337–360

Vincent, K. R., Bull, W. B., Cadwick, O. A., 1994, Construction of a Soil Chronosequence Using the Thickness of Pedogenic Carbonate Coating: Journal of Geological Education, v. 42, p. 316 – 324.

Zhou, Y., 2018, Anomalous mantle transition zone beneath the Yellowstone hotspot track: Nature Geoscience, v. 11, p. 449 – 453.

Zhou, Q., Liu, L., and Hu, J., 2017, Western US volcanism due to intruding oceanic mantle driven by ancient Farallon slabs: Nature Geoscience, v. 11, p. 70 – 76

Chapter ll: Alluvial Fan Morphology, Chronology, and Inferences of Climatic History

2.1 Fan units in the Nicholia and Blue Dome segments

This chapter describes alluvial fan morphology and chronology adjacent to the southern Beaverhead range. Dating the deposition of alluvial fans and comparing them to reconstructed regional paleoclimates will show how climate can influence the process of alluvial fan deposition. This is important for the reconstruction of alluvial fan deposition within the northern Basin and Range.

In addition, characterizing these alluvial fans may provide insight on seismic hazards assessment for the Idaho National Laboratory, located to the south of the study area. Haller (1988) showed that the youngest fans in the Nicholia segment are not cut by a fault scarp while older alluvial fans are. By dating the unfaulted fan and the faulted fans, we can constrain the last rupture timing along the Nicholia segment. Chapter 3 of this thesis documents patterns of faulting along the Nicholia and Blue Dome segments.

2.1.1 Spatial distribution of fan units

Five fan units (Qaf1 – Qaf5) were mapped along both the Nicholia and Blue Dome segments. Mapping was done using lidar imagery, and incorporated the relative geomorphic position of the alluvial fans, the caliche carbonate rind thickness, and the OSL ages from the fan units. The following sections describe the spatial distribution of fans along the Nicholia and Blue Dome segments, their soilcharacteristics, and OSL ages.

2.1.2 Nicholia segment

The alluvial fan map for the Nicholia segment is shown in Figure 2.1. The alluvial fans along the Nicholia segment form a bajada along the range front. These alluvial fans are broad and spread into Birch Creek basin with the exception of alluvial fans in Pierce Canyon where the bedrock of the Blue Dome segment restricts their spread. The distal ‘toes’ of the alluvial fans have been eroded away by Birch Creek. Qaf1 fans are mapped at the mouths of most canyons. Qaf1 fans are the lowest fan surface and other alluvial fan surfaces are topographically higher. There are two types of Qaf1 fans mapped in the Nicholia segment, Qaf1o being older and Qaf1y being younger. Qaf1o fans are inset by Qaf1y fans. Qaf1o are slightly lower topographically than Qaf1y fans. The Qaf3 and Qaf4 alluvial fans are found predominantly within the central to southern portion of the Nicholia segment. One Qaf5 fan was mapped in central portion of the Nicholia segment. Most of the Qaf3-Qaf5 fans are clear remnants of the older fans eroded prior to construction of the younger fans, so only the lateral portions of those fans remain. The Qaf1 and Qaf2 alluvial fans are larger and spread toward the center of the Birch Creek basin, only having been incised by Birch Creek and truncated by Birch Creek terraces. There are also small alluvial landforms mapped as Qaf1 between Scott and Willow Creek canyons. The Qaf1 fans are the only fans in the Nicholia segment not cut by a fault scarp. In the middle portion of the segment, near Scott Canyon, there are remnants of Qaf2 fans inset by Qaf1 fans towards the basin.

In the southern portion of the segment near and including Pierce Canyon, there are no large Qaf1 fans like those found elsewhere, but rather there is a large Qa unit that experiences ephemeral water flow and sediment transport. Generally, the alluvial fans at Pierce Canyon are elongate landforms rather than normal fan-shaped alluvial units. This is because the bedrock of the Blue Dome spur blocks the expansion of the alluvial fans to the south, confining them intoa narrow space and restricting their growth. This is in contrast to those in the northern section that freely spread out into Birch Creek basin.

2.1.3 Blue Dome segment

The alluvial fans, much like in the Nicholia segment, form a bajada and spread laterally into the Birch Creek basin (Figure 2.2). The Blue Dome segment range front is dominated by Qaf1 and Qaf3 fans. Just as in the Nicholia segment, Qaf1 fans extend directly from the canyon mouths. Qaf3 fans are generally adjacent to the Qaf1 fans. In the southern portion of the range near the mouth of the Birch Creek basin with the Snake River Plain, there is a section Qaf1y and Qaf1o fans along the narrow, low spur of bedrock along the range front. These fans have preserved braided stream patterns on their surfaces. These fans wrap around ~6 Ma basalt buttes and cinder cones (Skipp, 1985). The canyons that fed the fans have smaller drainage areas and would naturally have smaller fan areas. Only two Qaf2 units were mapped in the Blue Dome segment, one in the southern portion of Spring Canyon and another remnant near the end of Long Canyon. Qaf3 fans are the most common fan in the Blue Dome segment. They typically flank a Qaf1 fan. Qaf3 deposits are also present alongside the range front from Long Canyon to Scott Butte. These were mapped as late Holocenedeposits by Scott (1982) but our OSL ages confirm that they are late Pleistocene Qaf3 deposits. Qaf4 fan units appear at Long Canyon, Spring Canyon and Peterson Canyon. These fans are small in area compared to Qaf1 and Qaf3 fans.

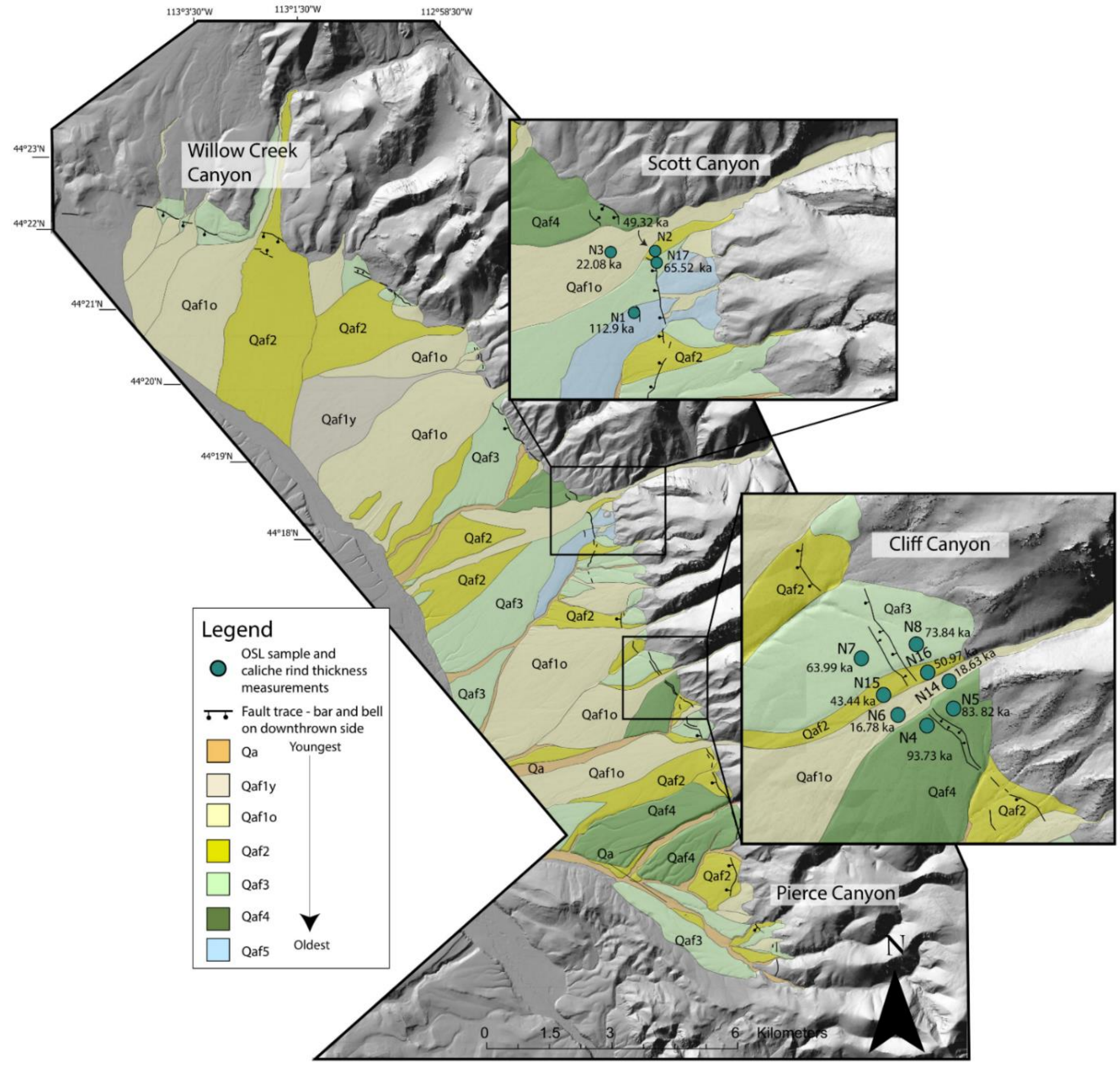

Figure 2.1: Alluvial fan mapping of the Nicholia segment showing the OSL sample locations in Scott and Cliff canyons. Fivefan units were identified in the Nicholia segment.

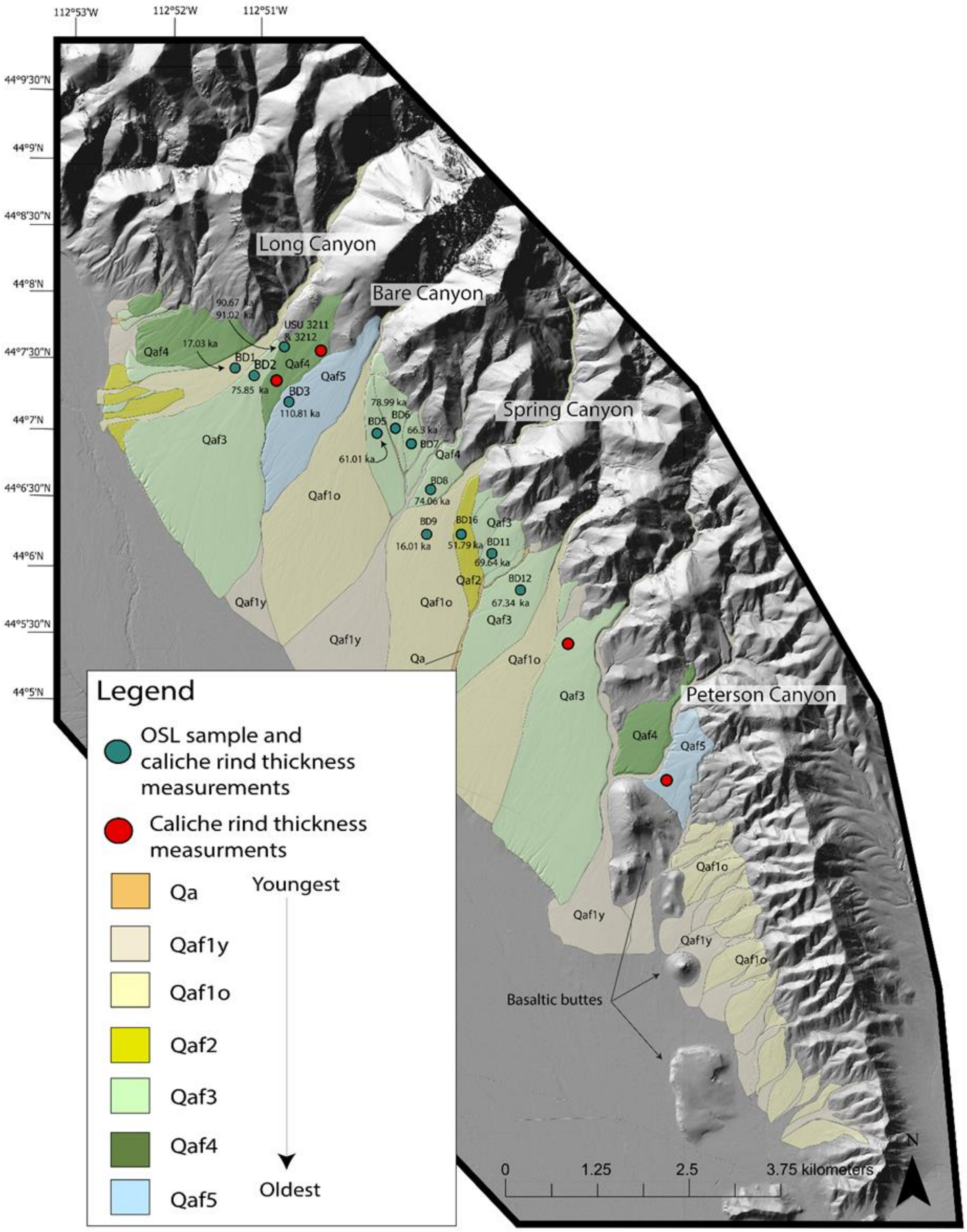

Figure 2.2: Alluvial fan mapping of the Blue Dome segment showing the locations of the OSL samples and their respective ages. Shown are also the additional sites where additional caliche rinds were measured. There are 5 alluvial fan units shown in Blue Dome section.

2.1.4 Fan unit description

General: In the southern portion of the Beaverhead Mountains, near the Blue Dome and Nicholia segments, the alluvial fans form bajadas filling the eastern third of the Birch Creek basin and terminate where cut by Birch Creek. Broad alluvial fans are missing from the range front of the Blue Dome spur, probably having been eroded by Birch Creek.

Alluvial fan deposits were observed in shallow (1.5-2 m) sampling trenches excavated by backhoe. The alluvial fans consist of coarse-cobble to pebble gravel in the upper 1.5 m below the ground surface, fining upward to pebbly gravel and silt interpreted as loess. The matrix ranges from coarse sand fining to sandy silt. Soil development in the gravels has disturbed the clasts and cause them to 'float' in the loessic cap. Gravels show imbrication, poorly expressed stratigraphy and poor sorting, indicating a high-energy fluvial setting. Most trench exposures also contained finely bedded pea gravel which is interpreted to be sheet flood deposits (see Figure 2.3, Appendix A). There were some deposits that were interpreted have been deposited by debris flows, but this was uncommon (Appendix A). The deposits that were matrixed supported and contained boulder clasts were classified as debris flows. One site, BD16, uniquely displayed a thick sand lens (30 cm), 1.5 m below the surface.

The soil profiles along the Nicholia and Blue Dome segments have similar soil horizons with varying thicknesses. The A soil horizon is typically a silt loam with granular texture with isolated pebbles. The A horizon reacts weakly to HCl. This horizon is about 15 cm, overlying ABk1 or Bk1 horizons. The ABk horizons were described as the transition zones between the A horizon and the Bk horizon. These layers still retained soil structures but had more pebble clasts as well as an increase of HCl reaction. The ABk horizons are 10 – 15 cm thick. The Bk horizon has a stronger HCl reaction, and more pebble clasts. Bk horizons were sub-divided based on carbonate accumulation and clast size and range in thickness from 10 – 20 cm. Most sites have at least 3 Bkhorizons (Bk1-Bk3). Clast size increases and gravels are more clast supported with depth.

Carbonate rinds were collected from average 30 cm depth in the Bk2 or Bk3 horizons. At 1.0 -1.5 m depth lies the upper portion of the CBk horizon, although this was not commonly observed because it lies below typical excavation depth. All of the soil horizons reacted to HCl, to varying degrees. The AB horizons reacted to the HCl weakly while the Bk horizons had a more moderate to violent reaction and the CBk horizons reacted weakly to moderately. The older alluvial fans had thicker carbonate rinds but the Bk soil horizon is consistent in thickness (Figure 2.3). The soil development on the fan deposits of small drainages limited to the range-front in the Blue Dome section was minimal, as defined by the lack of carbonate accumulation. Only one carbonate stage IV was identified, on an undated Qaf5 fan in Peterson Canyon in the southern Blue Dome segment. Detailed descriptions of the soil profiles and sedimentary units of each trench are in Appendix A.

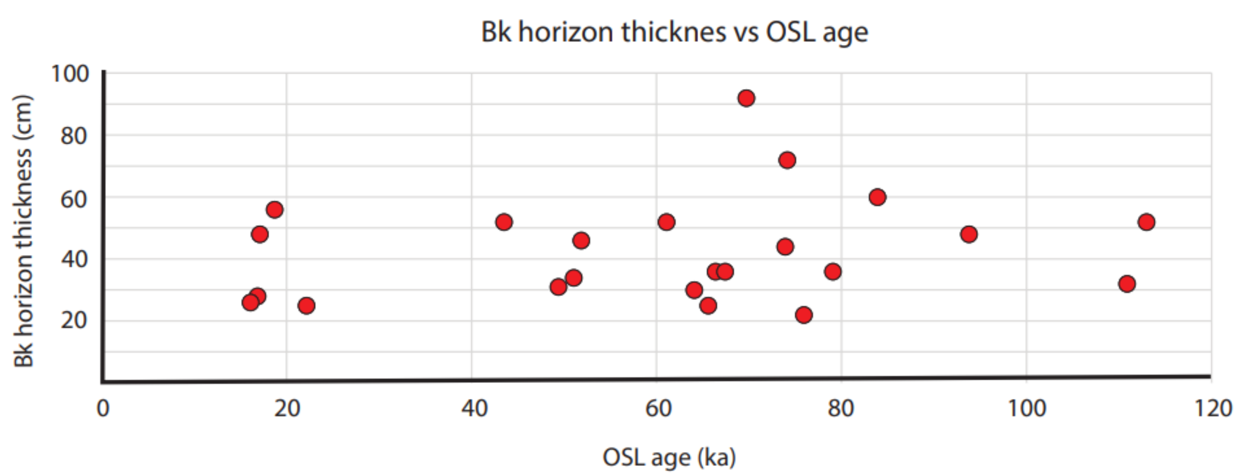

Figure 2.3: The thickness of the Bk horizon where the caliche samples were taken from plotted against the associated OSL age.

Qa: This is the youngest, most recently active, ephemeral stream deposit. These current ephemeral stream deposits are in channels cut into alluvial fans. The unit is most extensive in the southern portion of the Nicholia segment in Pierce Canyon.

Qaf1: This is the youngest alluvial fan unit in both the Nicholia and Blue Dome segments. OSL ages are 16 – 22 ka (see section 2.1). Both of the Nicholia and Blue Dome areas have Qaf1y (younger) and Qaf1o (older) fans. The Qaf1o fans are inset slightly lower than the Qaf1y fans, but there is otherwise not sufficient distinction to divide them into distinct units. These fans typically have braided stream channel patterns and deposits preserved on the landform surface. Soils in these fans are predominantly Stage I carbonate (see Birkeland, 1999) and are otherwise weakly developed. There is a thinner loessic cap on the soils and fewer large cobbles in the gravel as compared to Qaf2 - Qaf5 units. Figure 2.4 shows the stratigraphic profile of site N3 in the Qaf1 fan in Scott Canyon in the Nicholia segment.

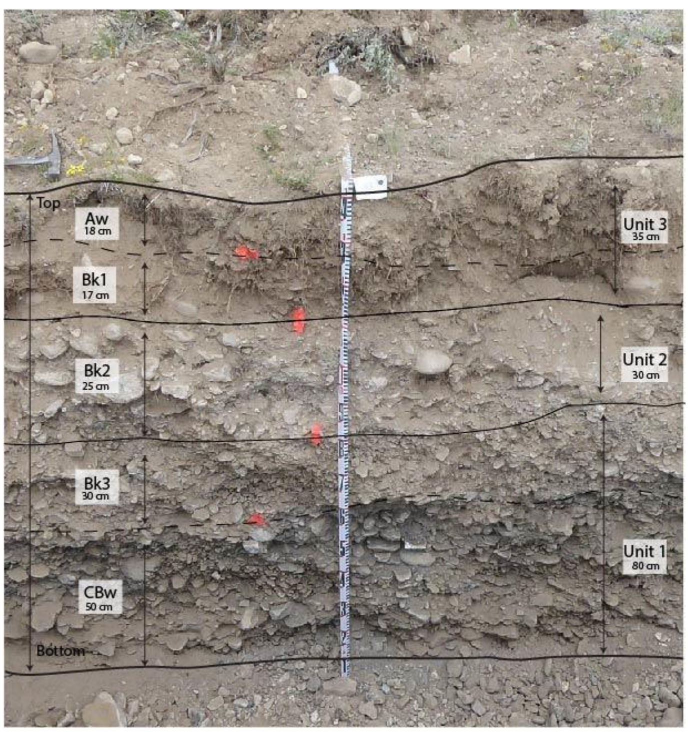

Figure 2.4: N3 trench wall on the Qaf1 fan at Scott Canyon in the central portion of the Nicholia section shown in Figure 2.1. Units on the left are the soil horizons while those on the right describe the sedimentary units.

Qaf2: Qaf2 fans are topographically higher than Qaf1 fans. These are normally narrow (1 – 1.5 km) remnants of the fans, adjacent to the canyon mouths. A few of these fans have braided stream patterns preserved, but generally do not. Qaf2 fans are more prominent in the Nicholia segment than in the Blue Dome segment. Qaf2 fans range in OSL ages from 35 – 55 ka (section 2.2.2). Stage I+ and Stage II carbonate development characterize the soils.

Qaf3: These fans are topographically higher than Qaf2 fans. These are broad range-front fans and show a smooth surface texture in LiDAR imagery, lacking braided stream channel patterns. The major distinction between Qaf2 and Qaf3 fans is geomorphic position with Qaf3 fans being slightly smoother than the Qaf2 counterparts. The soil carbonate stage for these fans is typically Stage II to Stage II +,with the exception of the mapped Qaf3 alluvial deposits at the mouths of small range front drainages (samples BD7, BD6, and BD11), which have Stage I carbonate. The base of the trenches inthe Qaf3 fans have more cobbles than those in the Qaf2 or Qaf1 fans. Figure 2.5 shows the trench site at N17, a mapped Qaf3 alluvial fan in Scott Canyon.

Qaf4: These alluvial fans are mostly mapped in the southern portion of the Nicholia segment and only locally in the Blue Dome segment. These fans have deeper drainage incisions along their edges as compared to Qaf3. These alluvial fans do not have braided stream channel patterns preserved on their surface. This is particularly the case in the southern portion of the Nicholia segment where the fans are smooth. These fans have abundant cobbles and Stage II to II+ pedogenic carbonate development.

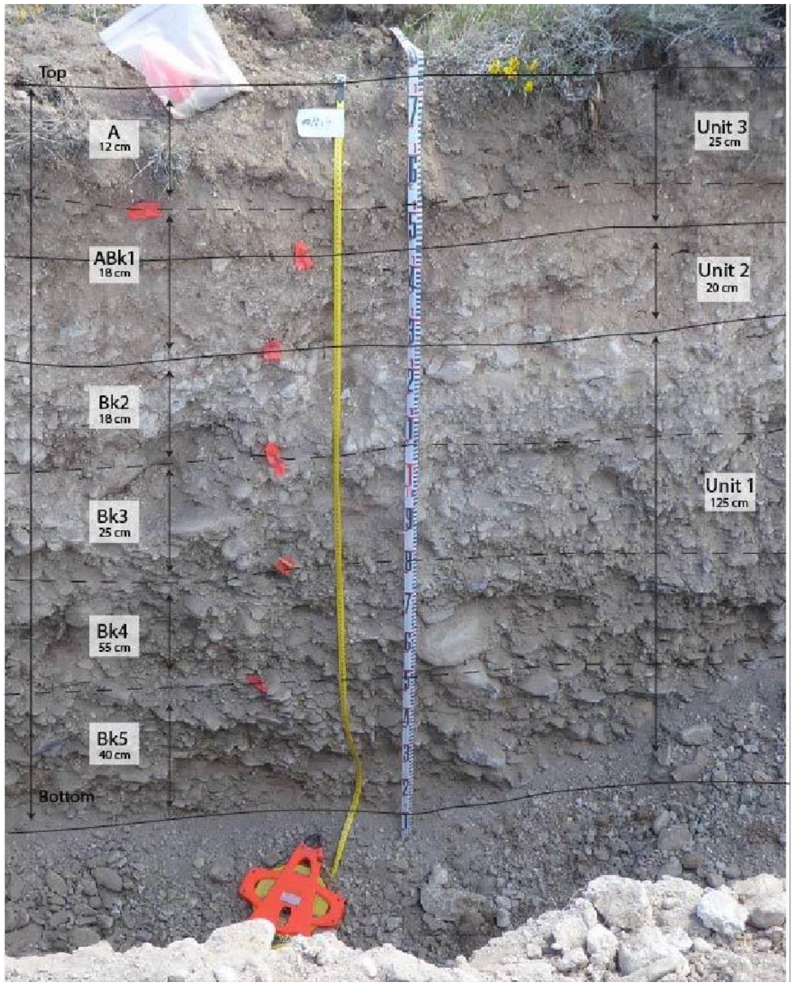

Figure 2.5: Trench site N17, mapped as a Qaf3 fan in Scott Canyon.

Qaf5: This is the oldest fan unit identified. Morphologically they are similar to Qaf4 fans but produced older OSL ages and displayed slightly stronger soil carbonate development than did Qaf4 fans. The Qaf5 fan in the Scott Butte area was mapped on the basis of the carbonate accumulation in the soil profile. One Qaf5 fan was identified in the Nicholia segment outside of Scott Canyon and the other in Bare Canyon within the Blue Dome segment. These fans have Stage II + to Stage III carbonate development and are incised deeply along their edges.

2.2 Optically stimulated luminescence age sequence and correlations to geomorphic position

2.2.1 Summary of OSL ages

We dated 25 OSL samples from 24 locations. Table 2.1 compiles the OSL ages from the Nicholia and Blue Dome segment alluvial fans. Locations and ages are shown in Figures 2.1 and 2.2. We dated two samples (USU-3211 and USU-3212) from one trench at Long Canyon in order to assess repeatability, and those two analyses produced very similar results. Five fan units and ages were identified and dated in both the Blue Dome and Nicholia segments. OSL ages range from 16 – 113 ka. Qaf1 hasages from 16 – 22 ka; Qaf2 43- 61ka; Qaf3 66– 74 ka; and Qaf4 84 – 94 ka. The oldest identified fan unit, Qaf5, had two ages 111 – 113 ka. The mean OSL ages are Qaf1 18.1 +/- 2.4 ka; Qaf2 48.88 +/- 3.6 ka; Qaf3 69.65 +/- 5.5 ka; Qaf4 89.81 +/- 3.6 ka and Qaf5 111.85 +/- 1.0 ka (Table 2.2). Dose-rate information is found in Appendix B.

2.2.2 OSL ages and correlation to geomorphic position

OSL ages correlate to geomorphic position and in general to our initial, purely geomorphic mapping. Examples of this geomorphic position-agecorrelation are shown in Cliff Canyon (Figure 2.6) and Long Canyon (Figure 2.7). There are four alluvial fan units mapped at the mouth of Cliff Canyon, where Qaf1 is topographically the lowest fan unit and Qaf4 is the highest fan unit. Eight OSL samples were collected on this fan sequence, from each geomorphic unit on either side of the fault scarp. The OSL ages increase with geomorphic position. This supports the accuracy of the geomorphic mapping and indicates that the surface of each alluvial fan consists of 1.5 m or more of gravel that was freshly deposited, as opposed to simple erosion and re-grading of an older alluvial fill. Kenworthy et al. (2014) found similar relationships in the Lost River Range.

Table 2.1: Results of the OSL ages.

Segment	Sample num.	Fan Unit	USU num.	Depth (m)	Num. of aliquots[1]	Dose rate (Gy/ka)	Equivalent Dose[2] ± 2σ (Gy)	OSL age ± 1σ (ka)
Nicholia	N3	Qaf1	USU-3400	1.3	18 (26)	1.19 ± 0.06	26.26 ± 1.64	**22.08 ± 1.98**
	N6	Qaf1	USU-3406	1.55	19 (27)	0.82 ± 0.05	13.82 ± 2.40	**16.78 ± 2.09**
	N14	Qaf1	USU-3407	1.5	21 (26)	0.84 ± 0.05	15.70 ± 2.42	**18.63 ± 2.20**
	N15	Qaf2	USU-3404	1.2	21 (28)	1.10 ± 0.05	47.87 ± 8.65	**43.44 ± 5.39**
	N2	Qaf2	USU-3401	1.3	21 (33)	1.22 ± 0.06	60.05 ± 8.36 [3]	**49.32 ± 5.86**
	N16	Qaf2	USU-3411	1.4	18 (27)	0.96 ± 0.05	49.04 ± 5.82	**50.97 ± 5.43**
	N7	Qaf3	USU-3405	1.3	18 (25)	0.89 ± 0.05	57.25 ± 7.25	**63.99 ± 6.99**
	N8	Qaf3	USU-3410	1.2	21 (33)	0.95 ± 0.05	70.07 ± 7.94	**73.84 ± 7.79**
	N17	Qaf3	USU-3402	1.5	21 (31)	1.02 ± 0.05	66.82 ± 8.17	**65.52 ± 6.92**
	N5	Qaf4	USU-3409	1.4	19 (26)	0.84 ± 0.05	70.51 ± 7.66	**83.82 ± 8.73**
	N4	Qaf4	USU-3408	1.5	18 (26)	0.68 ± 0.04	64.18 ± 10.66	**93.7 ± 11.8**
	N1	Qaf5	USU-3403	1.7	20 (35)	0.87 ± 0.05	98.28 ± 11.95	**112.9 ± 12.1**
Blue Dome	BD1	Qaf1	USU-3412	1.3	21 (31)	0.99 ± 0.05	16.90 ± 3.15 [3]	**17.03 ± 2.28**
	BD9	Qaf1	USU-3419	1.35	26 (32)	1.77 ± 0.08	28.33 ± 4.03 [3]	**16.01 ± 1.77**
	BD16	Qaf2	USU-3420	1.45	20 (26)	2.22 ± 0.09	114.9 ± 15.0	**51.79 ± 5.39**
	BD2	Qaf3	USU-3413	1.3	19 (26)	1.04 ± 0.05	79.10 ± 7.98	**75.85 ± 7.52**
	BD5	Qaf3	USU-3415	1.5	20 (28)	1.23 ± 0.06	75.08 ± 11.59	**61.01 ± 6.96**
	BD6	Qaf3	USU-3416	1.5	18 (24)	1.07 ± 0.05	84.56 ± 7.64	**78.99 ± 7.59**
	BD7	Qaf3	USU-3417	1.6	24 (47)	1.29 ± 0.06	85.55 ± 8.18	**66.30 ± 6.39**
	BD8	Qaf3	USU-3418	1.45	19 (36)	1.45 ± 0.06	107.6 ± 12.3	**74.06 ± 7.45**
	BD11	Qaf3	USU-3421	1.6	18 (26)	1.39 ± 0.06	97.06 ± 5.30	**69.64 ± 6.04**
	BD12	Qaf3	USU-3422	1.45	23 (41)	0.96 ± 0.05	64.86 ± 9.32	**67.34 ± 7.52**
	USU-3211	Qaf4	USU-3211	0.96	18 (43)	1.95 ± 0.08	176.4 ± 33.2	**90.7 ± 11.3**
	USU-3212	Qaf4	USU-3212	1.32	18 (32)	2.01 ± 0.09	183.3 ± 33.2	**91.0 ± 11.1**
	BD3	Qaf5	USU-3414	1.5	23 (29)	1.15 ± 0.05	127.8 ± 15.0	**110.8 ± 11.3**

Processed by Tammy Rittenour at the Utah State University's luminescence lab. For the Dose rate information see Appendix B.
[1]analysis using the single-aliquot regenerative-dose procedure of Murray and Wintle (2000) on 1-2 mm small-aliquots of quartz sand (USU-3211:3212 = 150-250 µm; USU-3400:3422 = 75-150µm). Number of aliquots used in age calculation and number of aliquots analyzed in parentheses.
[2] Equivalent dose (D_E) calculated using the Central Age Model (CAM) of Galbraith and Roberts (2012), unless otherwise noted.

Alluvial fan unit	OSL age range	Mean age ± 1σ (ka)
Qaf1	16 - 22 ka	18.1 ± 2.4
Qaf2	43 - 61 ka	48.88 ± 3.6
Qaf3	66 - 79 ka	69.65 ± 5.5
Qaf4	84 - 94 ka	89.81 ± 3.6
Qaf5	111 - 113 ka	111.85 ± 1.1

Table 2.2: Summary of alluvial fan units and associated OSL ages for both the Blue Dome and Nicholia segments.

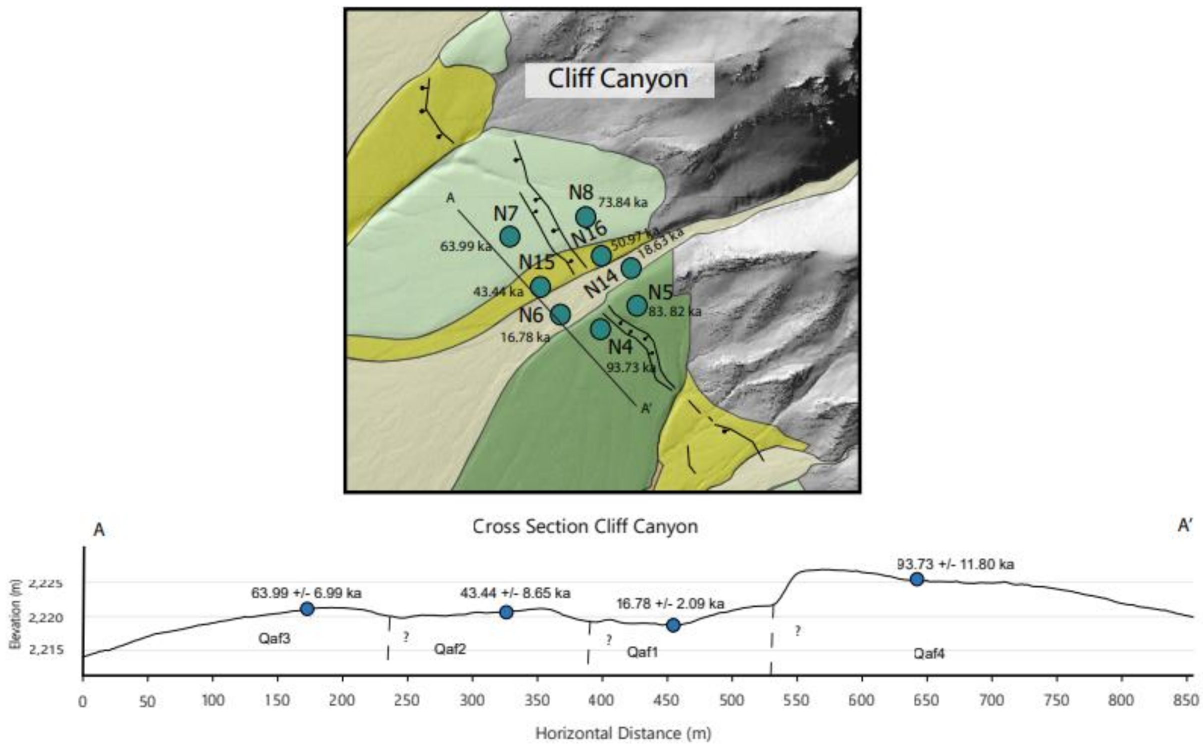

Figure 2.6: Geomorphic map of Cliff Canyon and showing the elevation profile drawn on A – A'. Cliff Canyon has 4 alluvial fan ages mapped out (Qaf1 – Qaf4). This shows the topographical relationship between OSL age and elevation on the mapped alluvial fans. Vertical exaggeration is 10x.

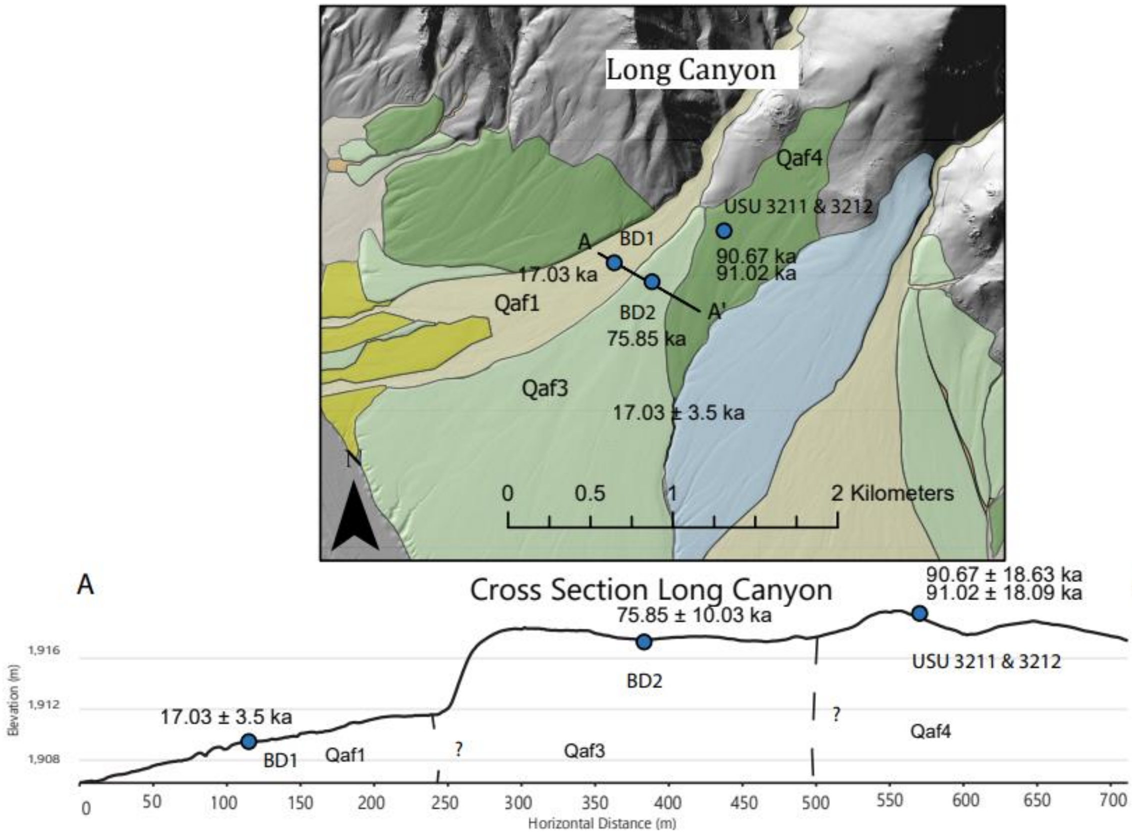

Figure 2.7: Geomorphic map of Long Canyon showing the elevation profile drawn on A – A'. The elevation profile showing the OSLages show OSL ages increase due to topographic relief. Vertical exaggeration is 12x.

2.3 Pedogenic carbonate rind data-fan age correlations

2.3.1 OSL age vs pedogenic rind thickness

Carbonate rinds were measured on clasts in the zone of maximum accumulation (ZMA), roughly 30 cm below the surface, at each OSL sample site and at several additional sites. The samples from the Nicholia segment were concentrated at the mouths of two canyons while the samples in the Blue Dome segment were from locations distributed along the range front. The mean thickness of pedogenic rinds (50 clasts) were calculated for each sampling site and plotted against the associated OSL age (Figure 2.7 and Table 2.3). While mean carbonate rind thicknesses in both segments increased with age, the Nicholia sample suite has a higher rate of accumulation (0.8 mm per 10 ka) than the Blue Dome sample suite (0.3 mm per 10 ka). The combined average pedogenic carbonate accumulation rate is 0.5 mm per 10 ka. The r^2 values for the Nicholia and for the Blue Dome segments are 0.47 and 0.24, respectively, which shows a weak correlation of the data. The r^2 value for all samples combined is 0.20. Soils generally would be expected to have a high variability, resulting in low r^2 values. The contrasting carbonate accumulation rates between the two areas may result from contrasting climatic conditions that can influence the rate of carbonate accumulation. In the field, it was observed that the Nicholia segment has larger sagebrush and generally denser vegetation than does the BlueDome segment. This suggests that the Nicholia segment has a higher rate of precipitation than the Blue Dome segment. Because the Blue Dome segment borders the ESRP, it most likely has a similar arid and windy climate, which could result in slower carbonate rind accumulation.

The carbonate rind data shows that relying solely on caliche thickness to determine landform age is possible, but that those ages should be considered to have substantial uncertainty, especially in older landforms. The soil carbonate accumulation is very dependent on the climate where the landform is located.

Outliers in the carbonate rind dataset include BD11, BD7, and BD6 for the Blue Dome segment. These samples have thin rinds (~1.0mm) with older OSL ages of 70 – 75 ka. These samples were collected from the alluvial deposits mantling small alluvial fans of small drainage basins limited to the range front. The soil here has thin carbonate rinds and there are few cobbles, and the contrast in rind thickness may arise from those differences. Another outlier is N4 in the Nicholia segment which has a mean of 2.1mm with a respective OSL age of 93.73 ka and is mapped as a Qaf4 alluvial fan. The mean caliche thickness in N5, in contrast, is 5.5 mm with an OSL age of 83 ka. The low r2 values and the outliers present within the dataset suggest that caliche rind thickness should be used with caution to estimate ages of individual alluvial fans. The strongly contrasting caliche accumulation rates (Figure 2.7) further indicates that calibration of caliche rind accumulation needs to be done locally rather than regionally, and that a larger calibration dataset may be needed.

Previous studies within the Lost River Range show that the carbonate accumulation rates vary from 0.6 mm per 10 ka (Pierce, 1985) to about 0.4 mm per 10 ka (Kenworthy, 2011). Our combined results (0.5 mm per 10 ka) do fit within that range, but our corresponding r^2 valueshow that there is a very weak positive correlation between OSL age and carbonate thickness. The r^2 values for Kenworthy (2011) was reported to be 0.66. Due to the alluvial fans selected having the same carbonate clast lithologies, we do not expect variation with clast lithology to influence the carbonate accumulation rates. Our results dosuggest that there are local climatic influences on carbonate accumulation rates.

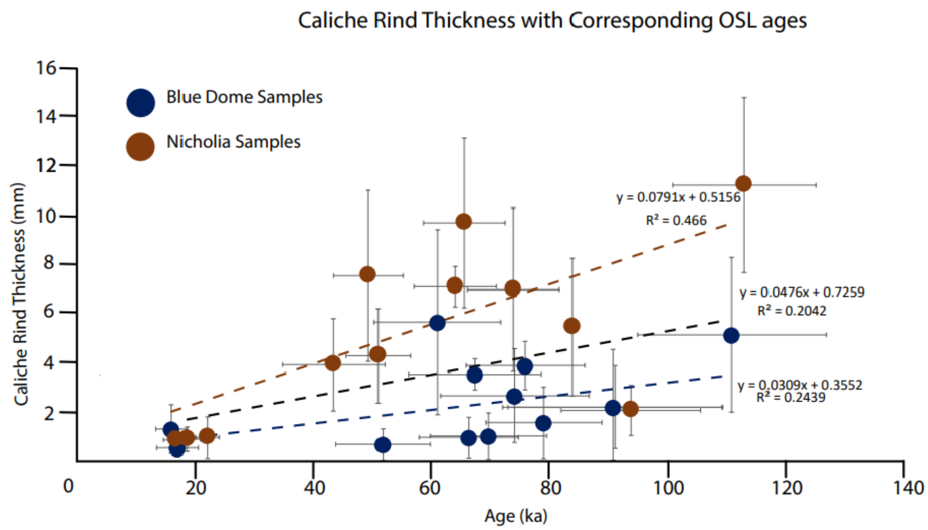

Figure 2.8: Mean pedogenic carbonate thicknesses plotted against the respective OSL age. Table 2 shows the respective graph. See Appendix C for the mean caliche calculated.

Sample Location	OSL age ± 1σ	Caliche Thickness ± 1σ
BD1	17.03 ± 3.5	0.55 ± 0.35
BD2	75.85 ± 10.03	3.90 ± 0.98
USU 3211	90.67 ± 18.63	2.21 ± 2.36
USU 3212	91.02 ± 18.09	2.21 ± 1.69
BD3	110.8 ± 15.95	5.16 ± 3.15
BD5	61.01 ± 10.72	5.67 ± 3.77
BD6	78.99 ± 9.79	1.59 ± 1.45
BD7	66.3 ± 8.42	0.98 ± 0.82
BD8	74.06 ± 12.54	2.68 ± 1.92
BD9	16.01 ± 2.63	1.32 ± 1.00
BD16	51.79 ± 7.97	0.69 ± 0.64
BD11	69.64 ± 9.88	1.04 ± 0.94
BD12	67.34 ± 11.26	3.55 ± 0.64
N1	112.9 ± 12.1	11.25 ± 3.56
N2	49.32 ± 5.86	7.56 ± 3.49
N3	22.08 ± 1.98	0.98 ± 0.84
N17	65.52 ± 6.92	9.72 ± 3.47
N7	63.99 ± 6.99	7.12 ± 0.82
N15	43.44 ± 8.65	3.94 ± 1.89
N6	16.78 ± 2.09	0.87 ± 0.44
N4	93.73 ± 11.8	2.08 ± 1.03
N8	73.84 ± 7.79	7.00 ± 3.33
N16	50.97 ± 5.43	4.30 ± 1.92
N14	18.63 ± 2.2	0.90 ± 0.50
N5	83.82 ± 8.73	5.47 ± 2.80

Table 2.3: Shows the OSL age and caliche rind thickness with 1σ standard deviation for each sam

2.4 Hypsometry of drainage basins and alluvial fan sequences

2.4.1 Hypsometry curves

Fan sequences and morphologies may be related to drainage basin characteristics. In order to investigate these relationships, we created hypsometry curves of selected canyons and compared them to fan sequences at the range front as well as to regional analyses of glacial snowline elevations. Figures 2.9 and 2.10 show selected source canyons and outlines of the alluvial fan areas for the Nicholia and Blue Dome segments respectively. These drainage basins were used for the hypsometry analysis. We primarily focused on selecting a variety of canyons and those that have alluvial fan OSL ages. Figure 2.11 shows the hypsometry plots for those canyons, in both the Blue Dome segment (in blue) and for the Nicholia segment (in orange). The tops of the Nicholia canyons start at a higher elevation (3200 m) than do the canyonsin the Blue Dome segment (Figure 2.8 and 2.9 respectively). The canyon with the lowest elevation in the Nicholia segment is Smelter Gulch (2800 m). Reconstruction of glacier equilibrium-line altitudes (ELA) during the last glaciation has been done by Locke (1990) in western Montana and was expanded into Oregon and Idaho by Meyer et al. (2004). The compiled late-Pleistocene ELA's are 2700 – 2800 m in the southern Beaverhead Mountains.

Comparing these values to those in the hypsometry curves in Figure 2.10, it is clear that the Nicholia drainages originate at higher elevations than do the Blue Dome ones. Comparing those elevations to the ELA's, it appears likely that during the last glaciation there was substantial summer snow pack in the mountains adjacent to the Nicholia segment while snowpack was likely less in the lower elevation mountains adjacent to the Blue Dome segment. This is because the canyons adjacent to the Nicholia segment extend further up into the calculated ELA zone of Locke (1990), while those adjacent to the Blue Dome segment likely did not to those high elevations where substantial snowpack was likely. It is noteworthy that Scott (1982) mapped a glacial outwash fan in the northern portion of the Nicholia segment near Smelter and Willow Creek canyons, but no glacial outwash elsewhere in the study area. There is a possibility that glaciers were present in the canyons of the Nicholia segment, but unlikely that they were adjacent to the Blue Dome segment. Whether glaciers were present or not, these results suggest that substantial snowpack was present and would generate sufficient discharge to transport gravel as suggested by Pierce and Scott (1982) and supported by Kenworthy et al. (2014).

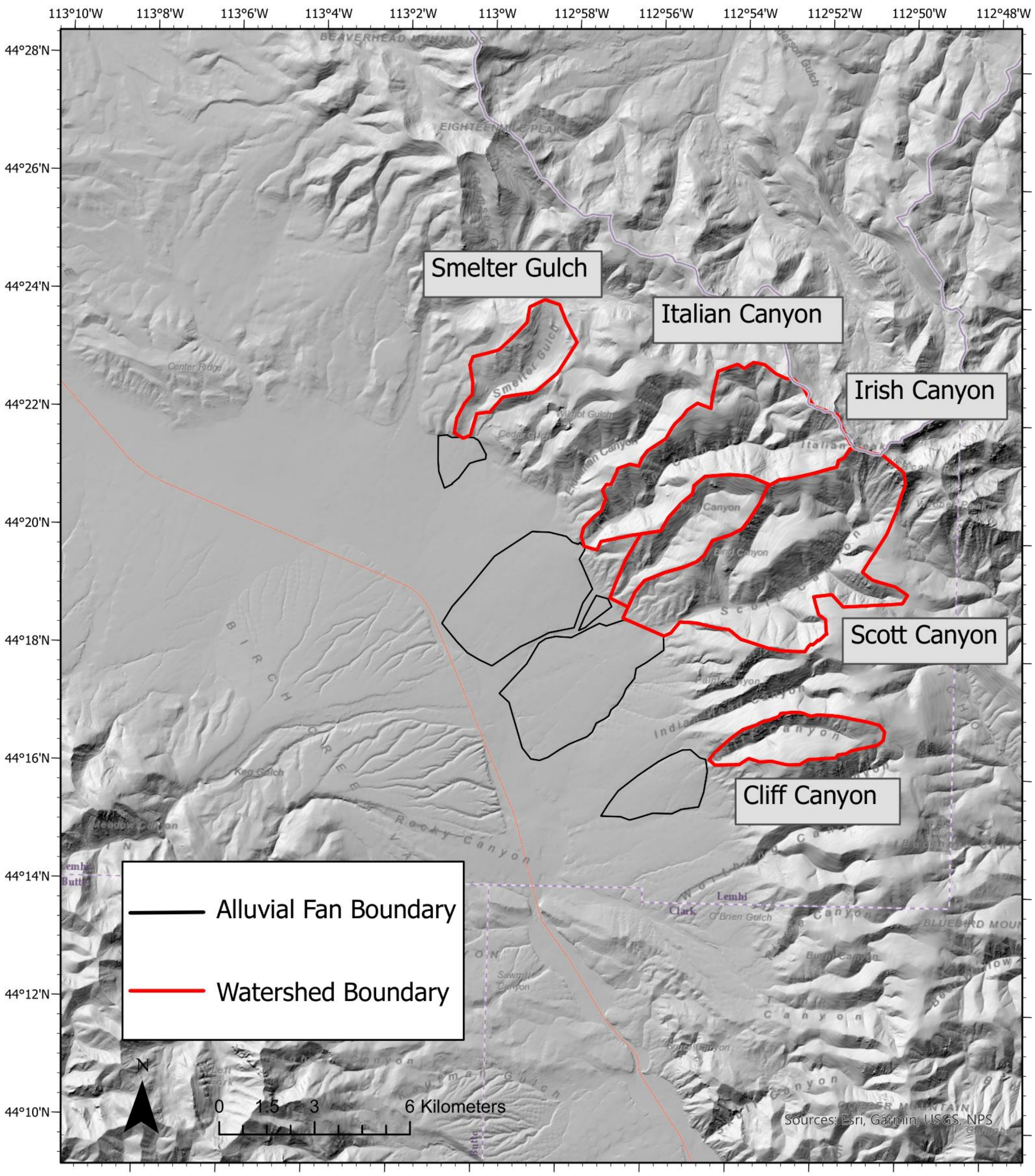

Figure 2.9: Map of the Nicholia segment showing the drainage basin (in red) for the hypsometry analysis shown in Figure 2.11. Five canyons were selected: Cliff, Scott, Irish, Italian, and Smelter canyons.

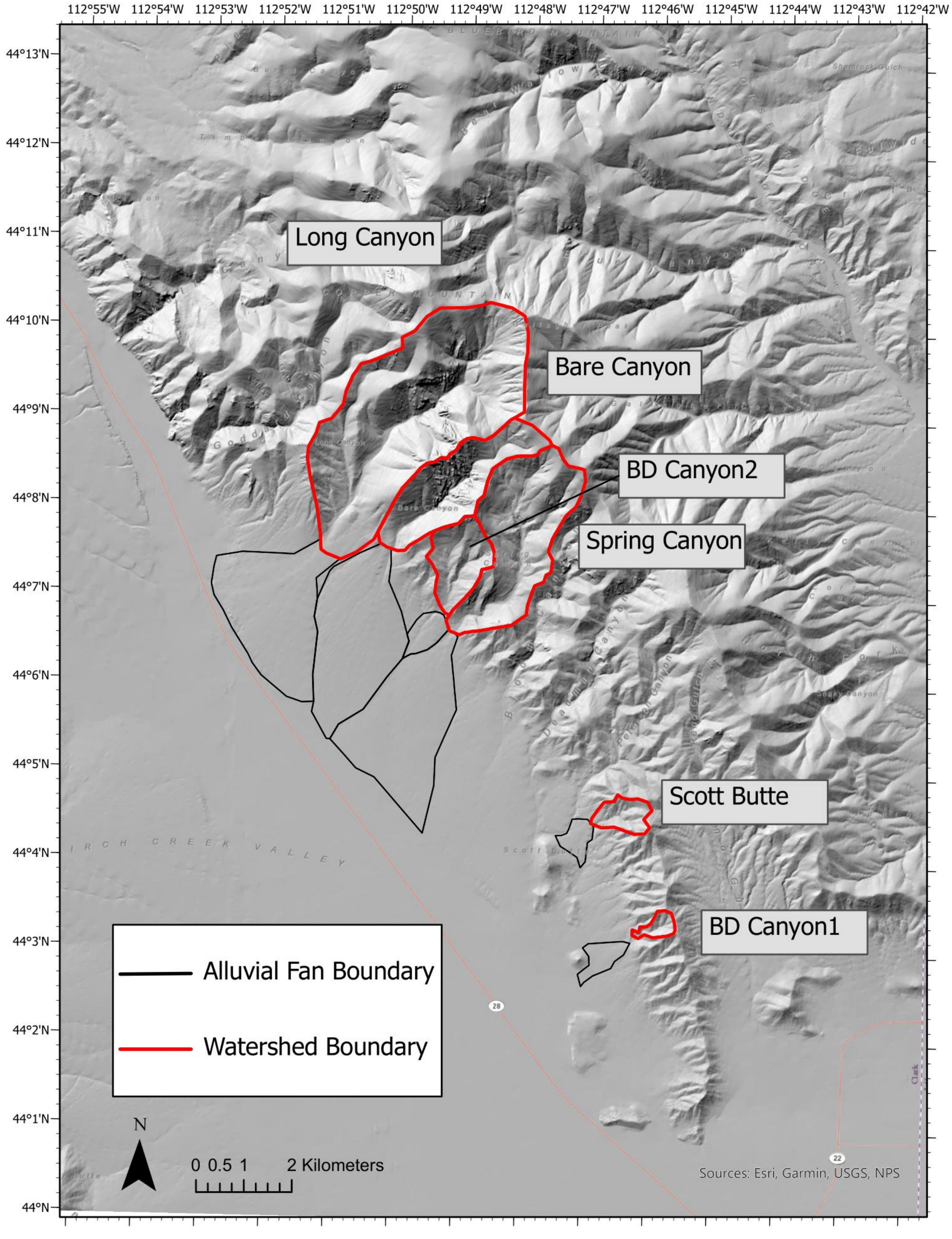

Figure 2.10: Map of the Blue Dome section highlighting the drainage basins for the hypsometry analysis shown in Figure 2.11. Six canyons were selected for this analysis, Long, Bare, Spring, and Scott Butte. Two additional canyons,BD Canyon 1 and BD Canyon 2 were also included.

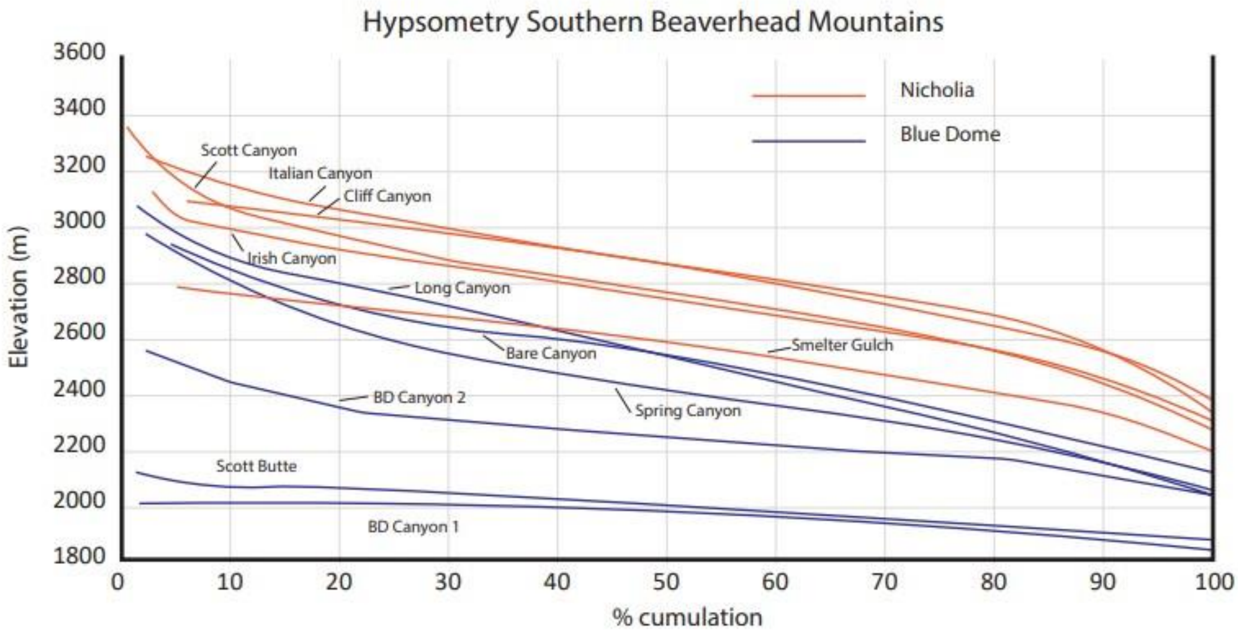

Figure 2.11: The hypsometry curves for the selected canyons shown in Figure 2 and 3. The blue curves show the selected canyons for the Blue Dome segment while the orange lines indicate the hypsometry curves for the Nicholia segment.

2.4.2 Drainage basin area vs fan area

Table 2.4 shows the alluvial fan area and the drainage basin area for each drainage and fan area adjacent to the Nicholia and Blue Dome segments (Figures 2.9, 2.10). Figure 2.12 shows the relationship between these two variables. Blue Dome canyons form two clusters: one includes BD Canyon 1, BD Canyon 2, (range front drainages) and Scott Butte Canyon while the other includes Long, Bare, and Spring canyons. The selected canyons show a slight positive correlation between drainage basin area and alluvial fan area. This would make sense that as a larger canyon would produce more sediment that would create a larger alluvial fan area.

Canyon Name	Alluvial Fan Area (km^2)	Drainage Basin Area (km^2)
Long Canyon (BD)	5.26	3.81
Bare Canyon (BD)	5.39	3.81
Spring Canyon (BD)	5.49	5.76
BD Canyon 1 (BD)	0.49	0.30
Scott Butte (BD)	0.42	0.69
BD Canyon 2 (N)	0.53	1.77
Scott Canyon (N)	12.59	29.77
Cliff Canyon (N)	4.39	6.04
Irish Canyon (N)	12.06	20.87
Italian Canyon (N)	0.44	6.83
Smelter Gulch (N)	1.59	7.90

Table 2.4: Alluvial fan area and drainage basin area for selected canyons. The annotations BD and N stand for the canyons located in the Blue Dome and Nicholia segments respectively.

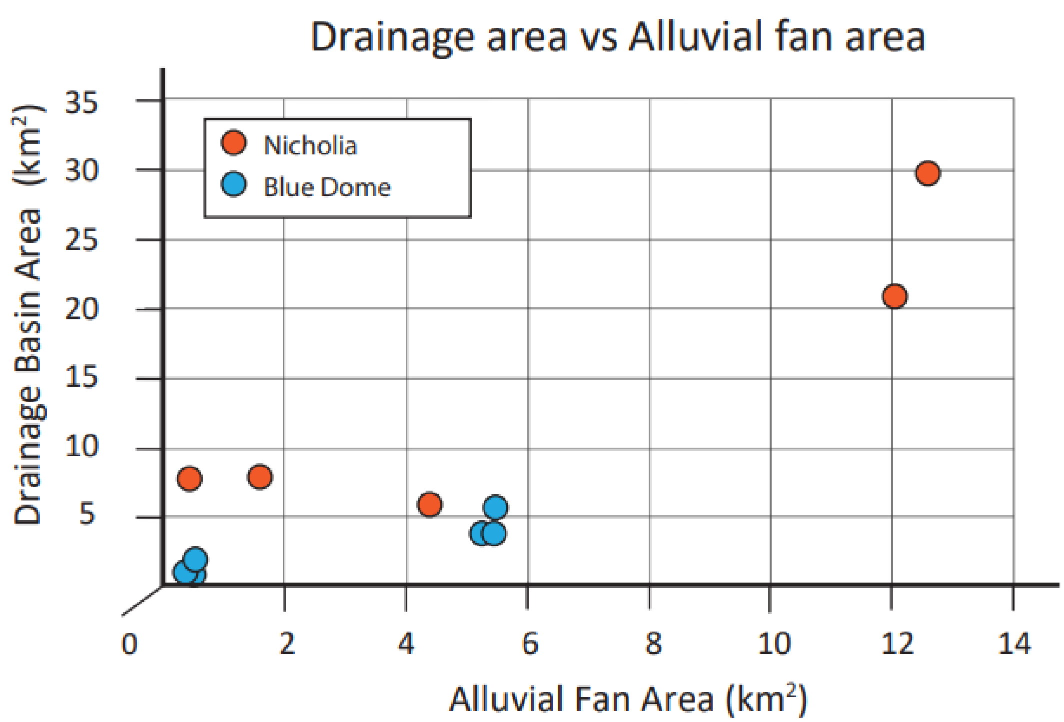

Figure 2.12: Alluvial fan areas and their respective drainages. (Data in Table 2.4)

2.5 Discussion: Alluvial fan processes and growth

2.5.1 Climatic linkages to alluvial fan growth

The main climatic drivers for alluvial fan aggradation are subject to debate. In the southwestern United States for example, there are two hypotheses for alluvial fan growth. The hypothesis supported by Bull (1991, 1977) is that alluvial fans grow during glacial cycles, particularly in transitional periods when the climate starts to warm. The glacial intervals would be characterized by higher rates of effective moisture which would increase erosion rates. An alternative hypothesis, the humid model, proposes that alluvial fans in the southern US would grow during interglacial cycles as this is when there is less vegetation density, and drier conditions would lead to increased erosion despite less precipitation (Harvey et al., 1999). Other studies have concluded that alluvial fans grow during a period of increasing precipitation. Miller et al., (2010) found that alluvial incision and deposition would increase during monsoonal seasons in the Mojave Desert and Owen et al, (2014) dated their alluvial fans to the Holocene and to marine isotope stage (MIS) 4.

In the northern Basin and Range province, where glaciers could influence alluvial fan growth, Pierce and Scott (1982) concluded that there are general climatic linkages to alluvial fan growth. They inferred from soil data that the most extensive alluvial fans are from the latest Pleistocene and coincide with the final glacial event of the last glaciation. Past studies have shown that the presence of a glacier in the drainage basin had little influence on the alluvial fan morphology (Pierce and Scott, 1982; Kenworthy et al., 2014), but that generally cooler climatic conditions during a glaciation can lead to fan growth.

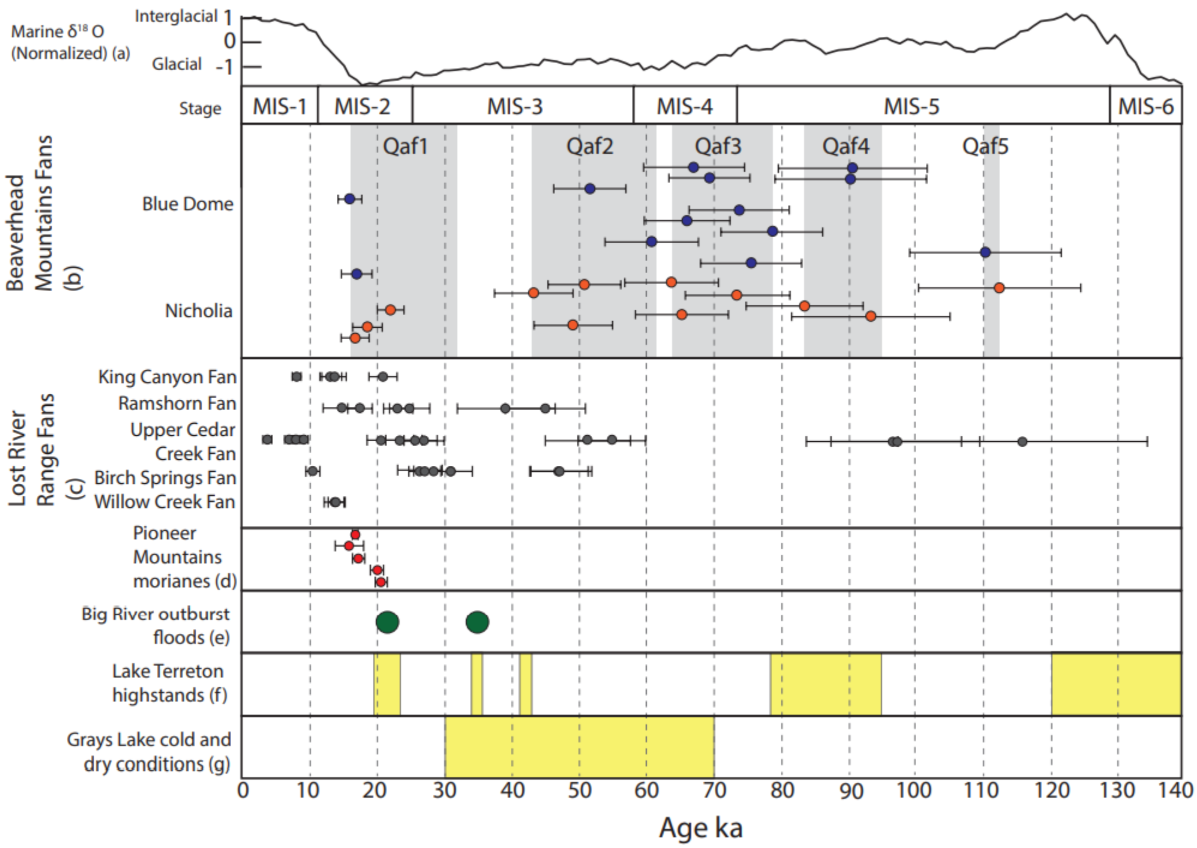

Figure 2.13: Comparison of regional climate records and other geochronological ages for the past 140 ka. A) Global normalized marine δ^{18}O from Lisiecki and Raymo (2015). B) OSL ages from this study. C) OSL samples from the central Lost River Range from Kenworthy et al. (2014). D) CRN ages from moraines from the Pioneer Mountains located in central Idaho (Warner, 2020). E) Outburst flood events estimated by Warner (2020). Two events were modeled, one at 22 ka and the other 35 ka. F) Highstands of Lake Terreton, a basin located along the SRP (Amidon et al., 2016 and Gianniny et al., 2002). G) Dry and cold conditions along Grays Lake, located along the ESRP, were estimated using pollen data shown from Grays Lake (Bieswenger, 1991).

Our OSL results and alluvial fan mapping show that fan aggradation occurred in five periods during MIS 5-2 (Figure 2.13). The Qaf1 fans were deposited in the late Pleistocene (16 – 23 ka) which correlates to MIS 2. During this time there have been apparent maximumglacial extents along the Wind River Range and elsewhere (Licciardi et al., 2004; Laabs et al., 2020), and presumably colder conditions than current Holocene conditions. A summary of OSL ages and other regional paleoclimatic proxies are shown in Figure 2.13.

Ages for Qaf2 (ca. 35 - 55 ka) and Qaf3 fans (60 – 80 ka) fall within MIS-3 and MIS-4 (Table 2.2:Figure 2.13). Qaf4 fan ages range from 80 – 90 while the Qaf5 fan ages ranged from 90 - 110 ka (MIS-5). None of the alluvial fan ages that were sampled dated to Bull Lake glaciation as typically interpreted (MIS-6, ca. 130- 180 ka). This does not mean that there were no alluvial fans formed during that period but rather that any evidence would have been buried by fan aggradation during MIS 5-2. The Qaf2-Qaf5 aggradation periods were not discerned by Pierce and Scott (1982), but are suggestive of cool and/or wet conditions as well. Kenworthy et al. (2014) found similar results regarding the development of alluvial fans in the Lost River Range. Most of their ages are late Pleistocene in age while there are a few in Holocene. The Holocene alluvial fans are much smaller and have finer sediment than their late Pleistocene counterparts. One difference in their results versus this study is that ours is that more of their fan ages are clustered to 15 – 30 ka while ours are from 15-22 ka and 45 – 80 ka. Kenworthy et al. (2014) lack OSL ages from 60 – 90 ka while our OSL samples contain several ages within that time period. This could indicate that even though the Lost River Range and the Beaverhead Mountains would be subjected to broadly similar climatic changes, there may be climatic differences between the two so that they would result in differences of alluvial fan ages.

Overall, Kenworthy et al. (2014) concluded that their alluvial fans are the result of cooler late-Pleistocene climates during apparent glacial intervals (Figure 2.13). This also supports the hypothesis of Pierce and Scott (1982) which says that the lower temperatures during the Pleistocene would lead to a lower evaporation rate and greater snowfall rate, thus leaving alarger snowpack. An increase of effective moisture during cold times would also increase stream input during the late summer. This increased stream flow during the late summer would then drive alluvial fan aggradation. Most of the canyons in our study area were unglaciated (Scott, 1982) or possibly glaciated (see hypsometry-snowline analysis above) and in either case would have generated greater summer snowmelt.

Regional alluvial fan, lake, and glacial studies support a cooler and/or wetter environment in the region during the late (and middle) Pleistocene. For example, Gianniny et al. (2002) dated high stands of Pleistocene Lake Terreton, immediately south of this study area, at 78 – 95 and 120 – 160 ka . The latter highstand correlates broadly with our alluvial fan ages for Qaf4 and Qaf5 and Amidon et al. (2016) estimated major high stands of the Terreton Basin at 42, 35, and 22 ka where the 22 ka highstand correlates to Qaf1 and 42 ka could correlate to the Qaf2 fans (Figure 2.13). Cool, dry conditions 70 – 30 ka were suggested from pollen data at Grays Lake, south of the ESRP, by Beiswenger (1991). Beiswenger (1991) also suggests that between 30 – 11 ka there were wet and warmer conditions for the region. Along the eastern central Lemhi Range, a 44 ka CRN age on moraine boulders could indicate the existence of glaciers and associated cool/wet climatic conditions (Colandrea, 2014; G. Thackray personal communication, 2021). Along the central Lost River Range, OSL and CRN ages on terraces and moraines range from 35 – 60 ka. In the Pioneer Mountains in central Idaho, Warner (2020) estimated that the Big Lost River outburst flood occurred at around 36 ka along with moraines dated between 16 – 22 ka (Figure 2.13). In conclusion, our OSL ages for the alluvial fans support Scott and Pierce (1982) model that alluvial fans in the northern Basin and Range record late

Pleistocene climate variation, such that fan formation occurred in association with cooler climates during glacial intervals. The cooler temperatures would allow for a snow pack to reside longer throughout the year and increase discharge from snowmelt in the late summer. Coarse-grained alluvial fans in particular were deposited during the late Pleistocene because frost wedging would create coarse sediments along the hillslopes that would then be transported by snowmelt streams and deposited in alluvial fans (Pierce and Scott, 1982).

2.5.2 Distribution of Fan Units between Nicholia and Blue Dome segments

All mapped alluvial fan units are present in the two segments, but Qaf2 fan units are more common along the Nicholia segment than in the Blue Dome segment. There are two plausible factors as to why that could be the case. Tectonically, the Nicholia segment has experienced faulting within the past 80 ka as this study (Chapter 3) and previous studies have shown (Haller, 1988). Our Qaf2 fan ages range from 43 – 61 ka, with the most recent surface fault scarp postdating those fans. Because normal fault rupture separates uplifted and down-dropped blocks, it may affect incision and aggradation and thus the presence or absence of fan surfaces of particular ages. If the primary driver of fan growth is climatic, then it is likely that Qaf2 fans were constructed at the canyon mouths in both segments. However, the lack of faulting in the Blue Dome segment may have allowed Qaf1 aggradation to bury Qaf2 surfaces in most areas, while in the Nicholia segment, fault offset could influence incision into the Qaf2 fan and isolate those surfaces more consistently above the Qaf1 aggradation level. Past studies such as Kenworthy (2011) and Owen et al. (2014) have suggested that tectonic influences aren’t the driving factors of alluvial fan growth in their study areas, but it is plausible that the timing of fault rupture events has affected the distribution of alluvial fans in space and time in east-central Idaho.

Another possibility is that relief contrasts, coupled with climatic conditions 41 – 61 ka produced Qaf2 alluvial fans in the Nicholia segment more readily than in the Blue Dome segment. As discussed in a previous section, the estimated glacial ELA's of the southern Beaverhead Mountains are 2700 – 2800 m (Locke, 1990). Our hypsometry curves indicate that the Nicholia segment has canyons with the ridge elevations ca. 3200 m to 2800 m. The Blue Dome segment has canyons ridge elevations 3000 m to 2000 m. While both of the segments have canyons that include the ELA's for the area, the canyons in the Blue Dome segment generally have lower elevations than those in the Nicholia segment. The lower elevation in the Blue Dome segment could contribute to lesser snowpack during the accumulation period of Qaf2 fans, but because the Nicholia elevations are higher, they would a snowpack to accumulate which would allow for the deposition of the Qaf2 fans. As proposed by Pierce and Scott (1982), persistent snowpack is likely an important influence on gravel transport and fan aggradation.

2.5.3 Conclusions

In conclusion, this research demonstrates that OSL ages in the study area correlate to geomorphic position, i.e., higher relative fan position correlates with older OSL age. The caliche data suggests that pedogenic rind thickness weakly correlates to OSL age. The overall calculated accumulation rate for our data is 0.48 mm per 10 ka while fans adjacent to the Nicholia segment had a higher accumulation (0.79 mm per 10 ka) than fans adjacent to the Blue Dome segment (0.31 mm per 10 ka). The differences in accumulation rates may be attributed to climatic differences between the them. Hypsometry curves show that most of the Nicholia canyons most likely had strong snowpack influences in the canyons, but canyons adjacent to the Blue Dome segment had weaker snowpack influences. Comparing basin vs alluvial fan areas, there is a weak positive correlation adjacent to the Nicholia segment. OSL ages correlate to periods during which regional late Pleistocene climate was probably cooler and included glacial intervals (Pierce and Scott, 1982). Cooler late Pleistocene climates would correlate to a prolonged snowpack and increased discharge during the late summer. Frost wedging and erosion would help generate sediment supply for these alluvial fans.

2.5.4 Future work

This chapter presents OSL ages from the southern Beaverhead Mountains that are generally consistent with Kenworthy's (2011) findings in the Lost River Range. Future work could include collecting OSL ages from the southern portion of the Lemhi Range and central portions of the Beaverhead Mountains. The central portion of the Beaverhead Mountains have glaciated valleys (Scott, 1982) and we could compare those OSL ages to those along the southern portion of the Beaverhead Mountains. We can hope to find an elusive 30 - 45 ka age on an alluvial fan that was not present with this thesis but was found in Kenworthy's (2011) study. Along the northern Lemhi fault, the Warm Creek segment, alluvial ages have been estimated to be 30 – 80 ka using soils and geomorphic position (Baltzer, 1990). We could test this age estimate with OSL dating on the geomorphic deposits. Having OSL ages along the northern portions of the faults would determine whether alluvial fan growth differs from wetter northern portions of the fault segment versus those in the southern segments where it is more arid.

References:

Amidon, W.H., Steele, J., Hollyday, A., and Gilbert, H., 2016, A 40 Kyr lacustrine record from the Terreton Basin, Idaho: Floods, climate change, or both?: Geological Society of America Abstracts with Programs, Vol. 48, No. 7.

Baltzer, E.M., 1990, Quaternary surface displacement and segmentation of the northern Lemhi fault, Idaho: Binghamton, State University of New York, unpublished M.S. thesis, 88 p.,2 pl., scale 1:62,500.

Beiswenger, J.M., 1991, Late Quaternary Vegetational History of Grays Lake, Idaho: Ecological Monographs v. 61, p. 165-182.

Birkeland, P. W. 1999, Soils and Geomorphology: New York, Oxford University Press, 430 p.

Bull, W.B., 1977. The alluvial-fan environment. Progress in Physical Geography 1, p. 220- 270. Bull, W.B., 1991. Geomorphic responses to climatic change. Oxford University Press, New York. 326 p.

Colandrea, H. A., 2016, Spatial and temporal patterns of late Pleistocene glaciation in the Lemhi Range, east-central Idaho [M.S. Thesis]: Pocatello, Idaho State University, 203 p.

Galbraith, R.F., Roberts, R.G., 2012. Statistical aspects of equivalent dose and error calculation and display in OSL dating: An Overview and some recommendations. Quaternary Geochronology, v. 11, p. 1-27.

Gianniny, G.L., Thackray, G.D., Kaufman, D.S., Forman, S.L., Sherbondy, M.J., and Findeisen, D. 2002. Late Quaternary highstands in the Mud Lake and Big Lost Trough subbasins of Lake Terreton, Idaho: Geological Society of America Special Paper v. 353 , p. 77-90.

Haller, K.M., 1988, Segmentation of the Lemhi and Beaverhead faults, east-central Idaho, andRed Rock fault, southwest Montana, during the late Quaternary [M.S. thesis]: Boulder, University of Colorado, 141 p.

Harvey, A.M., Wigand, P.E.,Wells, S.G., 1999. Response of alluvial fan systems to the late Pleistocene to Holocene climatic transition: contrasts between the margins of pluvial Lakes Lahontan and Mojave, Nevada and California, USA. CATENA, 36, p. 255–281.

Kenworthy, M.K., Rittenour, T.M., Pierce, J.L., Sutfin, N.A., and Sharp, W.D., 2014. Luminescence dating without sand lenses: An application of OSL to coarse-grained alluvial fan deposits of the Lost River Range, Idaho, USA: Quaternary Geochronology, v 23, p. 9-25.

Kenworthy, M.K., 2011, Optically stimulated luminescence dating of gravelly alluvial fan deposits: Links between climate and geomorphic response in the Lost River Range, Idaho[M.S. thesis]: Boise, Boise State University, 171 p.

Miller, D.M., Schmidt, K.M., Maham, S.A., McGeehin, J.P., Owen, L.A., Barron, J.A., Lehmkuhl, F., and Löhrer, R., 2010, Holocene landscape response to seasonality ofstorms in the Mojave Desert: Quaternary International, v. 215, p. 45-61.

Owen, L.A., Clemmens, S.J., Finkel, R.C., and Gray, H., 2014, Late Quaternary alluvial fans at the eastern end of the San Bernardino Mountains, Southern California: Quaternary Science Reviews, v. 87, p. 114-134.

Laabs B. J.C., Licciardi, J.M., Leonard, E.M, Munroe, J.S., and Marchetti, D.W., 2020, Updated cosmogenic chronologies of Pleistocene mountain glaciation in the western United States and associated paleoclimate inferences: Quaternary Science Reviews, v. 242, p. 1 – 36.

Lisiecki, L. E. and Raymo, M. E., 2005, A Pliocene-Pleistocene stack of 57 globally distributed benthic δ18O records, Paleoceanography, v. 20, p. 1 – 17.

Locke, W.W., 1990, Late Pleistocene glaciers and climate of western Montana, U.S.A. Arctic and Alpine Research, v. 22, p. 1-13.

Meyer, G.A., Fawcett, P.F., and Locke, W.W. 2004. Late-Pleistocene equilibrium-line altitudes, atmospheric circulation, and timing of mountain glacier advances in the interior northwestern United States, in Haller, K., and Wood, S.H., eds., Geological Field Trips in Southern Idaho, Eastern Oregon, and Northern Nevada. Geological Society of America Field Guide, p. 61-66.

Murray, A.S., Wintle, A.G., 2000. Luminescence dating of quartz using an improved single aliquot regenerative-dose protocol. Radiation Measurements, v. 32, p. 57-73.

Pierce, K.L. and Scott, W.E., 1982, Pleistocene episodes of alluvial-gravel deposition, southeastern Idaho in Bonnichsen, B., Breckenridge, R.M., eds., Cenozoic Geology of Idaho: Idaho Bureau of Mines and Geology Bulletin 26, p. 685-702.

Pierce, K. L., 1985, Quaternary History of Faulting on the Arco Segment of the Lost River Fault, Central Idaho, in Bonnichesen, B., and Breckenridge, R.M., eds., Proceedings of Workshop XXVII on the Borah Peak, Idaho Earthquake, U.S.G.S Open-File Report 85 - 290, p. 195 -206.

Skipp, Betty, 1985, Contraction and extension faults in the southern Beaverhead Mountains, Idaho and Montana: U.S. Geological Survey Open-File Report 85-545, scale 1:250,000.

Warner, B. M., 2020, Surficial geologic mapping and cosmogenic chronology of Pioneer Mountains glaciation and the Big Lost River floods, Pioneer Mountains and eastern Snake River Plain, Idaho [M.S. thesis]: Pocatello, Idaho State University, 124 p.

Chapter lll: Patterns and Chronology of Faulting along the Southern Beaverhead Fault

3.0 Fault scarp mapping and analysis

This chapter will discuss the faulting patterns of the Nicholia and Blue Dome segments. The observations from Chapter 2 allow us to describe the morphology of the fault scarps and bracket rupture event timing by comparing them with the OSL depositional ages. The main previous study by Haller (1988) documented fault scarps along the Nicholia segment, but found none within the Blue Dome segment.

3.1 Fault segment analysis: Nicholia segment

3.1.1 LiDAR Mapping and analysis, Nicholia segment

The Nicholia segment of the Beaverhead fault is well expressed by surface scarps which are present along most of the segment, from Pierce Canyon north to Willow Creek canyon (Figure 3.1). Overall, the Nicholia segment strikes ca. N 40° W. Fault scarps overall are discontinuous along the range front and typically appear to reflect a single-strand fault. Antithetic scarps were observed along portions of the fault cutting fans at the mouths of Cliff Canyon, Scott Canyon, and Willow Creek Canyon. Scarps vary in length but are typically 2 – 5 km. Scarp height varies from 1-5 m.

Fault scarps were observed in lidar imagery along 28 km of the Nicholia segment, from Pierce Canyon NW to Willow Creek. Haller (1988) also included a 13 km northern extension of the Nicholia segment from Willow Creek NNW to near Gilmore Summit (shown as dashed line in Figure 3.2). Lidar data coverage extended NW only to Willow Creek, and we examined that extended section only in field reconnaissance and on 10 m DEMs, and did not observe fault scarps. The fault may be buried in that area. If that extension to Gilmore Summit were included, the Nicholia segment would be 41 km in length, but we lack clear evidence to confirm that extended length.

The fault scarp pattern displays two prominent steps or bends. The fault at Willow Creek steps 2 km to the left and at Scott Canyon steps 1 km to the right. Synthetic and antithetic fault scarps cut Qaf2 – Qaf5 fans at Cliff Canyon, Willow Creek Canyon, and Scott Canyon. Nowhere do scarps cut Qaf1 fan units, an observation that Haller (1989) also made. This is in contrast to the mapped fault in the USGS Fold and Fault Database (Haller et al. 2010), which is depicted as continuous (Figure 3.2).

The 28 km confirmed length of the Nicholia segment in this fault scarp analysis lies between Haller's (1988) proposed length of 42 km and USGS Fold and Fault Database's (Haller et al. 2010) mapped length of 25 km. The USGS depiction of the fault includes the main portion of the fault trace with visible fault scarps, but omits the northern portion of the segment extended by Haller (1988), shown by the dashed line in Figure 3.2, as we do here.. By doing the fault mapping in 0.5 m resolution LiDAR we can observe the fault only in the 28 km fault length northwest to its termination near Willow Creek.

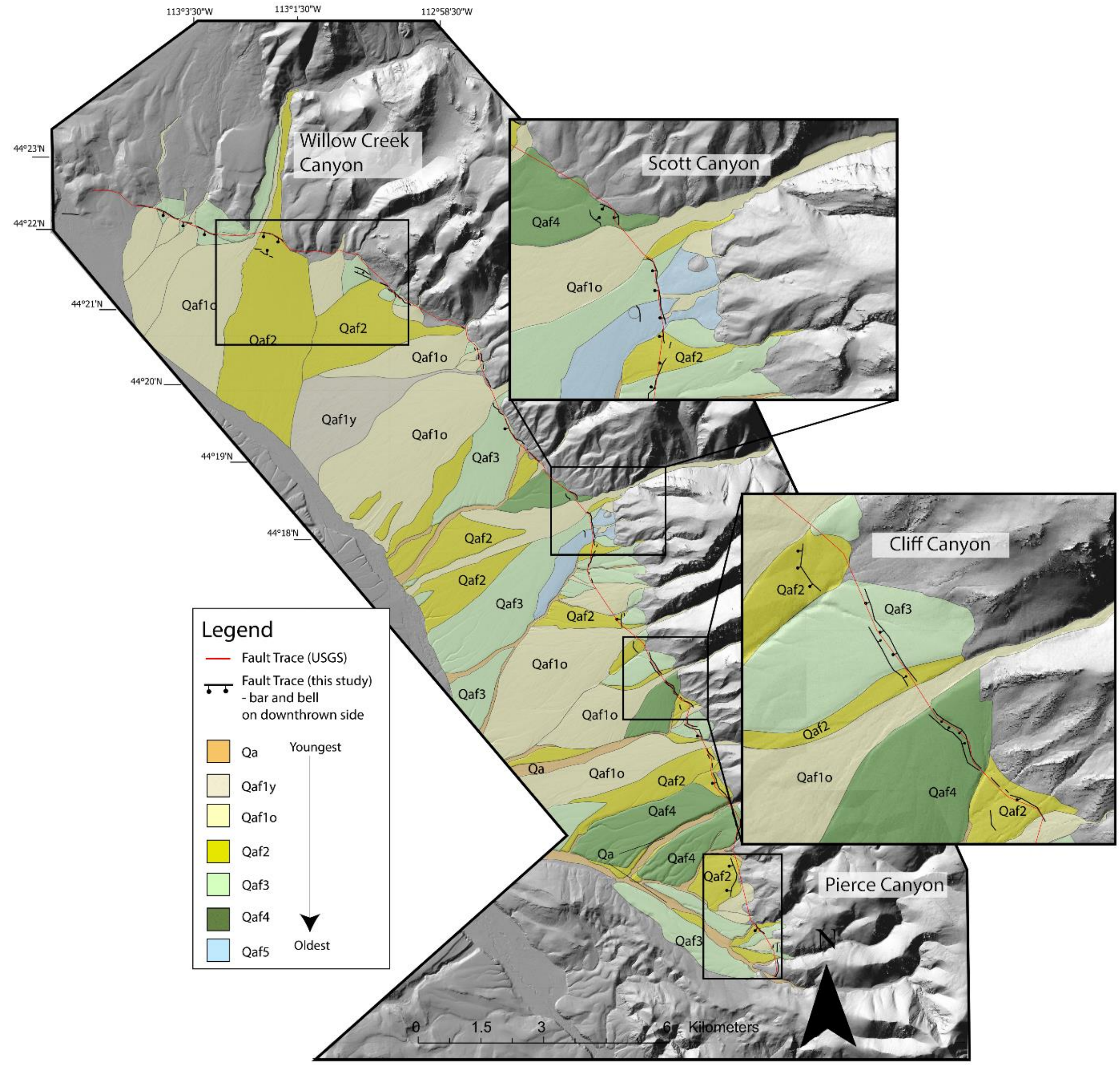

Figure 3.1: Fault trace of the Nicholia segment. Black lines show the fault scarp trace determined in this project while the red line is from the current Nicholia segment mapped by the U.S Geological Survey (2019). Boxed areas show where the fault does not cut through Qaf1 fans.

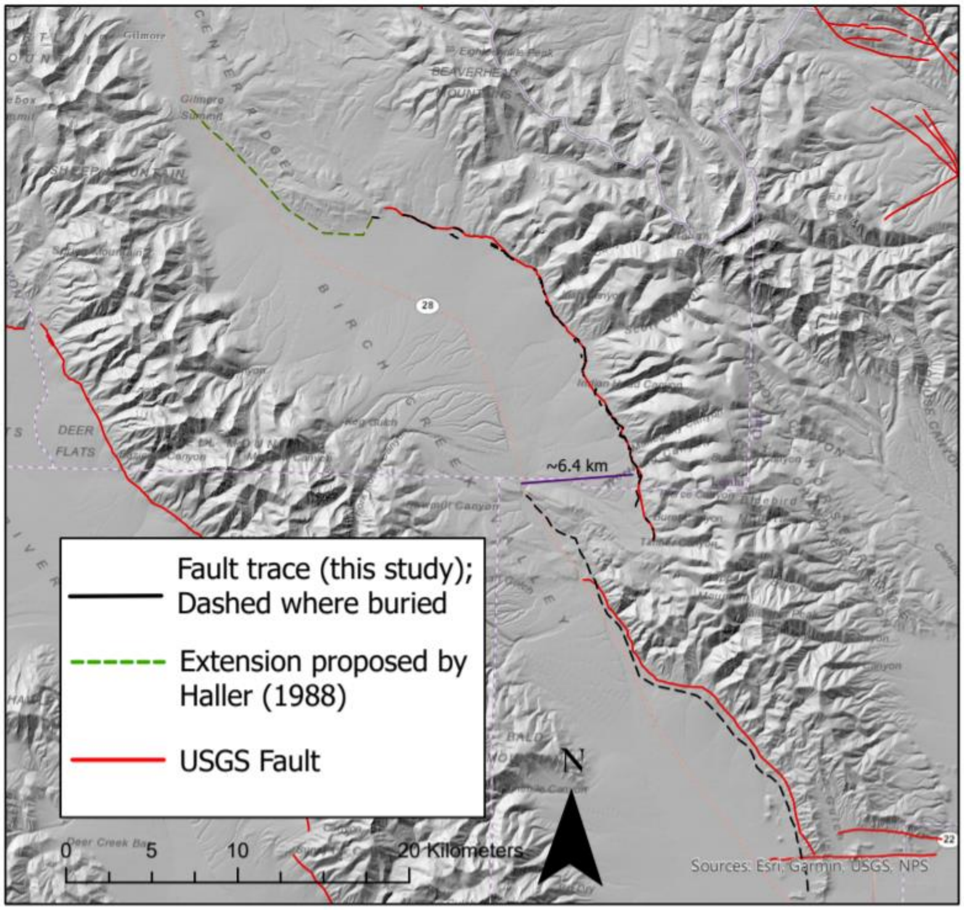

Figure 3.2: Red line shows the USGS Quaternary fault shape file and black is the proposed fault segment. Dashed line iswhere the fault is buried. Green line is the extension of the northern Nicholia segment boundary proposed by Haller (1988). Black boxes show the location of 'kink' along the fault segments for the Blue Dome and Nicholia segments

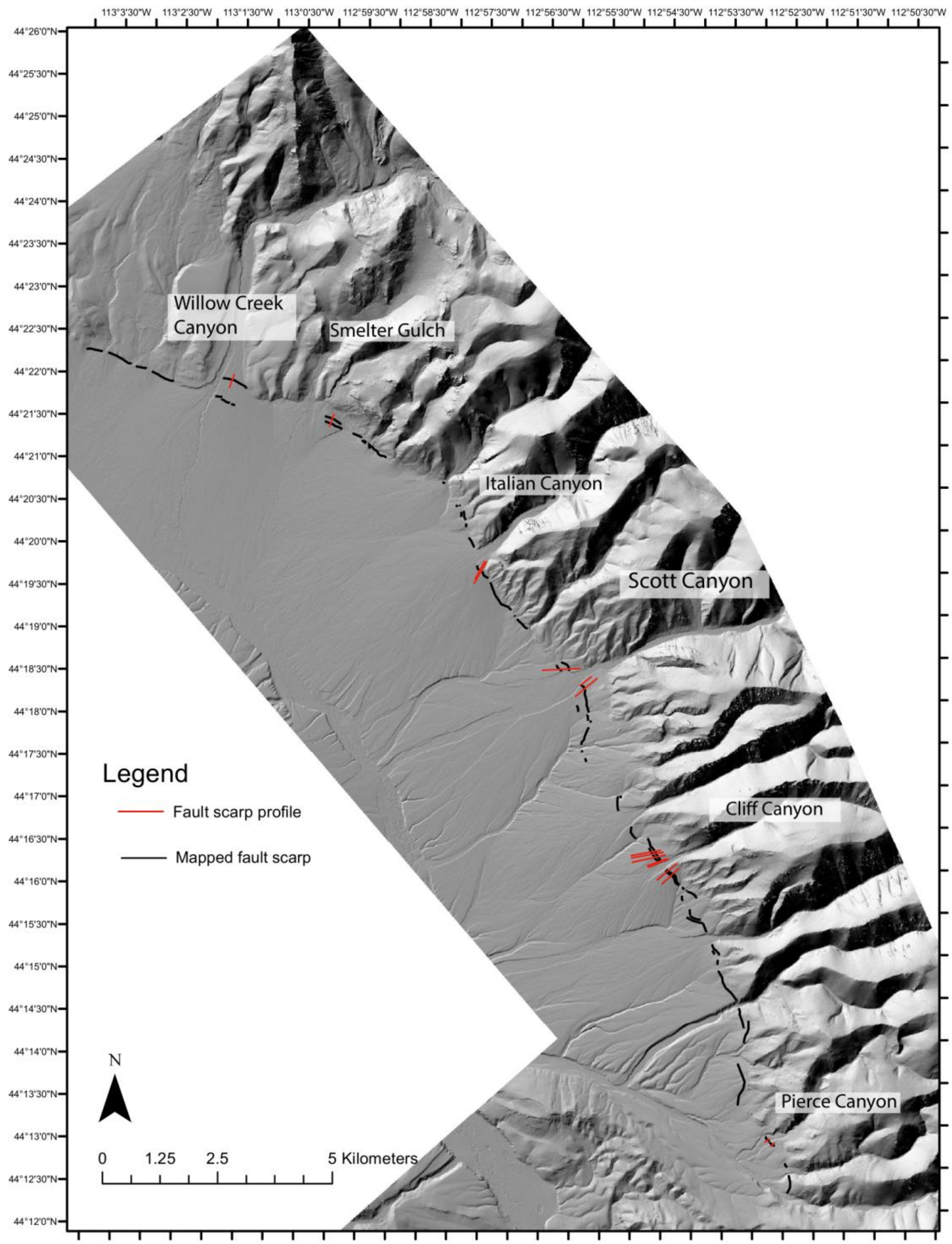

Figure 3.3: Red lines indicate fault scarp profiles taken along the Nicholia segment.

A.

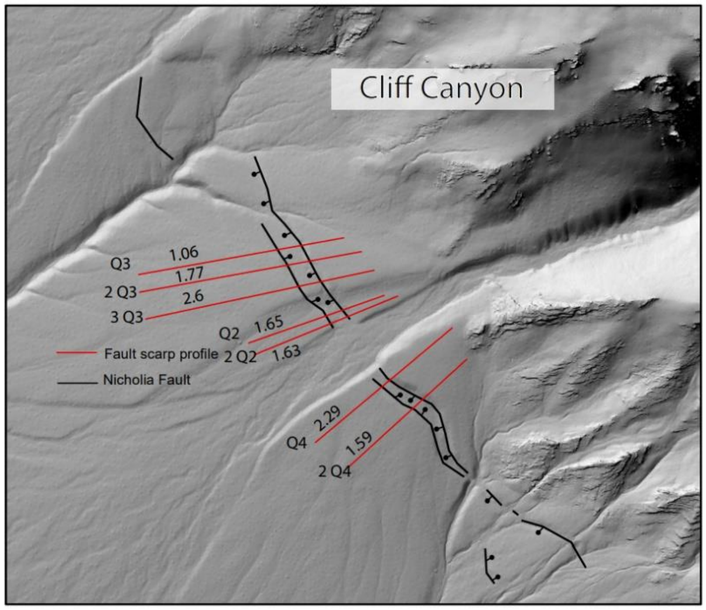

B.

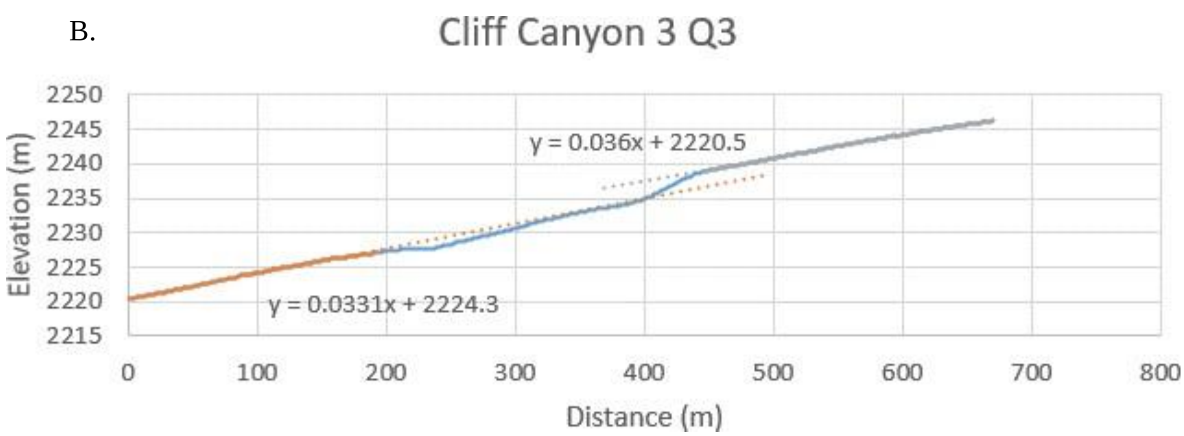

Figure 3.4: A: Location of the fault scarp profiles along Cliff Canyon in the Nicholia segment. B: Fault scarp profile of Cliff Canyon 3 Q3 showing vertical separation determination of the fault scarp cutting a Qaf3 alluvial fan. The slope of the hanging wall and footwall were calculated, then the VS was found by measuringthe vertical distance between the profiles at a point halfway up the main, synthetic scarp (i.e., at ca. 415 m distance).

3.1.2 Fault scarp offset vs alluvial fan age

Figure 3.3 shows the location of the 16 topographic profiles drawn across fault scarps in the Nicholia segment. These profiles were used to calculate the vertical separation of the fault scarp for each alluvial fan cut by a fault scarp (Qaf2 – Qaf5). Fault scarp profiles and offsets were calculated using the methods describe in Chapter I under Methods 2.0 (as described by Amos et al., 2016; Thompson et al., 2002). Fan unit designations for alluvial fans in the northern section of the Nicholia segment, such as at Willow Creek and Smelter Gulch, were based on geomorphic correlation to the OSL-dated fans at Cliff and Scott canyons.

As shown in Table 3.1, vertical separation measured along Nicholia segment fault scarps ranges from 1.3 to 4.1 m. There is a general relationship between alluvial fan unit age and fault scarp vertical separation (VS). In particular, the majority of the VS measurements on Qaf3 fans are greater than those on Qaf2 fans, but there is some overlap. Additionally, VS measurements of scarps cutting Qaf4 fans are well within the range of VS measurements from Qaf3 fans. These relationships suggest that the penultimate rupture event happened between construction of the Qaf2 and Qaf3 fans. At Cliff Canyon, average VS increases slightly with alluvial fan age (Figure 3.4; Table 3.1).

The variation in VS could be attributed to two factors. First, the generally greater VS of scarps cutting older fans suggests that multiple slip events have occurred along the same scarps, such that scarps cutting older fans (Qaf3 and Qaf4) record two or more events while the scarps cutting younger fans (especially Qaf2) may record just a single event. Second, the observation that VS is greater in the center of the segment (Italian Canyon where Vs= 4.1 and 3.3m for Qaf3 fans) than closer to the south end at Cliff Canyon (VS= 2.2, 1.8, and 2.6 m for Qaf3 fans) may indicate higher displacement in the middle portion of the segment rather than the ends, for the same number of slip events. This characteristic of fault segments has been documented elsewhere by Haller (1998) and Crone and Haller (1991).

Canyon	Fan Unit	VS (m)	Hanging Wall Surface Slope	Footwall Surface Slope	Slope contrast
Cliff	Q2	1.7	0.039	0.046	-0.007
Cliff	2 Q2	1.0	0.037	0.036	0.001
Scott	Q2	1.3	0.529	0.036	0.493
Pierce	Q2	1.6	0.102	0.081	0.021
Willow Creek	Q2	1.8	0.019	0.025	-0.006
Italian	Q3	4.1	0.024	0.026	-0.002
Italian	2 Q3	3.3	0.015	0.014	0.001
Scott	Q3	1.5	0.019	0.018	0.001
Scott	2 Q3	3.2	0.018	0.025	-0.007
Pierce	Q3	2.4	0.103	0.126	-0.023
Smelter Gulch	Q3	1.2	0.046	0.047	-0.001
Cliff	Q3	2.2	0.070	0.073	-0.003
Cliff	2Q3	1.8	0.075	0.071	0.004
Cliff	3 Q3	2.6	0.036	0.033	0.003
Cliff	Q4	2.6	0.080	0.099	-0.019
Cliff	2 Q4	1.6	0.086	0.094	-0.008

Table 3.1: The associated VS measurements and their respective canyons and fan units.

3.2 Fault segment analysis: Blue Dome segment

3.2.1 Blue Dome segment analysis

In contrast to the Nicholia fault segment, the Blue Dome segment is not defined by scarps cutting alluvial fan surfaces. Our LiDAR analysis confirms the lack of a fault scarp on the surface. Instead, the fault is inferred to exist at depth based on range front morphology (Haller, 1988), buried beneath alluvial fans, and following the range front over a length of ca. 30 km from the Blue Dome bedrock spur in the north to the Snake River Plain, where the bedrock tapers to merge with the land surface.

At the northern end of the Blue Dome segment, the Blue Dome spur projects northwestward into Birch Creek Valley, creating a major right step between the Blue Dome and Nicholia segments. The spur consists of late Miocene bedrock cut by three NW-striking fault splays (Rodgers and Anders; 1990). Slip on these splays occurred at some time after 6.5 Ma, the minimum age of bedrock in the spur.

At the south end of the Blue Dome segment near the ESRP, two south-dipping normal faults were mapped by Witkind (1975). These faults are depicted cutting through the bedrock along the low ridge of the southernmost portion of the Beaverhead Mountains. However, Breckenridge et al. (2003) did not include these faults in their compilation, and LiDAR analysis for this study revealed no surface evidence of faulting.

3.2.2 Blue Dome segment fault scarp analysis

In contrast to the Nicholia segment, no fault scarp has been observed to define the Blue Dome segment (Haller, 1988). To further investigate the presence or absence of fault scarps in the Blue Dome segment, we carefully analyzed alluvial fanslopes using high resolution LiDAR data, augmented with field observations. We also flew two drones (Trinity F90 and Phantom Pro V4) (Figure 3.5) in the northern section of the Blue Dome segment and created orthomosaic imagery and digital elevation models (DEM) using structure for motion (SfM) analysis. More details on the specific flight paths are found in Chapter 1. Detailed processing and errors of the SfM DEM are in Appendix D.

3.2.3 Structure from motion analysis and field observations: Blue Dome segment

Figure 5 shows the drone images (Figure 3.5a) and the hillshade (Figure 3.5b) created for Long Canyon and Bare Canyon in the Blue Dome segment, using structure from motion (SfM) analysis through Agisoft Metashape v 1.7 software and ArcGIS Pro v 2.8. The SfM images show that sagebrush is spaced evenly in the region with no linear clustering on any of the alluvial fans in the area, as would be expected if water collected in scarp-related depressions or if water were emitted from the fault zone. This was also confirmed by field study: there was no linear slope break observed along the alluvial fans. Because of these observations, we conclude that there is no discernible fault scarp associated with the Blue Dome segment.

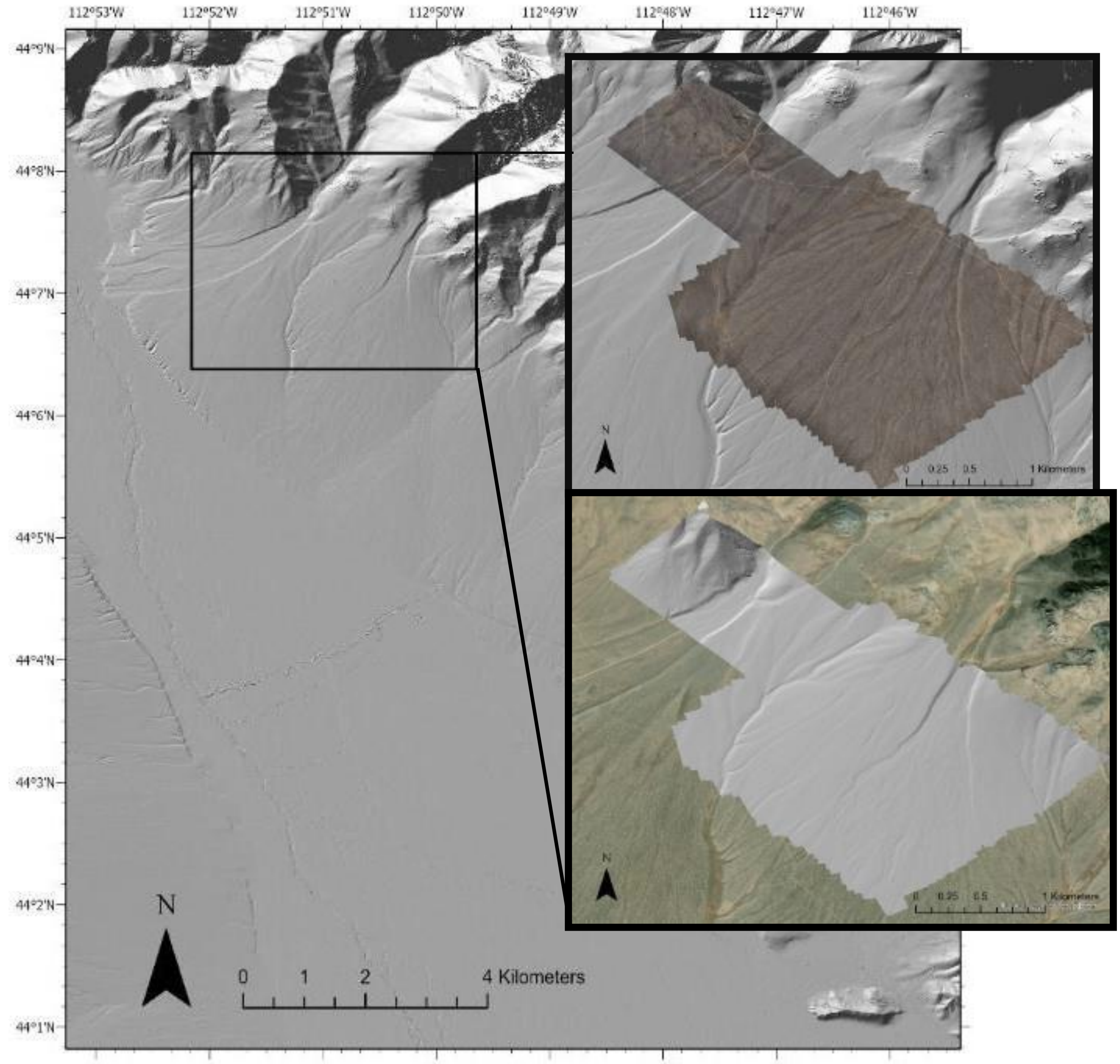

Figure 3.5: Black box shows the location for the Blue Dome study area where drones (Trinity F90 and Phantom V4 were flown) The orthomosaic is shown in A, and the hillshade model from the DEM derivedby the SfM is shown in B.

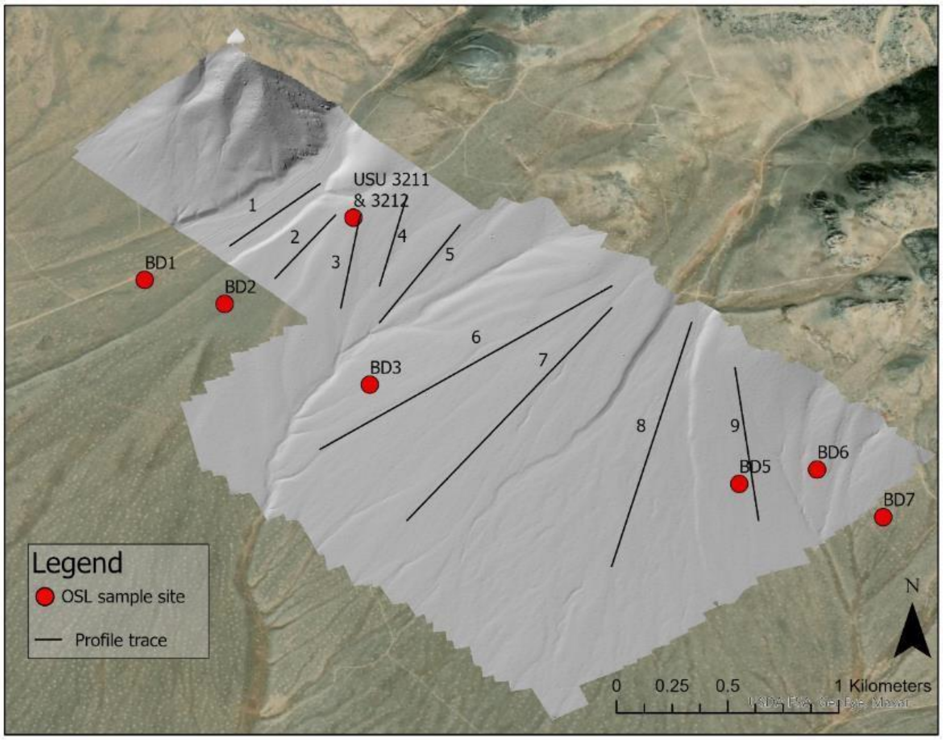

Profile 4

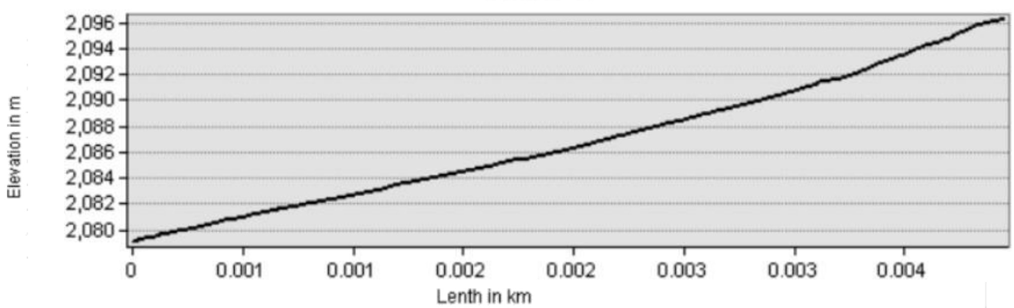

Profile 6

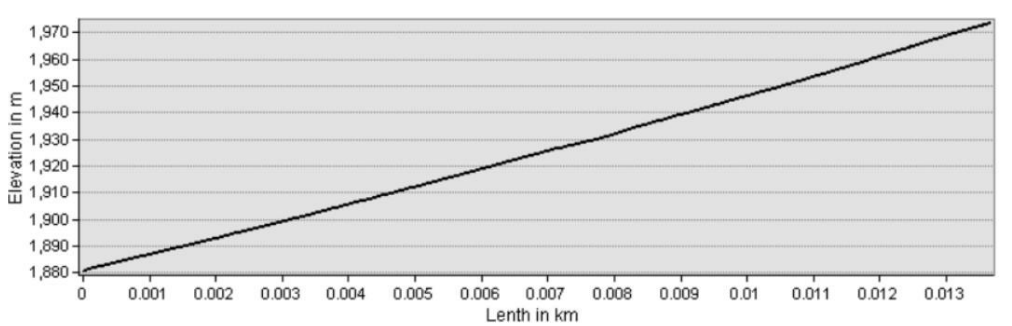

Figure 3.6: Topographic profiles drawn on the from the combined Hillshade model from the DEM derived from the SfM imagery in AgiSoft Pro 4. Topographic profiles 4 and 6 show an unbroken slope.

3.2.4 DEM and profiles along Blue Dome segment

Topographic profiles of the potential fault zone from Long and Bare canyons are shown in Figure 3.6. These profiles were extracted from the SfM DEMs using the hillshade images, along each alluvial fan that has an OSL age. Each of these profiles produced a smooth, unbroken surface slope, confirming field and lidar observations. Profile 4 (Figure 3.6) spans the Qaf4 fan, on which there is no clear break of the topography. Profile 6 is drawn across the oldest alluvial fan surface, Qaf5, and also does not show a change in surface slope suggestive of a normal fault scarp.

Neither the DEM nor SfM visual images reveals a possible fault scarp cutting the surface of the fans. This suggests that the last rupture along the Blue Dome segment occurred prior to ca. 110 ka years ago, which is the OSL age of the oldest fan (Qaf5, USU-3414) at Bare Canyon. Another alternative is that a fault scarp cut that surface but has diffused so much that it is not apparent on the surface in the field nor in the highly detailed imagery and DEMs. A step in the landscape would nonetheless be expected, and is not apparent.

3.3 Faulting History: Cosmogenic radionuclide ages on the faultscarp and OxCal model results of OSL ages

3.3.1 CRN ages on Faulted surface

Cosmogenic radionuclide (CRN) ages were obtained along the fault scarp and alluvial fan in the southern Nicholia segment. By determining the exposure age of the boulders along thefault scarp, we hoped to determine 1) the age of the alluvial fan and 2) the exposure age of boulders exposed in the degrading fault scarp. Figure 7 shows the location of sampled boulders along the Qaf2 alluvial fan surface and fault scarp at Pierce Canyon, in the southernmost Nicholia segment. Table 2 shows the calculated cosmogenic ages for the boulders. The ages range from

33 ka to 500 ka and the average age of all boulders is 144 +/- 119ka (Figure 8a). If the 33 ka and the 500 ka ages are removed as outliers (Figure 8b), then the weighted mean is 188 +/- 54 ka. When other outliers are removed, samples BHPC04, BHPC01, BHPC06, and BHPC07 remain, with a weighted mean of 193+/- 16 ka. The boulders on the fault scarp itself have a wide range of ages between 130 – 500 ka (BHPC05 – BHPC08).

Sample name	Located on fault scarp?	Nuclide	Age (yr)	Interr (yr)	Exterr (yr)
BHPC01	No	Be-10 (qtz)	205707	4566	19321
BHPC02	No	Be-10 (qtz)	321870	4079	33244
BHPC03	No	Be-10 (qtz)	33372	645	2661
BHPC04	No	Be-10 (qtz)	185683	2041	16742
BHPC05	Yes	Be-10 (qtz)	131562	1388	11257
BHPC06	Yes	Be-10 (qtz)	175905	2189	15745
BHPC07	Yes	Be-10 (qtz)	216589	2829	20179
BHPC08	Yes	Be-10 (qtz)	583516	6829	79068

Table 3.2: Sample names and location and their respective calculated ages.Ages were calculated using CRONUS vs and used the Lm data set. Interr (yr) is the internal uncertainty which measures uncertainties on the nuclide concentration. Exterr (yr) is the external uncertainties which includes uncertainties of both measurement and production rate.

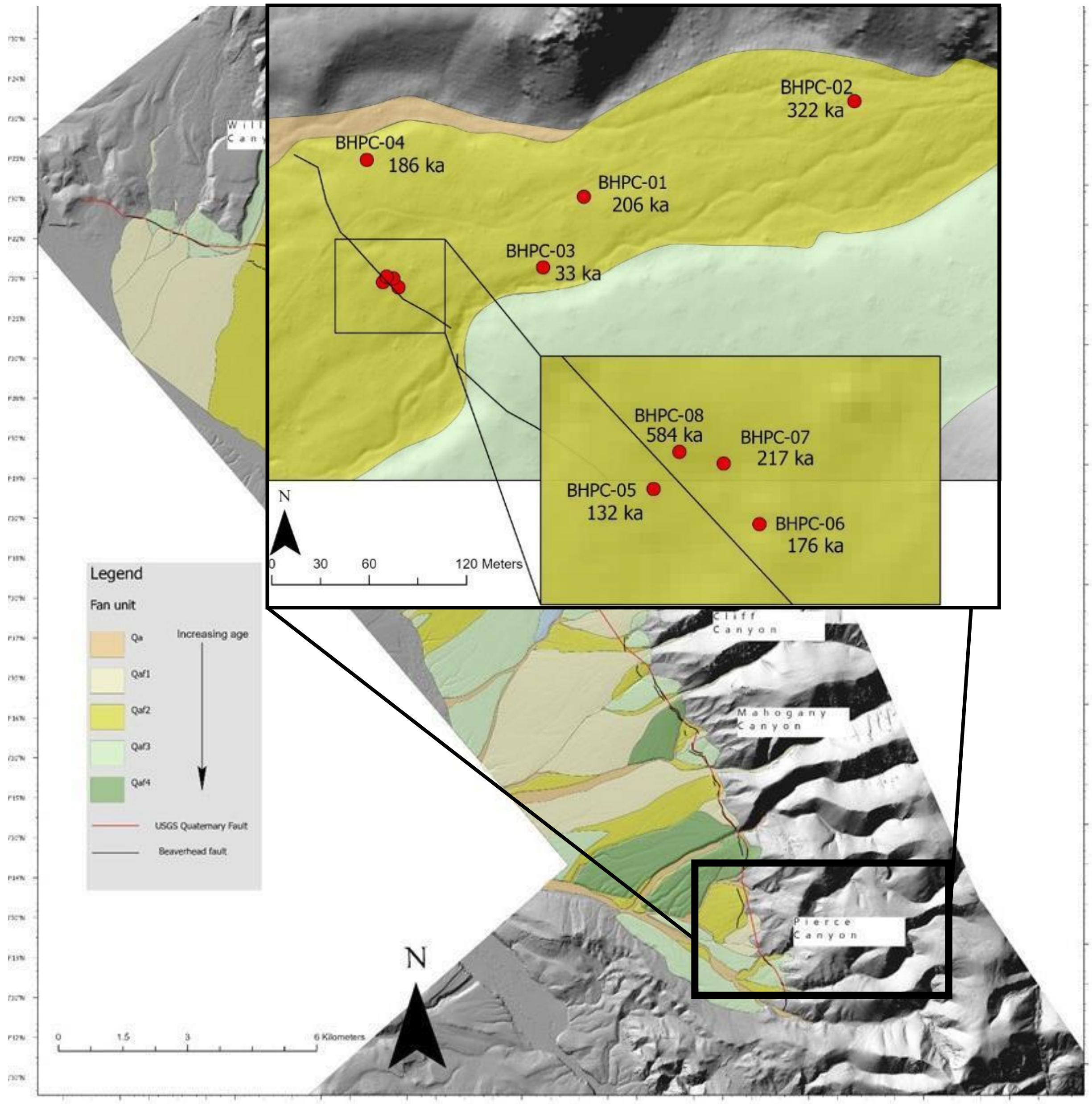

Figure 3.7: Map showing the location of Pierce Canyon, which is located in the southern portion of the Nicholia segment. Four samples, BHPC-01, BHPC-04, BHPC-03, and BHPC-02 are located on a mapped Qaf2 fan surface. The other four samples, BHPC-05, BHPC-06, BHPC-07, and BHPC-8 were collected in a vertical transect on the fault scarp.

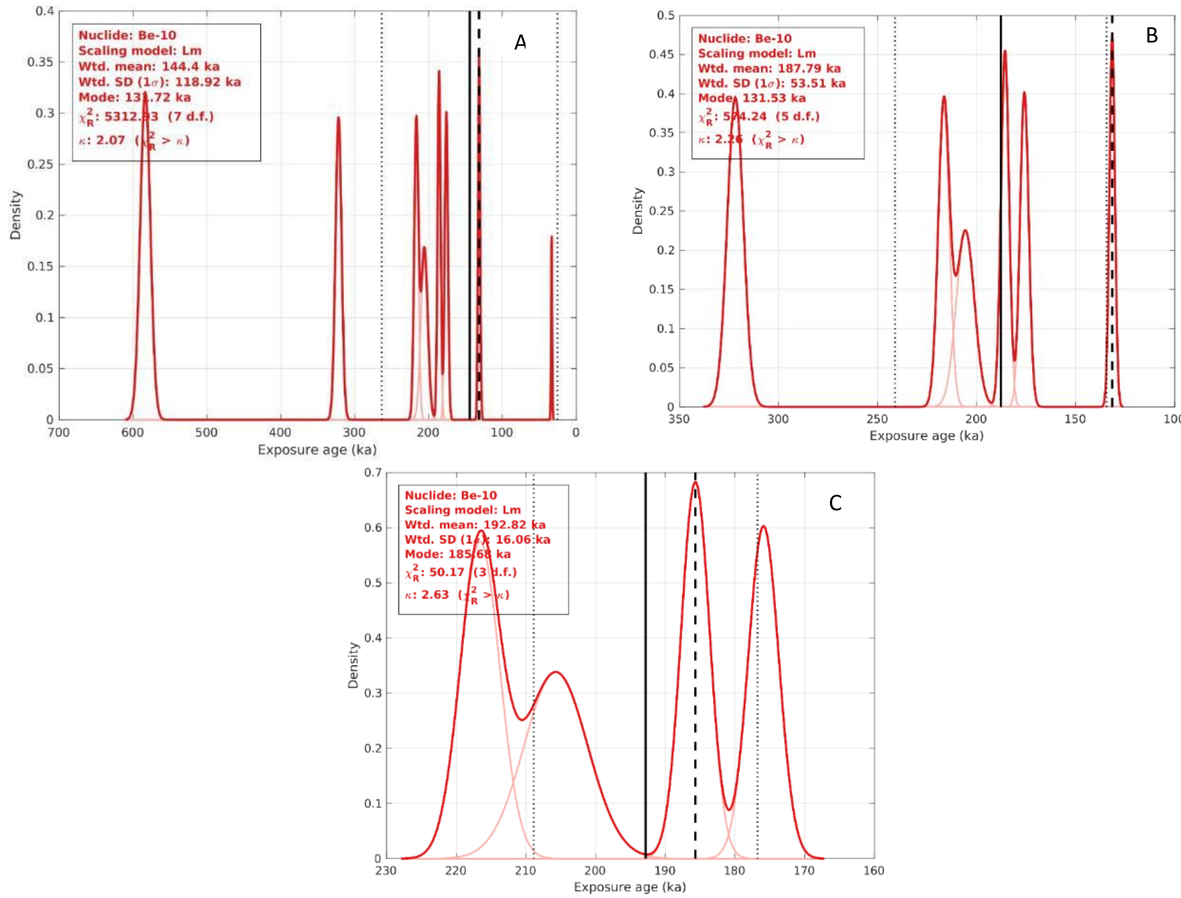

Figure 3.8: Weighted mean CRN boulder ages for a variety of outlier assumptions. A) is the calculated weighted mean for all of the ages (144.4 +/- 118.9 ka). B) Removing BHPC03 and BHPC08, the weighted mean is 187.8 +/ - 52.5 ka. C) is the weighted mean calculated when BHPC01,BHPC04, BHPC06, and BHPC07 192.8 +/- 16.1 ka.

The generally very old and highly variable cosmogenic ages most likely reflect inheritance of preexisting ^{10}Be isotopes from a previous exposure history of the boulders. This makes the calculated ages much older than the OSL age of the alluvial fan gravels. Inheritance is common in unglaciated watersheds because there is less erosion of the boulders to remove the preexisting ^{10}Be prior to deposition in and on the alluvial fan. Because these ages are much older than all 25 OSL ages, these ages cannot be used to draw further conclusions on faulting history nor be used to estimate the alluvial fan age.

3.4 OxCal model results of OSL ages

3.4.1 OxCal modeling results of OSL fan ages and fault scarps

As described in Chapter 2, we obtained 12 OSL ages from fans at Scott Canyon and Cliff Canyon in the Nicholia segment (Table 3.3). S. Olig (personal communication, 2021) used a two- event model for the Nicholia segment based on the OSL ages and inferences from vertical separation measurements at Cliff Canyon. For the model, samples from Cliff Canyon (Figure 3.9) were used to bracket the most recent rupture along the Nicholia segment (Figure 3.10). Qaf4 samples N14 and N5 along with Qaf3 samples N7 and N8 were used to estimate the age of the penultimate event. The last rupture was modeled by using the Qaf2 samples N15 and N16 with the Qaf1 samples N6 and N14. With the ages and assumptions, the model results show, that the last faulting occurred ca. 32 +/- 7.3 ka (95.4% confidence interval; Figure 3.10, model CFC1). For the penultimate event (CFC2 in the model), ages N4, N5 and N7, N8 were used to bracket the event (Figure 3.10). The modeling shows that the penultimate event occurred ca. 77.4 +/- 6.7 ka (95.4% confidence interval).

Table 3.3: Results of the OSL ages.

Segment	Sample num.	Fan Unit	USU num.	Depth (m)	Num. of aliquots[1]	Dose rate (Gy/ka)	Equivalent Dose[2] ± 2σ (Gy)	OSL age ± 1σ (ka)
Nicholia	N3	Qaf1	USU-3400	1.3	18 (26)	1.19 ± 0.06	26.26 ± 1.64	**22.08 ± 1.98**
	N6	Qaf1	USU-3406	1.55	19 (27)	0.82 ± 0.05	13.82 ± 2.40	**16.78 ± 2.09**
	N14	Qaf1	USU-3407	1.5	21 (26)	0.84 ± 0.05	15.70 ± 2.42	**18.63 ± 2.20**
	N15	Qaf2	USU-3404	1.2	21 (28)	1.10 ± 0.05	47.87 ± 8.65	**43.44 ± 5.39**
	N2	Qaf2	USU-3401	1.3	21 (33)	1.22 ± 0.06	60.05 ± 8.36 [3]	**49.32 ± 5.86**
	N16	Qaf2	USU-3411	1.4	18 (27)	0.96 ± 0.05	49.04 ± 5.82	**50.97 ± 5.43**
	N7	Qaf3	USU-3405	1.3	18 (25)	0.89 ± 0.05	57.25 ± 7.25	**63.99 ± 6.99**
	N8	Qaf3	USU-3410	1.2	21 (33)	0.95 ± 0.05	70.07 ± 7.94	**73.84 ± 7.79**
	N17	Qaf3	USU-3402	1.5	21 (31)	1.02 ± 0.05	66.82 ± 8.17	**65.52 ± 6.92**
	N5	Qaf4	USU-3409	1.4	19 (26)	0.84 ± 0.05	70.51 ± 7.66	**83.82 ± 8.73**
	N4	Qaf4	USU-3408	1.5	18 (26)	0.68 ± 0.04	64.18 ± 10.66	**93.7 ± 11.8**
	N1	Qaf5	USU-3403	1.7	20 (35)	0.87 ± 0.05	98.28 ± 11.95	**112.9 ± 12.1**
Blue Dome	BD1	Qaf1	USU-3412	1.3	21 (31)	0.99 ± 0.05	16.90 ± 3.15 [3]	**17.03 ± 2.28**
	BD9	Qaf1	USU-3419	1.35	26 (32)	1.77 ± 0.08	28.33 ± 4.03 [3]	**16.01 ± 1.77**
	BD16	Qaf2	USU-3420	1.45	20 (26)	2.22 ± 0.09	114.9 ± 15.0	**51.79 ± 5.39**
	BD2	Qaf3	USU-3413	1.3	19 (26)	1.04 ± 0.05	79.10 ± 7.98	**75.85 ± 7.52**
	BD5	Qaf3	USU-3415	1.5	20 (28)	1.23 ± 0.06	75.08 ± 11.59	**61.01 ± 6.96**
	BD6	Qaf3	USU-3416	1.5	18 (24)	1.07 ± 0.05	84.56 ± 7.64	**78.99 ± 7.59**
	BD7	Qaf3	USU-3417	1.6	24 (47)	1.29 ± 0.06	85.55 ± 8.18	**66.30 ± 6.39**
	BD8	Qaf3	USU-3418	1.45	19 (36)	1.45 ± 0.06	107.6 ± 12.3	**74.06 ± 7.45**
	BD11	Qaf3	USU-3421	1.6	18 (26)	1.39 ± 0.06	97.06 ± 5.30	**69.64 ± 6.04**
	BD12	Qaf3	USU-3422	1.45	23 (41)	0.96 ± 0.05	64.86 ± 9.32	**67.34 ± 7.52**
	USU-3211	Qaf4	USU-3211	0.96	18 (43)	1.95 ± 0.08	176.4 ± 33.2	**90.7 ± 11.3**
	USU-3212	Qaf4	USU-3212	1.32	18 (32)	2.01 ± 0.09	183.3 ± 33.2	**91.0 ± 11.1**
	BD3	Qaf5	USU-3414	1.5	23 (29)	1.15 ± 0.05	127.8 ± 15.0	**110.8 ± 11.3**

Processed by Tammy Rittenour at the Utah State University's luminescence lab. For the Dose rate information see Appendix B.
[1]analysis using the single-aliquot regenerative-dose procedure of Murray and Wintle (2000) on 1-2 mm small-aliquots of quartz sand (USU-3211:3212 = 150-250 µm; USU-3400:3422 = 75-150µm). Number of aliquots used in age calculation and number of aliquots analyzed in parentheses.
[2] Equivalent dose (D_E) calculated using the Central Age Model (CAM) of Galbraith and Roberts (2012), unless otherwise noted.

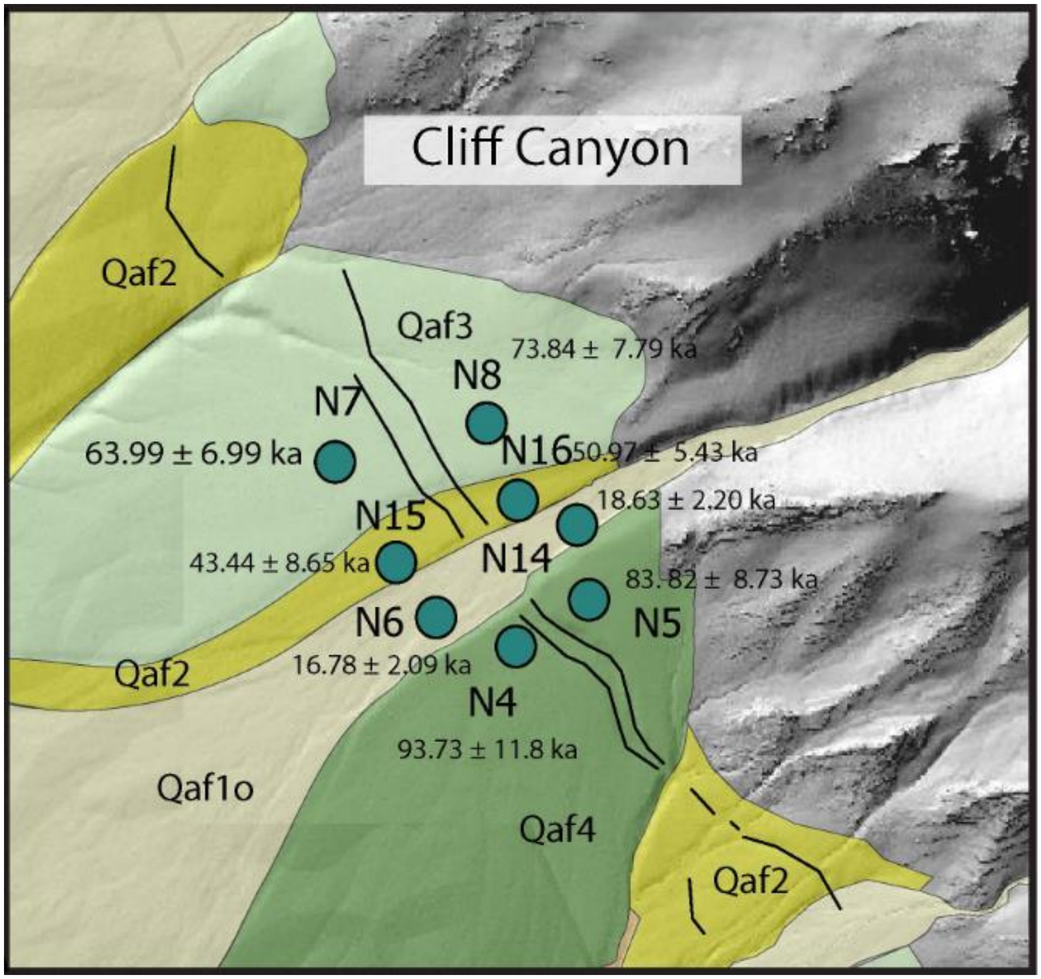

Figure 3.9: Sample locations for the OxCal model (Figure 3.10) shown here. N6 and N14 are on theunfaulted Qaf1 fan and N15 and N16 are on the faulted Qaf2 surface.

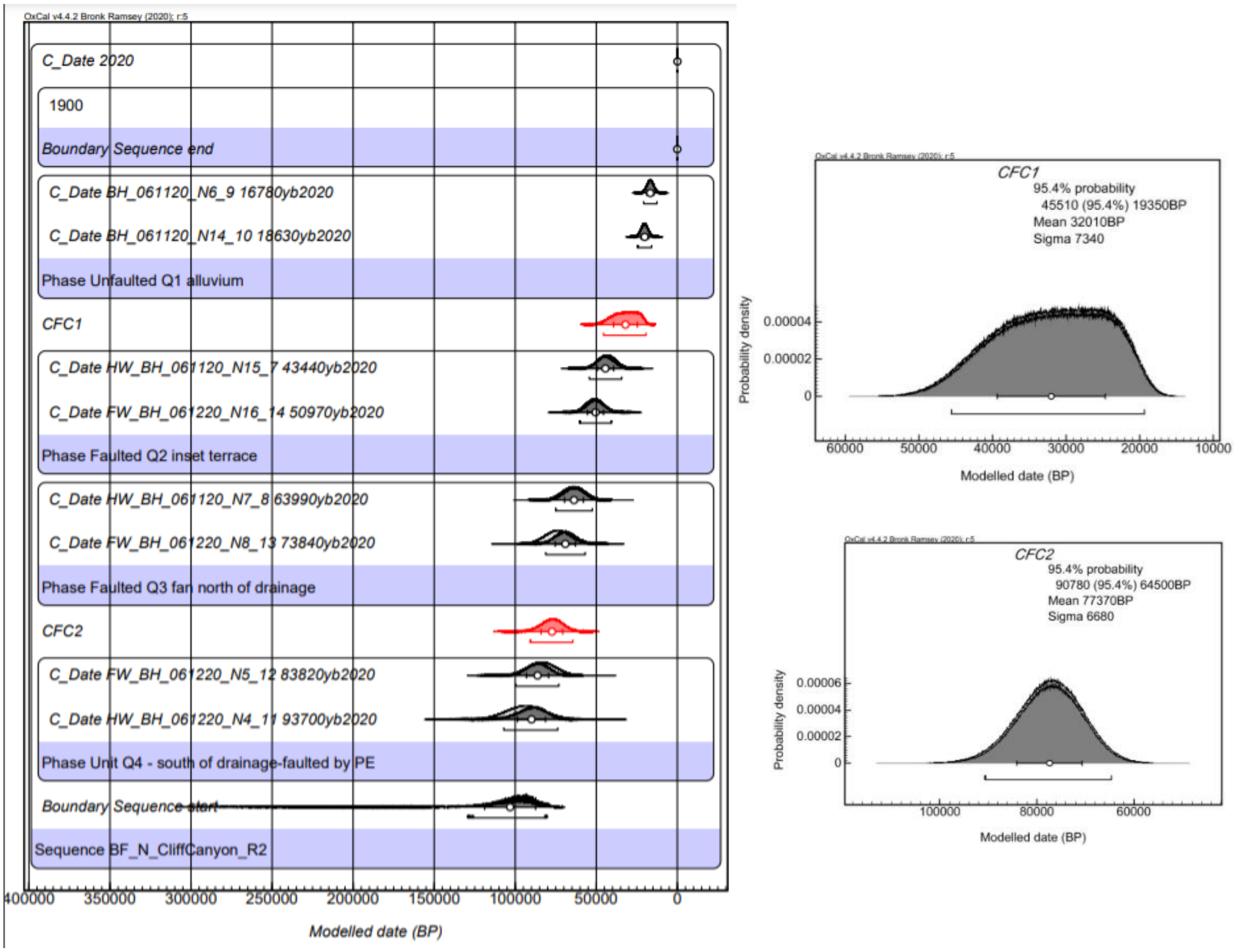

Figure 3.10: OxCal v4 results provided by S. Olig personal communication (2021). They calculated the ages of two seismic events by using the OSL ages from Cliff Canyon (See Chapter 2). For the first event, OSL ages N6 and N14 from the Qaf1 fanand OSL ages N15 and N16 were used from the Qaf2 fan to bracket the last event (32.0 +/- 7.3 ka). OSL ages from the Qaf3 fan N7 and N8 as well as Qaf4 fan ages N5 and N4 were used to estimate that the penultimate event occurred ca. 77.3 +/- 6.7 ka. Both models have a 95.4% probability estimation.

3.5. Discussion: Faulting History and segmentation

Previous studies have shown that the Nicholia and Blue Dome segments are separated by a right en-échelon step (Haller, 1988; Skipp and Hait, 1977). The spacing of the step between these two segments is 6.4 km. The results of our study confirm the segment boundary described by Haller (1988) and others.

3.5.1 Nicholia segment: OxCal age modeling results discussion

OxCal modeling by S. Olig (personal communication, 2021), using mapped scarps, VS measurement comparisons, and OSL ages of faulted alluvial fans, indicates that the last two ruptures along the Nicholia segment occurred 32 +/- 7.3 ka and 77 +/- 6.8 ka. These results are an improvement on estimates by Haller (1988), who used soil profiles and fault scarp morphology to infer two faulting events from 10 – 15 ka and 15 – 30 ka. The lack of scarps cutting Qaf1 fans indicates that Nicholia segment clearly has not ruptured since 16-22 ka.

3.5.2 Blue Dome segment: Why has it not ruptured?

There is no fault scarp on the Blue Dome segment that is discernible in the field, in lidar imagery, or in drone imagery, with oldest fan dated at ca. 110 ka (sample USU-3414, BD3, Table 3.1, Figure 3.6). From these detailed observations, we infer that the Blue Dome segment has not ruptured during the past 110 ka. The Blue Dome segment is different from the southernmost segments of the Lemhi fault and the Lost River fault (Howe and Arco, respectively) in terms of late Pleistocene faulting history. Scarp mapping and sediment dating from the Arco and Howe segments suggest that the most recent faulting occurred 15 – 30 ka (Haller, 1988). More recent analysis indicates that the most recent fault occurred 20-21 ka (Olig et al., 1995) for the Arco segment and 15 – 18 ka for the Howe segment (Gorton, 1995; Hemphill-Haley, 1992).

Here we hypothesize why the Blue Dome segment has not ruptured in a similar time frame to the

Howe and Arco segments. The transition from Basin and Range normal faulting to the Centennial region north of the Beaverhead Mountains could be a factor. The Centennial block could be an extra ‘weight’ for the footwall of the Beaverhead fault causing greater rigidity and would require more strain for an earthquake to occur. This area also contains the Red Rock fault, which in contrast to the other faults in east central Idaho, is thought to have either two (Haller, 1988; Greenwell, 1997) or three segments (Harkins et al., 2005). The Red Rock fault could show that normal fault growth ceases southward toward the interior Centennial block.

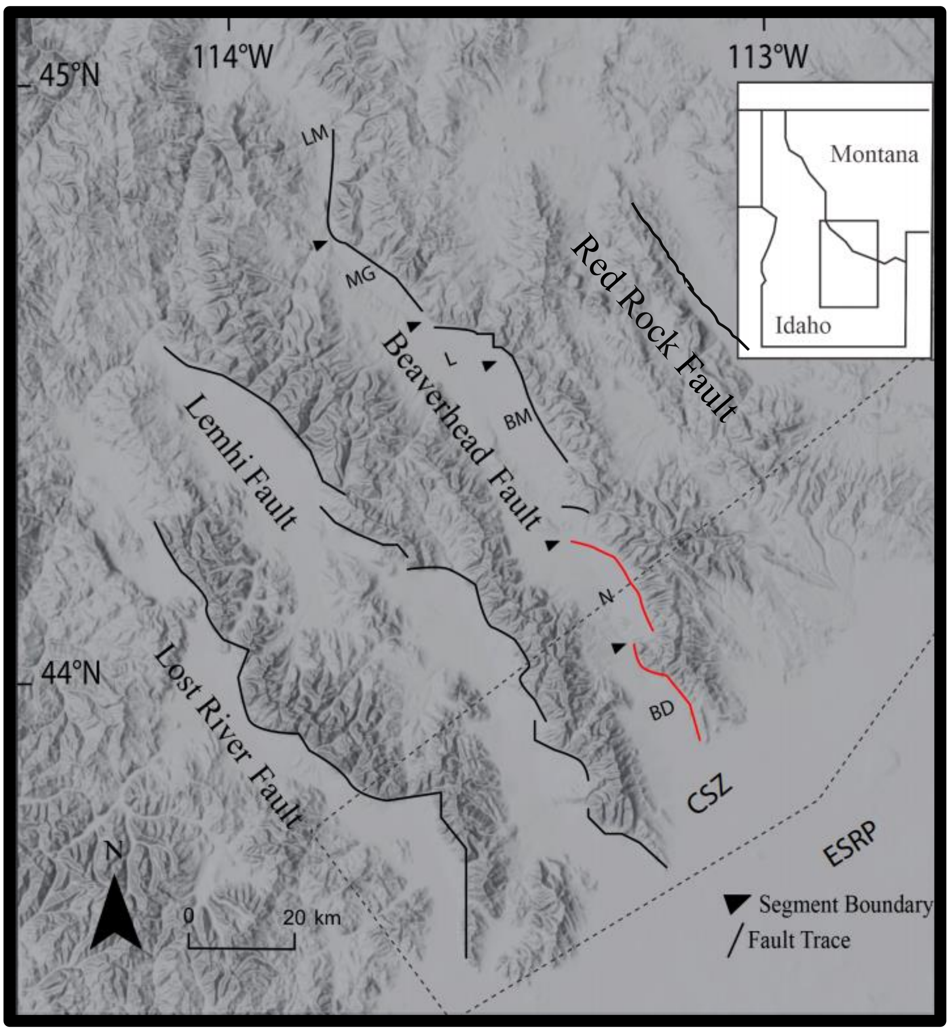

Figure 3.11: Map showing possible tectonic relationships. Beaverhead, Lemhi, and Lost River ranges are shown perpendicular to the eastern Snake River Plain (ESRP). The Centennial shear zone (CSZ) is outlined with a dashed line (Payne et al. 2008). Red line shows the trace of the Beaverhead fault in the study area. Segments on the Beaverhead fault are: BD, Blue Dome;N, Nicholia; BM, Balding Mountain; L, Leadore; MG, Mollie Gulch; LM, Lemhi. Modified from Haller, 1988.

3.5.3 The Centennial Shear Zone

The Centennial shear zone (Figure 3.11) separates two domains that move southwestward at contrasting rates relative to the Stable North American Reference Frame. Using GPS data over a time span of 1994 to 2010, Payne et al. (2008, 2012) showed that the velocity of the Eastern Snake River Plain was $-0.1 \pm 0.4 \times 10^{-9}$ mm/yr while the Centennial Tectonic Belt moved at $3.5 \pm 0.2 \times 10^{-9}$ mm/yr. Located between these two domains, rocks in the Centennial Shear Zone should experience northeast-oriented right-lateral shear, with the shear rate diminishing from northeast to southwest.

In the Beaverhead fault area, Payne et al. (2012) located the Centennial zone in the area between the northern Nicholia segment and the south end of the Blue Dome segment. However, my high-resolution LiDAR analysis of alluvial fans did not yield any indication of NE-striking faults. In fact, two NE-striking faults previously mapped by Witkind (1975) at the south end of the Blue Dome segment are interpreted to be false, since they have no topographic manifestation in the LiDAR data. Ultimately, I found no faults that might be associated with the Centennial Shear Zone.

Given the absence of shear structures as well as the absence of surface rupture along the Blue Dome segment during the past 110 ka, it is possible that the southern end of the Beaverhead Range, despite its Basin & Range morphology, is currently experiencing such low internal strain that it should be considered tectonically as part of the rigid Eastern Snake River Plain tectonic block. In support of this hypothesis, I note that several basaltic cinder cones and other eruptive centers occur west of the Blue Dome segment, which may reflect the outward expansion of volcanism from the ESRP to "off-axis" areas.

The southern fault segments of adjacent ranges, including the Howe segment (Lemhi

Range) and Arco segment (Lost River Range), have experienced late Pleistocene faulting (Haller, 1988; Crone and Haller, 1991), unlike the Blue Dome segment. Notably, the basins associated with these segments do not expose off-axis volcanic rocks, so in these locations the current boundary between Basin & Range and ESRP tectonic blocks may coincide with its morphologic boundary.

3.5.4 Further Research

Further research could be done in areas along the Lost River, Lemhi, and Beaverhead faults that have yet to have faulting constrained by OSL ages. For example, the Baldy Mountain segment of the Beaverhead fault, north of Nicholia segment, has an apparent fault scarp cutting the surface of terraces and fans, but no geomorphic feature has been dated (Haller, 1988). Dating those faulted surfaces would determine if our estimations for the timing of Nicholia segment ruptures contrast with the timing of other segments (Haller, 1988). As noted above, rupture event ages proposed here are earlier than those inferred by Haller (1988), and that may be the case in other segments as well. This would refine Crone and Haller's (1991) model indicating that faults in the northern Basin and Range experience similar faulting patterns overall. There should also be more research into the Blue Dome segment and why it has not ruptured in the past 110 ka, in contrast to the Howe and Arco segments. Geophysical studies could determine depth of the basin and indicate if there is a fault beneath the surface. Liberty et al. (1997) found that the southern portion of Birch Creek Valley contains a shallow basin that is a few hundred meters below depth. This study did not include the portion of Birch Creek Valley in the northern portion of the Blue Dome segment.

References:

Amos, C. B., Kelson, K. I., Rood, D. H., Simpson, D. T., and Rose, R. S., 2016, Late Quaternary slip rate on the Kern Canyon fault at Soda Spring, Tulare County, California: Lithosphere, v. 2, p. 411 – 417.

Breckenridge, R.M., Lewis, R.S., Adema, G.W., and Weisz, D.W., 2003, Miocene and Younger Faults in Idaho: Idaho Geological Survey Map M-8, scale 1:1,000,000.

Gorton, A.E., 1995, Late Quaternary surface displacements and segmentation along the southern Lemhi fault, east-central Idaho, [MS thesis]: State University of New York at Binghamton, 103 p.

Crone, A.J., and Haller, K.M., 1991, Segmentation and the coseismic behavior of Basin and Range normal faults: examples from east-central Idaho and southwestern Montana, U.S.A.: Journal of Structural Geology, v. 13, p. 151-164.

Greenwell, R.A., 1997, Alluvial fan development, the key to segmentation of the Red Rock fault, Southwestern Montana. [M.S. Thesis]: Columbia, University of South Carolina.

Haller, K.M., 1988, Segmentation of the Lemhi and Beaverhead faults, east-central Idaho, andRed Rock fault, southwest Montana, during the late Quaternary [M.S. thesis]: Boulder, University of Colorado, 141 p.

Haller, K.M., Wheeler, R.L., and Adema, G.W., compilers, 2010, Fault number 603e, Beaverhead fault, Nicholia section, in Quaternary fault and fold database of the United States: U.S. Geological Survey website, https://earthquakes.usgs.gov/hazards/qfaults, accessed 012/07/2020.

Harkins, N.W., Anastasio, D.J., and Pazzaglia F. J., 2005, Tectonic geomorphology of the Red Rock fault, insights into segmentation and landscape evolution of a developing range front normal fault: Structural Geology, v. 27, p. 1925 – 1939.

Hemphill-Haley, M.A., Sawyer, T.L., Kneupfer, P.L.K., Forman, S.L., and Wong, I.G., 2000, Timing of faulting events from thermoluminescence dating of scarp-related deposits, Lemhi fault, southeastern Idaho, *in* Stratton-Noller, J., Sowers, J.M., and Lettis, W.R., eds., Quaternary geochronology—Methods and applications: Washington D.C., American Geophysical Union Reference Shelf v. 4, p. 541-548.

Liberty L.M., Barrash, W., Knoll, M.D., Hudson, W.K., Bolger, R.D., 1997, Geophysical Investigations of Birch Creek Valley near the Northern Boundary of the INEEL – Year 1 Report: Boise State University, Technical Report BSU CGISS 96-06, p. 20.

Olig, S.S., Gorton, A.E., Bott, J.D., Wong, I.G., Knuepher, P.L.K., Forman, S. L., Smith, R.P., and Simpson, D., 1995, Paleseismic investigation of the southern Lost River fault zone, Idaho: Lockheed Idaho Technologies Company, Technical Report INEL-95/0508, 82 p.

Payne, S.J., McCaffrey, R., and King, R.W., 2008, Strain rates and contemporary deformation in the Snake River Plain and surrounding Basin and Range from GPS and seismicity: Geology, v. 36, p. 647–650, doi:10.1130/G25039A.1.

Payne, S.J., McCaffrey, R., King, R.W., and Kattenhorn, S.A., 2012, A new interpretation of deformation rates in the Snake River Plain and adjacent Basin and Range regions from GPS measurements: Geophysical Journal International, v. 189, p. 101–122, doi:10.1111 /j.1365-246X.2012.05370.x.

Rodgers, D.W., and Anders, M.H., 1990, Neogene evolution of Birch Creek Valley near Lone Pine, Idaho, *in* Roberts, S., ed., Geologic field tours of western Wyoming and parts of adjacent Idaho, Montana and Utah: Geol. Survey Wyoming Pub. Info. Circ. 29, p. 26-38.

Skipp, B., and Hait, M.H., Jr., 1977, Allochthons along the northeast margin of the Snake River Plain, Idaho, *in* Heisey E.L., Lawson, D.E., Norwood, E. R., Wach, P.H., and Hale, L.A., eds., Rocky Mountain Thrust Belt Geology and Resources: Wyoming Geological Association 29th Annual Field Conference, p. 499-515.

Thompson, S. C., Weldon, R. J., Rubin, C. M., Abdrakhmatov, K., Molnar, P., and Berger, G.W., 2002, Late Quaternary slip rates across the central Tien Shan, Kyrgyzstan, central Asia: Journal of Geophysical Research, v. 107, p. 1 – 32.

Witkind, I.J., 1975, Preliminary map showing known and suspected active faults in Idaho: U.S. Geological Survey Open-File Report 75-278, 71 p. pamphlet, 1 sheet, scale 1:500,000.

Chapter IV: Summary of findings

4.0 Alluvial fan morphology and chronology of the southern Beaverhead Mountains

Chapter 2 contains results and discussion for the alluvial fan morphology and chronology along the southern Beaverhead Range. The mapping results are shown in Figure 4.1 for Nicholia segment and Figure 4.2 for the Blue Dome segment. The teal dots on both maps are the locations of optically stimulated luminescence ages and additional caliche measurement sites . Both of these maps have 5 distinct units (Qaf1 – Qaf5). Qaf1 fans are mapped as the lowest topographic unit and normally extends directly from the canyon mouths. Qaf2 – Qaf5 fans were mapped based on the soil and alluvial fan morphology and have successive topographically higher positions. A summary of the OSL ages are shown in Table 4.1.

Alluvial fan unit	OSL age range	Mean age ± 1σ (ka)
Qaf1	16 - 22 ka	18.1 ± 2.4
Qaf2	43 - 61 ka	48.88 ± 3.6
Qaf3	66 - 79 ka	69.65 ± 5.5
Qaf4	84 - 94 ka	89.81 ± 3.6
Qaf5	111 - 113 ka	111.85 ± 1.1

Table 4.1: Summary of alluvial fan units and associated OSL ages for both the Blue Dome and Nicholia segments.

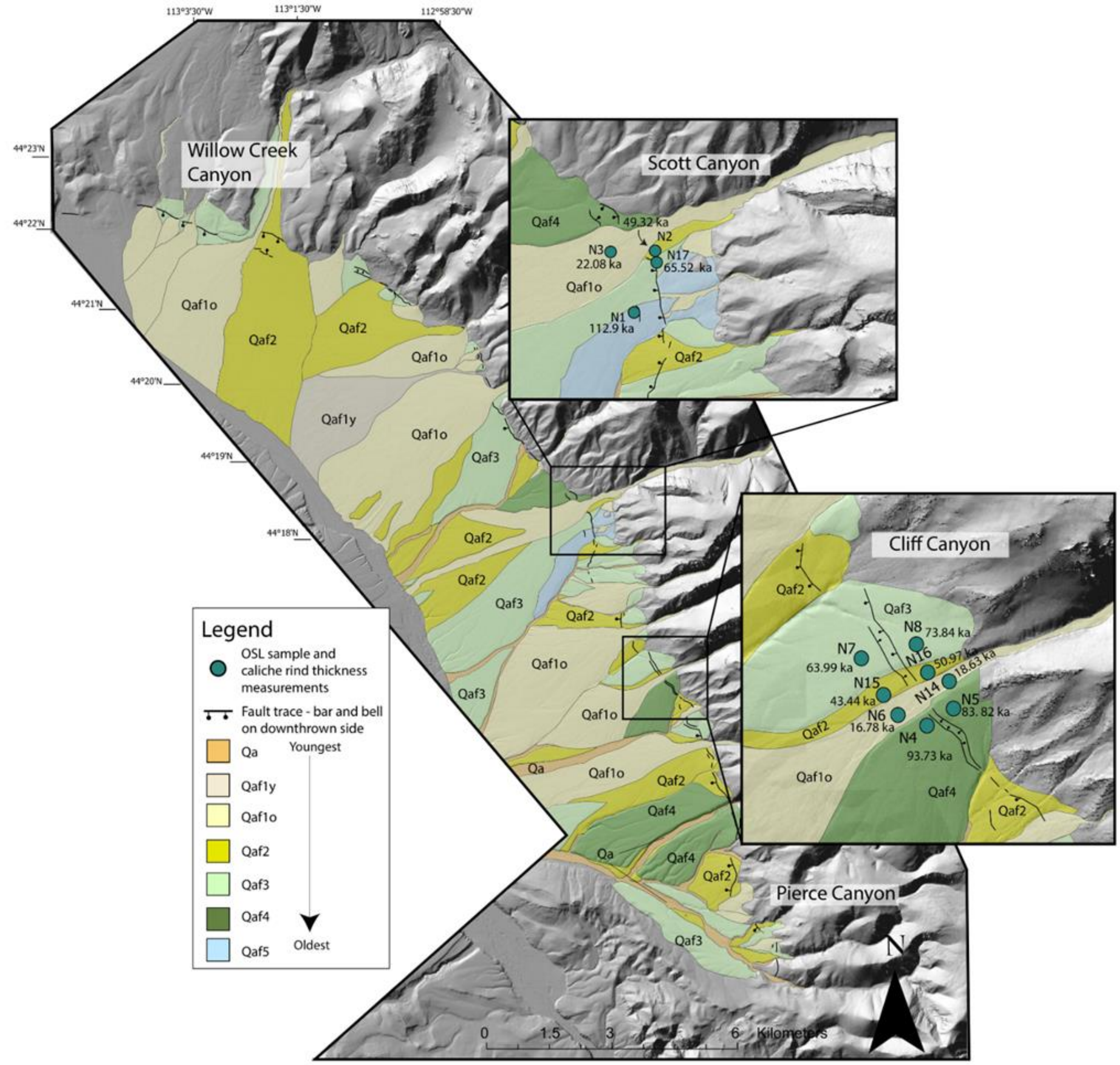

Figure 4.1: Alluvial fan mapping of the Nicholia segment showing the OSL sample locations in Scott and Cliff canyons. Fivefan units were identified in the Nicholia segment, Qaf1 – Qaf5.

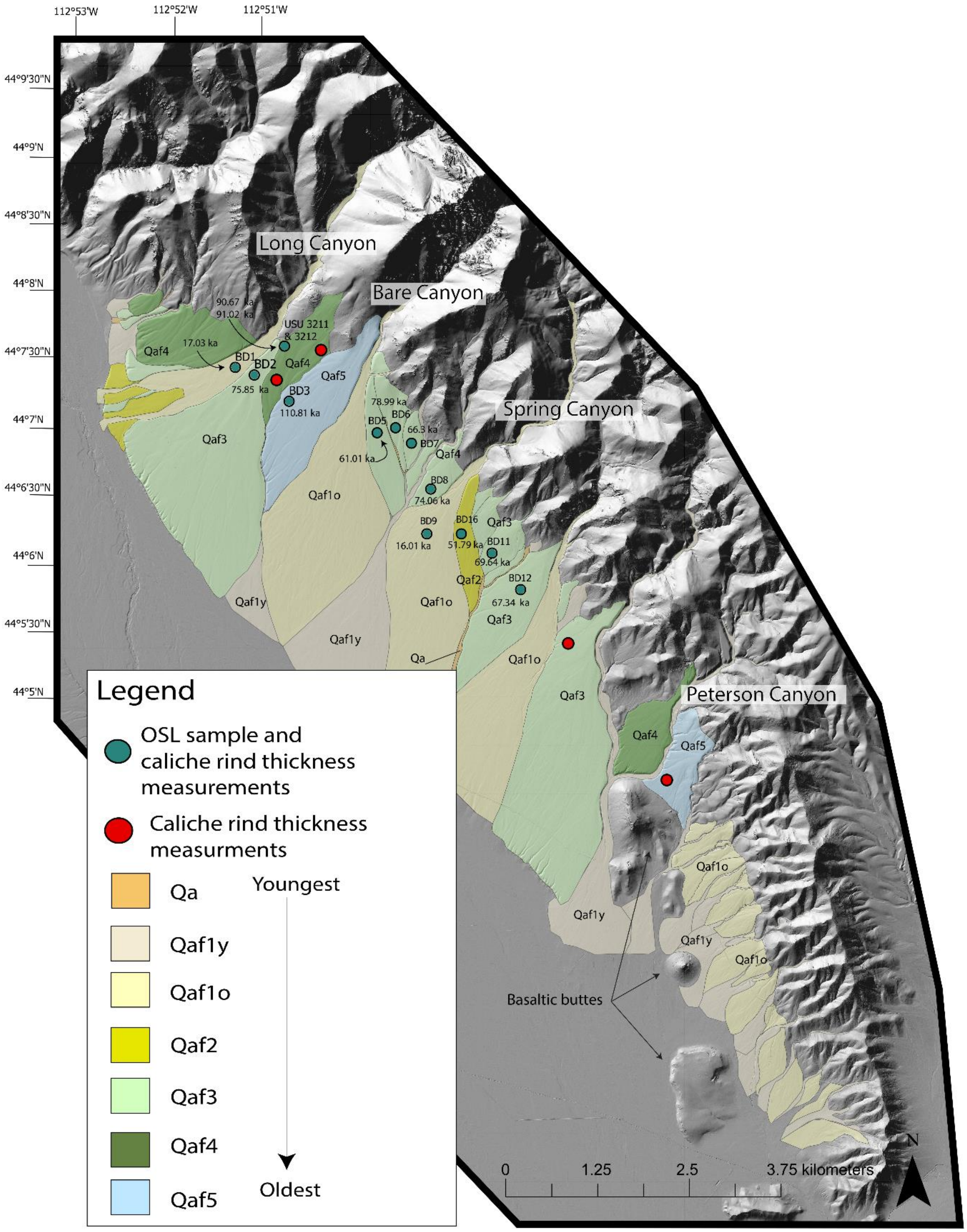

Figure 4.2: Alluvial fan mapping of the Blue Dome segment showing the locations of the OSL samples and their respective ages. Shown are also the additional sites where additional caliche rinds were measured. There are 5 alluvial fan units shown in Blue Dome section.

Qaf1 alluvial fans have an age range of 16 – 22 ka; Qaf2 43 – 61 ka; Qaf3 66 – 74 ka; Qaf4 84 – 94 ka; and Qaf5 from 111 – 113 ka. The means of all ages are Qaf1 18.1 +/- 2.4 ka; Qaf2 48.88 +/- 3.6 ka; Qaf3 69.65 +/- 5.5 ka; Qaf4 89.81 +/- 3.6 ka and Qaf5 111.85 +/- 1.0 ka (Table 4.2). We infer that the timing of fan aggradation correlates to cooler and/or wetter late Pleistocene climatic episodes. According to Pierce and Scott (1982) cooler climates would have prolonged a snowpack at higher elevations and would create intense dischargeduring the late summer snowmelt to ensure gravel transport into alluvial fans. These cooler conditions would have created more effective moisture within the soil; reducing the erosion of finer sediment. Frost wedging would have also occurred and created course-grained colluvium deposits along hillslopes that would have been transferred downstream.

Our hypsometry curves show that the elevation from the tops of the selected Nicholia canyons range from 3200 – 2800 m while the Blue Dome canyons have a range of 3000 – 2000 m. These elevations exceed the estimated regional glacial equilibrium-line altitude (ELA) of 2700 – 2800 m (Locke 1990; Meyer et al., 2004). The ELA's suggest that there would have been snowpack in the Nicholia segment drainages and in portions of the Blue Dome segment drainages. With this analysis we can infer that melting snowpack was the primary driver of alluvial fan aggradation for the Nicholia segment and likely for portions of the Blue Dome segment.

In conclusion, as with Kenworthy (2011), we infer that alluvial fans within the northern Basin and Range form during cool late Pleistocene conditions. This inference is partially supported by data from other regional paleoclimatic proxy records, such as the Lake Terreton highstands dated by Amidon et al. (2016) and isolated CRN moraine boulder ages.

4.1 Faulting histories along the Blue Dome and Nicholia segments

Chapter 3 describes the faulting history of the Blue Dome and Nicholia segments. The two segments are separated by a 6.5 km right en echelon step. As previous studies have shown (Haller,1988) and the findings in the Chapter 3, the Blue Dome segment does not appear to have a fault scarp cutting its alluvial fans. Our oldest OSL age along the Blue Dome segment is around 110 ka and therefore we infer that no faulting has occurred along the Blue Dome segment in the past 110 ka.

The Nicholia segment in contrast has fault scarps cutting alluvial fan surfaces. The fault scarps are present along Qaf2 – Qaf5 alluvial fans but are lacking along the youngest alluvial fan unit, Qaf1. Fault scarp vertical separation (VS) generally increases with alluvial fan age, as shown at Cliff Canyon. The OxCal modeling provided by S. Olig (personal communications 2021) modeleda two-event rupture history along the Nicholia segment. The model infers fault ruptures occurred 32 +/- 7.3 ka and 72 +/- 6.7 ka based on the OSL ages from Cliff Canyon. These estimations are older than what Haller (1988) suggested.

References:

Haller, K.M., 1988, Segmentation of the Lemhi and Beaverhead faults, east-central Idaho, and Red Rock fault, southwest Montana, during the late Quaternary [M.S. thesis]: Boulder, University of Colorado, 141 p.

Kenworthy, M.K., 2011. Optically stimulated luminescence dating of gravelly alluvial fan deposits: Links between climate and geomorphic response in the Lost River Range, Idaho[M.S. thesis]: Boise, Boise State University, 171 p.

Locke, W.W., 1990, Late Pleistocene glaciers and climate of western Montana, U.S.A. Arcticand Alpine Research, v. 22, p. 1-13.

Meyer, G.A., Fawcett, P.F., and Locke, W.W. 2004. Late-Pleistocene equilibrium-line altitudes, atmospheric circulation, and timing of mountain glacier advances in the interior northwestern United States, in Haller, K., and Wood, S.H., eds., Geological Field Trips in Southern Idaho, Eastern Oregon, and Northern Nevada. Geological Society of America Field Guide, p. 61-66.

APPENDIX A:
Soil descriptions were made from the top-downward
Sedimentary descriptions were made from bottom up

Site: N3
Coordinates: N 44.30449 W 112.94054
GPS Elevation: 2165 m

USU-3400
Fan unit: Qaf1
OSL age: 22.08 ± 1.98 ka
Depth collected: 1.3 m

Soil Horizons

Aw: 0 – 18cm
- Pebbly silt loam
- Weakly Granular Structure

Bk1 : 18 – 35cm
- Pebbly silt loam
- Platy, weak structure
- 10YR 5/4 – Yellowish Brown
- Diffuse upper contact

Bk2: 35 – 60cm
- Silty Gravel
- Platy texture
- 10 YR 7/2 – Light gray
- Abrupt upper contact
- Stage II carbonate soil – clasts collected from this horizon
- Abrupt upper contact

Bk3: 60 – 90cm
- Pebble-gravel
- weak platy structure
- 10 YR 6/3 – Pale brown

C/Bw 90 – 140 cm
- Pebble-gravel
- no soil structures
- 10 YR 5/3 – Brown

Sedimentary Units

Unit 1: 0 – 80cm
- 3-4 cycles of coarsening and fining upward sequences (couplets)
- Couplets are 25 – 30 cm each
- Matrix supported
- Subrounded – rounded clasts (5 – 7cm)
- Smaller pea shaped clasts present

Interpretation : Sheet wash deposit

Unit 2: 80 – 110cm
- Matrix supported
- Heterogenous composition of grains
- Matrix is fine to medium sand (carbonate)
- Weakly bedded and stratified

Interpretation: Sheet wash deposit but has been disturbed; soil disturbed alluvial gravel

Unit 3: 110 – 145cm
- Massive; no bedding
- Matrix supported
- Clasts (2cm) loaded in silt
- Pebbly silt to fine sand matrix

Interpretation: Loessic cap with soil mixing

Site: N2
Coordinates: N 44. 30453 W 112.93542
GPS Elevation: 2177 m

Soil Horizons

A: 0 – 16cm
  Pebbly silt loam
  weakly granular
  10 YR 6/3 – Pale brown

Bk1: 16 – 28cm
  Silty pebbly gravel
  weakly Platy
  10 YR 6/4- Light yellowish brown

Bk2: 28 – 45cm
  Silty pebble gravel
  Platy
  10 YR 6/4 -Light yellowish brown

Bk3: 45 – 63cm
  Silty pebble gravel
  more massive, less platy than Bk3
  10 YR 6/4 -Light yellowish brown

Bk4: 63 – 94cm
  Pebble-gravel
  No soil structure
  10 YR 6/3 – Pale brown
  Stage II + carbonate stage
  Clasts collected from this horizon

Bk5 94 – 145cm
  Pebble-gravel
  No soil structure
  10 YR 6/2 – Light brownish gray

USU-3401
Fan unit: Qaf2
OSL Age: 49.32 ± 5.86 ka
Sample Depth: 1.3 m

Sedimentary Units

Unit 1: 0 – 83cm
  Pebble gravel with occasional cobbles
  Stratified
  Largely clast supported
  Sub-angular to sub-rounded

Interpretation: Alluvial gravel deposit

Unit 2: 83 – 118cm
  Massive Pebbly silt
  Matrix supported; Tabular

Interpretation: Loessic, wind blown deposits with pebbles, bioturbated

Unit 3: 118 – 145cm
  Massive, Pebbly fine sand
  Roots throughout
  Darker than Unit 2

Interpretation: Soil developed in loessic cap

Site: N17
Coordinates: N44.30357 W112.93526
GPS Elevation 2176 m

USU-3402
Fan unit: Qaf3
OSL age: 65.52 ± 6.92 ka
Sample depth: 1.5 m

Soil Descriptions

A: 0 – 20cm
- Pebbly silt loam
- Granular
- weak HCl reaction
- 10 YR 6/3 – Pale brown

ABk1: 20 – 32cm
- Pebbly silt loam
- Granular
- Mild HCl reaction
- 10 YR 6/4 – light yellowish brown

Bk2: 32 – 50cm
- Silty pebbly gravel
- Platy
- 10 YR 7/3 – very pale brown

Bk3: 50 – 75cm
- Pebble gravel
- No soil structure
- 10 YR 6/2 – light brownish gray
- carbonate pendants present
- Stage II + stage carbonate
- Clasts collected here

Bk4: 75 – 130cm
- Pebble gravel
- No soil structure
- 10 YR 6/2 – Light brownish gray
- Carbonate pendants

Bk5: 130 – 170cm
- Pebble gravel
- No soil structure
- 10 YR 6/3 – Pale brown
- Carbonate pendants

Sedimentary Units

Unit 1: 0 – 1.25 m
- Pebble gravel, occasional cobbles
- Subrounded to rounded
- Interbedded coarser and finer gravel
- Stratified; broadly tabular
- Clast supported

Interpretation: Alluvial fan gravel

Unit 2: 1.25 – 1.45 m
- Silty pebble gravel
- Massive
- Matrix supported
- Diffuse contact with Unit 1
- Randomly oriented clasts
- Subangular clasts

Interpretation: Bioturbated gravels in soil

Unit 3: 1.45 – 1.70 m
- Pebbly sandy silt
- Massive
- Matrix supported
- Smaller clasts than Unit 2
- Subangular

Interpretation: Soil development in loessic cap. Bioturbation of lower gravel

Site: N1
Coordinates: N44.29946 W112.93794
GPS elevation: 2162

Soil Horizons

A: 0- 18cm
- Pebbly silt loam
- Granular
- 10 YR 5/3 – Brown

ABk1: 18 – 28cm
- Pebbly silt loam
- Granular
- 10 YR 5/4 – Yellowish brown

Bk2: 28 -52cm
- Pebbly silt loam (more pebbles than previous horizon
- Weak granular
- 10 YR 7/3 – Very pale brown

Bk3: 52 – 74 cm
- Silty pebble
- No soil structure
- 10 YR 7/4 – Very pale brown
- White appearance on outcrop

Bk4: 74 – 128cm
- Silty pebble
- No soil structure
- small carbonate pendants

Bk5: 128 – 180cm
- Pebble gravel
- No soil structure
- 10 YR 7/3 – Very pale brown
- Stage II + carbonate
- Rind measurements were collected from here

USU-3403
Fan unit: Qaf5
OSL age: 112.9 ± 12.1 ka
Sample depth: 1.7 m

Sedimentary Units

Unit 1: 0 – 60cm
- Cobbly Pebble gravel
- Clast supported
- Heterogeneous mixture
- Subangular – subrounded clasts
- Stratified
- Imbrication

Interpretation: Alluvial fan gravel

Unit 2: 60 – 120cm
- Base of Unit 2 has gypsum
- Massive
- Matrix supported
- Angular – subangular pebble gravel
- Vertical clasts (%50)
- Uniform sized clasts (1 – 5cm)

Interpretation: Some kind of massive movement (debris?) channel fill deposit

Unit 3: 120 – 135cm
- Massive matrix supported pebbly silt
- Subangular clasts
- no orientation of clasts
- Similar to Unit 2 in size and character

Interpretation: Soil and bioturbated unit with loess

Unit 4: 155 – 178cm
- Pebbly sandy silt
- Massive
- Smaller clasts than Unit 2

Interpretation: Loessic cap with bioturbation of gravels from below

Site: N15
Coordinates: N44.26833 W112.91721
GPS elevation: 2218

Soil Horizons
A: 0 – 18cm
- Pebbly silt loam
- Granular
- Roots present
- Weak HCl reaction
- 20 YR 6/2 – light brownish gray

ABk1: 18 – 28cm
- Pebbly silt loam
- Granular
- Mild HCl reaction
- Diffuse upper boundary
- 10 YR 6/3 – Pale brown

Bk2: 28 – 68cm
- Loamy pebbly gravel
- Boundary based on color
- 10 YR 7/3 – Very pale brown
- Diffuse lower boundary based on color

Bk3: 68 – 120cm
- Cobble pebble gravel
- No soil structure
- Stage II carbonate
- Lower boundary picked on reduced carbonate pendants
- 10 YR 6/3 – Pale brown
- carbonate clasts collected here

C: 120 – 140cm
- Cobble pebble gravel
- No soil structure
- No carbonate present
- 10 YR 5/4 – yellowish brown

USU-3404
Fan unit: Qaf2
OSL age: 43.44 ± 5.39 ka
Sample depth: 1.2 m

Sedimentary Units
Unit 1: 0 – 70cm
- Cobble pebble gravel
- Imbrication on larger clasts
- Clast supported
- Subrounded clasts
- Weakly stratified
- Pods of pebbles
- Uniformly distributed

Interpretation: Channel deposit of alluvial fan

Unit 2: 70 – 115cm
- Matrix supported
- Cobbly pebbly gravel
- Clasts randomly oriented
- Subrounded clasts
- Heterogenous distribution

Interpretation: Soil disturbed gravel with loessic addition

Unit 3: 115- 140cm
- Matrix supported gravely silt
- clasts much finer than Unit 2
- More massive than Unit 2

Interpretation: Loessic cap with bioturbated clasts

Site: N7
Coordinates: N44.27021 W112.91881
GPS elevation: 2224m

Soil Horizons
A: 0 – 20cm
Fine pebble silt loam
Granular
Mild HCl reaction
10 YR 6/4 – Light yellowish brown
roots present
ABk1 20 – 34cm
Pebbly silt loam
Platy textures; little granular
weak – moderate HCL reaction
10 YR 6/4 – Light yellowish brown
Gradual contact between A – ABk1; boundary defined by roots
Bk2 34 – 66cm
Pebbly silt loam
Weakly granular
Strong HCl reaction
abrupt lower contact
10 YR 7/2 – Light gray
Bk3: 66 -96cm
Pebble cobble gravel
No soil structure
Carbonate pendants present
Stage II
10 YR 6/2 – Light brownish gray
Gradual lower contact based on carbonate pendants
Bk4: 96 – 150cm
Pebble gravel
Thinner carbonate pendants than Bk3
No soil structure
10 YR 6/3 – Pale brown

USU-3405
Fan unit: Qaf3
OSL age: 63.99 ± 6.99 ka
Sample depth: 1.3 m

Sedimentary Units
Unit 1: 0 – 55cm
Pebble gravel with occasional cobbles
Stratified and roughly layered
Larger clasts are imbricated
Subrounded clasts
Moderately well sorted
Interpretation: Sheet flow; washed

Unit 2: 55-90cm
Pebble cobble gravel
Bottom of Unit 2; subdivided into two beds
bed 1: Mostly large pebble to small cobble clasts in a fine matrix
Matrix supported; Poorly sorted
Debris flow (20cm thick)
bed 2: Coarse gravel
clasts supported
Moderately sorted
Interpretation: Bed 1 is a debris flow and bed 2 is a coarse fluvial deposit

Unit 3: 90 -130cm
Matrix supported
Silty pebbly gravel
randomly oriented clasts
Poorly sorted
Interpretation: soil modified gravel with loess

Unit 4: 130 – 150cm
Silt with small pebbles
Matrix supported
Very poorly sorted
Interpretation: Soil with loessic cap

Site: N6
Coordinates: N44.26730 W112.91616
GPS elevation: 2228m

Soil Horizons

A: 0 – 22cm
- Silt loam with some pebbles
- Mild HCl reaction
- Granular
- Roots throughout
- 10 YR 5/3 – Brown
- Basal clear because of roots

Bk1: 22-46cm
- Silty pebble gravel
- Moderate HCl reaction
- No structure

10 YR 6/3 – Pale brown
- Diffuse basal boundary

Bk2: 46 – 74cm
- Pebble gravel
- No soil structure
- Stage I carbonate
- 10 YR 7/2 – Light gray
- Basal contact seen as carbonate sits between clasts

CBk3: 74 – 155cm
- Pebble gravel with minor carbonate
- No soil structure
- 10YR 6/2 – Light brownish gray

USU-3406
Fan unit: Qaf1
OSL age: 16.78 ± 2.09 ka
Sample depth: 1.55 m

Sedimentary Units

Unit 1: 0 – 1.15 m
- Pebble cobble gravel
- Imbrication of clasts
- Clasts supported
- Subrounded clasts
- Couplets of coarsening and fining upwards
- The coarsening sequences are thicker than the finer sequences

Interpretation: Sheet floods, fluvial influence

Unit 2: 1.20 – 1.40 m
- Massive matrix supported pebble gravel
- Silty fine sand matrix
- No orientation of clasts
- Subrounded – subangular clasts

Interpretation: Soil developed from gravels with loess addition; Bioturbation present

Unit 3: 1.40 – 1.55 m
- Pebbly silt
- Massive
- Finder clasts than Unit 2
- More angular clasts than Unit 2

Interpretation: Loessic cap and soil

Site: N14
Coordinates: N44.26898 W112.91235
GPS elevation: 2255m

Soil Horizons

A: 0-14cm
- Silt loam with pebbles
- Granular
- Roots throughout
- Mild HCl reaction
- 10 YR 5/3 – Brown

ABk1: 14 – 32cm
- Silt loam with more pebbles than A
- Granular; weakly plated
- Mild – moderate HCl reaction
- Boundary contact with A is defined by roots and texture
- 10 YR 6/4 – Light yellowish brown

Bk2: 32 – 50cm
- Pebbly silt loam
- Weakly granular
- Moderate – strong HCl
- Gradual boundary with ABk1
- 10 YR 7/3 – Very pale brown

Bk3: 50 – 78cm
- Silty pebble gravel
- No soils structure
- Basal boundary defined by less silt; no carbonate pendants
- 10 YR 7/2 – Light gray

Bk4: 78 – 134cm
- Pebble gravel
- No soil structure
- Stage I + carbonate
- Basal boundary defined by reduction of carbonate
- 10 YR 7/2 – Light gray

CBk5: 134 – 165cm
- Pebble cobble gravel
- No soil structure
- Lack of pedogenic rinds
- 10 YR 6/2 – Light brownish gray

USU-3407
Fan unit: Qaf1
OSL age: 18.63 ± 2.20 ka
Sample depth: 1.5 m

Sedimentary Units

Unit 1: 0 – 85cm
- Pebble cobble gravel
- Couplets of fining and coarsening upwards
- Clast supported
- Subrounded clasts
- imbricated clasts

Interpretation: Sheet flood cooping alluvial fan gravel

Unit 2: 85 – 135cm
- Matrix supported pebble gravel with some cobble
- Clasts have different orientations
- subrounded to subangular clasts

Interpretation: Soil influenced bioturbated with loess addition

Unit 3: 135 – 165cm
- Massive matrix pebbly silt
- No orientation of clasts
- Smaller pebbles than Unit 2
- Sandy silty matrix
- Subrounded clasts

Interpretation: Soil developed in loess cap over alluvial gravel with bioturbation

Site: N4
Coordinates: N44.26674 W112.91403
GPS elevation: 2238m

Soil Horizon

A: 0 – 20cm
- Silt loam with pebbles
- Granular
- Abundance of roots
- Mild reaction to HCl
- 10 YR 6/3 – Pale brown

ABk1: 20 – 38cm
- Silt loam with more pebbles than the A horizon
- Granular
- Moderate HCl reaction
- Some roots
- 10 YR 6/4 – Light yellowish brown

Bk2: 34- 62cm
- Silty pebble gravel with loam
- Subangular blocky texture
- Carbonate coats on clasts
- 10 YR 7/2 – Light gray
- Basal contact based on color and matrix

Bk3: 62 – 110cm
- Pebble gravel
- No soil structure
- Stage II carbonate
- 10 YR 7/1 – Light gray
- Basal contact diffuse of carbonate

CBk4: 110 – 160cm
- Pebble gravel
- No soil structure
- Some carbonate pendants
- 10 YR 6/2 – Light brownish gray

USU-3408
Fan unit: Qaf4
OSL age: 93.7 ± 11.8 ka
Sample depth: 1.5 m

Sedimentary Units

Unit 1: 0 – 1m
- Clast supported
- Pebble gravel with cobbles
- Clasts are imbricated
- Subrounded clasts
- Coarsening and fining sequences and equal in thickness
- Incision on unit where it is consistent

Interpretation: Sheet flood deposit alluvial gravel with the occasional debris flow incision

Unit 2: 1 – 1.25m
- Matrix, massive pebble, gravel
- Weak imbrication
- Matrix is fine silty sand
- Weakly stratified
- Same pebble size as Unit 1 but larger clasts are less present

Interpretation: Soil influence bioturbated with loess addition

Unit 3: 1.25 – 1.60 m
- Matrix supported
- Pebbly silt
- Fine sand to silty
- Smaller pebbles than Unit 2
- Randomly oriented
- Poorly sorted

Interpretation: Soil developed in loess cap

Site: N5
Coordinates: N44.26759 W112.91206
GPS elevation: 2262 m

Soil Horizons
A: 0 – 20cm
Silty loam with small pebbles
Granular
Ample roots
Mild HCl reaction
Basal contact defined by lack of roots
10 YR 6/3 – Pale brown
ABk1: 20 – 44cm
Silty loam with pebbles clasts larger than A horizon
Granular
Less roots than A horizon
Moderate HCl reaction
Basal contact defined by silt loam
10 YR 6/4 – Light yellowish brown
Bk2: 44 – 66cm
Pebble gravel with silt loam
No soil structure
Carbonate coating present
Strong HCl reaction
10 YR 8/2 – Very pale brown
Basal contact defined by increase of carbonate
Bk3: 66 -126cm
Pebble gravel with some cobble
No soil structure
Strong HCl reaction
Prominent mammillary on rinds
Stage II carbonate
Basal contact defined by diffusion of carbonate
10 YR 6/2 – Light brownish gray
CBk4: 126 – 150cm
Pebble gravel
No soil structure
10 YR 6/2 – Light brownish gray

USU-3409
Fan unit: Qaf4
OSL age: 83.82 ± 8.73 ka
Sample depth: 1.4 m

Sedimentary Units
Unit 1: 0 – 1.05m
Pebble gravel with some cobbles
Clast supported
Imbricated clasts
Couplets of fine and coarse grained
Subrounded clasts
Well – moderately sorted
Interpretation: Sheet flood deposit with alluvial gravel

Unit 2: 1.05 – 1.32m
Matrix supported pebbly silt
Massive
Poorly sorted
Subrounded clasts
Randomly oriented clasts
Coarse to fine sand silt matrix
Interpretation: Bioturbated soil developed with loess from Unit 1

Unit 3: 1.32 – 1.50m
Pebbly silt, clasts are smaller than Unit 2
Massive, poorly sorted
Interpretation: Loessic cap with soil development

Site: N8
Coordinates: N44.27089 W112.91474
GPS elevation: 2258m

USU-3410
Fan unit: Qaf3
OSL age: 73.84 ± 7.79 ka
Sample depth: 1.2 m

Soil Horizons
A: 0 – 16cm
- Silt loam with pebbles
- Granular
- Roots throughout
- Mild HCl reaction
- 10 YR 5/4 – Yellowish brown

ABk1: 16 – 32cm
- Silt loam with more pebbles than the A horizon
- Granular
- Less roots than the A horizon
- 10 YR 6/4 – Light yellowish brown

Bk2: 32 – 60cm
- Pebble gravel with silt loam matrix
- No soil structure
- some roots present
- Strong reaction to HCl
- Basalt contact due to increase of carbonate present
- 10 YR 8/2 – Very pale brown

Bk3: 60 – 104cm
- Pebble gravel
- No soil structure
- Stage II + carbonate
- No roots
- 10 YR 7/2 – Light gray

CBk4: 104 – 145cm
- Pebble gravel
- No soil structure
- 10 YR 6/3 – Pale brown

Sedimentary Units
Unit 1: 0 – 0.85 m
- Pebble gravel with some cobbles
- Mostly clast supported
- Imbricated clasts
- Couplets of coarsening and fining
- Subrounded clasts
- Moderately sorted

Interpretation: Alluvial fan gravel with fluvial influence

Unit 2: 0.85 -1.15 m
- Matrix supported
- Massive gravel
- Large pebbles with very few cobbles
- Undulating basal contact
- Silty sand matrix
- Poorly sorted
- Random oriented clasts
- Coarser clasts than Unit 1

Interpretation: Bioturbated soil influenced loess addition

Unit 3: 1.15 – 1.45m
- Silt with small pebbles large at basal contact
- Massive
- Pebbles are smaller than Unit 2

Interpretation: Soil in loess cap

Site: N16
Coordinates: N44.26945 W112.91393
GPS elevation: 2254

Soil Description
A: 0 – 22cm
Silt loam with pebbles
Granular
Roots present
Mild reaction to HCl
Basal contact defined by roots and HCl
10 YR 5/4 – yellowish brown
Bk1: 22 – 36cm
Silt loam with more pebbles than the A horizon
Granular
Strong reaction to HCl
10 YR 7/3 – Very pale brown
Bk2: 36 – 66cm
Pebble gravel with silt loam matrix
Carbonate rinds present
No soil structure
Few roots
10 YR 7/3 – Very pale brown
Bk3: 66 – 100cm
Pebble gravel
No soil structure
Stage II carbonate
Basal contact defined by lack of rinds
10 YR 7/2 – Light gray
CBk4: 100 – 160cm
Pebble cobble gravel
No soil structure
Some boulders present
10 YR 6/2 – Light brownish gray

USU-3411
Fan unit: Qaf2
OSL age: 50.97 ± 5.43 ka
Sample depth: 1.4 m

Sedimentary Units
Unit 1: 0 – 0.85m
Pebble cobble gravel with boulders
Clast supported
Subrounded clasts
Slightly stratified
Some imbrication
Moderately sorted
Interpretation: Fluvial influenced gravel

Unit 2: 0.85 – 1.25m
Weakly stratified
Matrix supported
Pebble gravel with some cobble
Fine silt and fine sand matrix
Poorly to moderately sorted
Subrounded clasts
Gradual basal contact
Interpretation: Soil disturbed with loess addition

Unit 3: 1.30 – 1.60m
Pebbly silt
Massive
Poorly sorted
Gradual contact
Interpretation: Soil with loess cap and bioturbated

Site: BD1
Coordinates: N44.12293 W112.85955
GPS elevation: 1916

Soil Horizons

A: 0 – 20cm
- Silty loam with pebbles
- Granular
- Mild HCl
- Roots
- 10 YR 6/2 – Light yellowish brown
- Basal contract change in color; roots

Bk1: 20 – 60cm
- Silty pebble gravel
- Weakly granular
- Moderate HCl reaction
- Diffuse basal contact
- 10 YR 6/3 – Pale brown

Bk2: 60 – 112cm
- Pebble gravel
- No soil structure
- Loss of roots
- Basal defined as beginning of carbonate
- 10 YR 6/2 – Light brownish gray

Bk3: 112 – 160cm
- Pebble gravel
- No soil structure
- Stage I carbonate
- 10 YR 6/2 – Light brownish gray

USU-3412
Fan unit: Qaf1
OSL age: 17.03 ± 2.28 ka
Sample depth: 1.3 m

Sedimentary Units

Units 1: 0 – 90cm
- Clast supported pebbled gravel with occasional cobble
- Coarsing and finding upwards
- Subrounded – rounded larger clasts
- Moderate to poorly sorted
- Weakly stratified
- Imbrication

Interpretation: Fluvial influenced alluvial fan deposit

Unit 2: 90 – 130cm
- Pebbly gravel with silty matrix
- Matrix supported
- Weakly stratified
- Subrounded – subangular clasts

Interpretation: Soil influenced bioturbated gravel with loess addition

Unit 3: 130 – 150cm
- Silty pebbly gravel
- Massive
- Pebbles are suspended in matrix
- Random orientation
- Subrounded clasts
- Fewer clasts than Unit 2

Interpretation: Soil developed on loessic cap and bioturbated

Site: BD2
Coordinates: N44.12196 W112.85632
GPS elevation: 1924m

Soil Horizons

A: 0 – 14cm
- Silty loam with pebbles
- Granular
- Abundance of roots
- Mild reaction to HCl
- Basal contact defined by lack of roots and HCl reaction
- 10 YR 6/3 – Pale brown

ABk1: 14 – 36cm
- Silty loam with more pebbles than the A horizon
- Weakly granular
- Moderate reaction to HCl
- 10 YR 6/4 – Light yellowish brown

Bk2: 36 – 58cm
- Pebble gravel with some loam
- No soil structure
- Very strong reaction to HCl
- Stage II carbonate
- 10 YR 7/2 – Light gray

Bk3: 60 – 90 cm
- Pebble gravel
- No soil structure
- less carbonate rinds than Bk2
- 10 YR 6/2 – Light brownish gray
- Basal contact defined by color

CBk4 90 – 160cm
- Pebble gravel
- No soil structure
- Less carbonate
- 10 YR 6/3 – Pale brown

USU-3413
Fan unit: Qaf3
OSL age: 75.85 ± 7.52 ka
Sample depth: 1.3 m

Sedimentary Units

Unit 1: 0 – 1.05 m
- Pebble gravel with cobbles
- Moderately sorted
- Clast supported
- Fining and coarsening upward sequences
- Subrounded clasts

Interpretation: Alluvial deposit with fluvial deposits

Unit 2: 1.05 – 1.45m
- Pebble gravel with fine silty sand matrix with cobbles
- Matrix supported
- Some clasts have random orientation
- Subrounded – subangular clasts

Interpretation: Soil developed in gravel pedogenic disturbance; bioturbated by roots with loess addition

Unit 3: 1.45 – 1.60 m
- Silty pebble gravel
- Fine silty matrix
- Random orientation of clasts
- Pebble clasts smaller than Unit 2
- Poorly sorted

Interpretation: Soil developed in loess cap and bioturbation

Site: BD3
Coordination: N44.11869 W112.85045
GPS elevation: 1921 m

Soil Horizons

A 0 – 16cm
- Mild HCl reaction
- Silty loam with pebbles
- Granular
- Abundance of roots
- 10 YR 6/3 – Pale brown
- Basal contact defined by HCl; less roots; different texture

ABk1 16 – 28cm
- Silty loam with pebbles, more than A
- Granular
- Less roots, moderate HCl reaction
- 10 YR 6/3 – Pale brown
- Basal contact carbonate increase and change in color

Bk2 28 – 58cm
- Pebble gravel with silty loam
- Weakly granular
- Less roots than ABk1
- 10 YR 7/3 – very pale brown
- Basal contact defined by carbonate increase

Bk3 58 – 90 cm
- Pebble gravel
- No soil structure
- Stage II +
- 10 YR 6/3 – Pale brown
- Basal contact diffuse and less carbonate and color change

CBk4 90 – 160cm
- Pebble gravel
- No soil structure
- Some carbonate present
- 10 YR 6/3 – Pale brown (could also be 6/4)

USU-3414
Fan unit: Qaf5
OSL age: 110.8 ± 11.3 ka
Sample depth: 1.5 m

Sediment Units

Unit 1: 0 – 0.75m
- Pebble cobble gravel with some boulders
- Clasts supported
- Subrounded clasts
- Overall fining upwards
- Moderately sorted
- Imbricated clasts

Interpretation: Alluvial deposit with fluvial deposit

Unit 2: 0.75 – 1.35 m
- Overall matrix supported pebble gravel with cobbles
- Some stratification towards the base of unit
- Subrounded clasts
- Weak imbrication
- Silty to fine sand matrix

Interpretation: Soil developed from gravel bioturbated with loess addition

Unit 3: 1.35 – 1.60 m
- Silty with pebbles
- Massive
- Matrix supported
- Random orientation of clasts
- Silty to fine sand matrix

Interpretation: Soil developed in loess cap and bioturbated with roots

Site: BD5
Coordinates: N44.11468 W112.83551
GPS elevation: 1937m

Soil Horizons

A: 0 – 18 cm
- Silty loam with pebble
- Granular
- Mild HCl reaction
- Abundance of roots
- 7.5 YR 5/4 – Brown
- Basal contact defined by lack of loam, HCl, and less roots

ABk1: 18 – 30cm
- Silty loam with more pebbles than A
- Weakly granular
- Less bioturbated than A
- Moderate HCL reaction
- 7.5 YR 6/3 – light brown
- Basal contact defined by loss of loam and carbonate

Bk2: 30 – 68cm
- Silty pebble gravel with loam
- No soil structure
- Beginning of carbonate accumulation
- Strong HCl reaction
- 7.5 YR 8/1 – White
- Basal contact defined by color and more carbonate

Bk3: 68 – 118cm
- Pebble gravel with loam
- No soil structure
- Carbonate present
- 7.5 YR 7/2 – Pinkish gray

Bk4: 118 – 170cm
- Pebble gravel
- No soil structure
- Carbonate rind accumulation
- Stage II
- 7.5 YR 7/3 – Pink

USU-3415
Fan unit: Qaf3
OSL age: 61.01 ± 6.96 ka
Sample depth: 1.5 m

Sedimentary Units

Unit 1: 0 – 0.75m
- Pebble gravel with some cobble
- Clast supported
- Subrounded clasts
- Imbrication
- Sequences fining upwards
- 2 – 3 pea gravel lenses

Interpretation: Alluvial deposits with fluvial influence

Unit 2: 0.75 – 1.5m
- Matrix supported pebble gravel with cobbles
- Clasts are more randomly oriented
- Fining upwards sequences
- Silty find sand matrix

Interpretation: Soil development in gravel; bioturbated with loess addition

Unit 3: 1.5 – 1.7 m
- Silt with pebbles
- Pebbles are smaller than Unit 2
- Subrounded clasts
- Find sand matrix

Interpretation: Soil developed in loessic cap with bioturbation

Site: BD6
Coordinates: N44.11529 W112.83236
GPS elevation: 1993m

Soil Horizons
A: 0 – 8cm
Silty loam with pebble
Granular structure
Mild HCl;
Roots
7.5 YR 5/3 – Brown
Basal contact defined by HCl and less roots and loam
ABk1: 8 – 22cm
Silty loam with more pebbles than A
Granular
Moderate HCl reaction
Root bioturbation
7.5 YR 6/3 – Light brown
Basal defined by carbonate and color change
Bk2: 22 – 58cm
Pebble gravel with traces of loam
No structure
Strong HCl reaction
Carbonate present
10 YR 8/1 – White
Basal contact defined color change and texture change
Bk3: 58 – 78cm
Silty gravel loam with small pebbles
No soil texture
Carbonate is less present
7.5 YR 6/3 – light brown
Basal contact was defined by carbonate rinds
Bk4: 78 – 114cm
Pebble gravel with some cobbles
No soil structure
Stage I carbonate development
7.5 YR 7/2 – Pinkish gray
Basal contact defined by less carbonate
CBk5: 114 – 136cm
Pebble gravel (small pebbles)
No soil structure
Lack of carbonate
10 YR 7/3 – very pale brown
Basal contact defined by color
CBk6: 136 – 160cm
pebble gravel with loam
No soil structure
Paleo soil?
Less carbonate
10 YR 8/2 – very pale brown
(looks pink by the human eye)

USU-3416
Fan unit: Qaf3
OSL age: 78.99 ± 7.59 ka
Sample depth: 1.5 m

Sedimentary Units
Unit 1: 0 – 0.25m
Clast supported
Pebble gravel
Fine to silty matrix
Imbricated clasts
Interpretation: Alluvial deposit could be a weak paleosol

Unit 2: 0.25 – 0.45m
Pea pebble gravel
Rounded clasts
Clast supported
Well sorted
Fine sand matrix
Interpretation: Localized channel fill or sheet flood deposit

Unit 3: 0.45 – 0.85m
Clast supported pebble gravel with cobbles
Random orientation of clasts
Undulating contact from below
Subrounded – subangular clasts
Fine silty sand matrix
Interpretation: Soil developed from below with alluvial deposit

Site BD6 continued

Unit 4: 0.85 – 1.35 m

Matrix supported
Pebble gravel
Coarsening upwards sequence
Random orientation of clasts
Subrounded – subangular clasts

Interpretation: Soil development in gravel; in a channel flow

Unit 5: 1.35 – 1.60m

Matrix silt with pebbles
Slight fining upwards
Subrounded – subangular clasts
Fine silty sand matrix

Interpretation: Soil developed in loessic cap with bioturbation

Site: BD7
Coordinates: N44.11334 W112.82969
GPS elevation: 1924 m

Soil Horizons

A: 0 – 26cm
- Silty loam with pebbles
- Granular structure
- Mild HCl reaction
- Abundance of roots
- 10 YR 5/3 – Brown
- Basal contact by less roots stronger HCl reaction and lighter color change

ABk1: 26 – 46cm
- Silty loam with pebble with some larger clasts
- Weakly granular
- Moderate HCl reaction
- Less roots
- 10 YR 6/4 – Light yellowish brown
- This horizon could just be a Bk1
- Basal contact defined by color increase carbonate less loam and less roots

Bk2: 46 – 80cm
- Pebble gravel with loam
- No soil structure
- Carbonate appears
- 10 YR 8/2 – Very pale brown
- Basal contact defined by color and increase of carbonate coatings

Bk3: 80 – 118cm
- Pebble gravel with loam
- No soil structure
- 10 YR 8/2 – Very pale brown looks white

Bk4: 118 – 154 cm
- Pebble gravel
- No soil structure
- Stage I
- 10 YR 6/4 – Light yellowish brown
- Basal contact defined by diffused carbonate

CBk5: 154 – 180cm
- Pebble gravel
- No soil structure
- Diffuse of carbonate
- 10 YR 7/3 – very pale brown

USU-3417
Fan unit: Qaf3
OSL age: 66.30 ± 6.39 ka
Sample depth: 1.6 m

Sedimentary Units

Unit 1: 0 – 80cm
- Pebble gravel with few cobbles
- Subrounded – subangular clasts
- Fine sand matrix
- Clast supported
- Imbrication
- Stratified

Interpretation: Alluvial deposit with channel fill deposits

Unit 2: 0.80 – 1.55m
- Matrix supported
- Pebble gravel with some cobbles
- Lower portion of the unit is weakly stratified
- Subrounded clasts
- Fine silty sand matrix
- Basal contact gradual and slightly undulates

Interpretation: Soil developed on gravel with some root bioturbation with loess

Unit 3: 1.55 – 1.80m
- Massive
- Matrix supported silt with pebbles
- Smaller pebbles than Unit 2
- Fine sand silty matrix

Interpretation: Soil developed on loess cap with bioturbation

Site: BD8
Coordinates: N44.10770 W112.82651
GPS elevation: 1892 m

Soil Horizons

A: 0 – 16cm
- Silt loam with pebbles
- Granular
- Mild HCl reaction
- Abundance of roots
- 10 YR 6/5 – Light brown
- Basal contact defined by HCl, diffuse of roots

ABk1: 16 – 36cm
- Silt loam with pebbles and some cobbles
- Weakly granular
- Moderate HCl reaction
- Cobbles have rinds
- Stage I +
- Will not sample here due for constancy
- 10 YR 7/3 – Very pale brown
- Basal contact diffuse of loam and increase carbonate

Bk2: 36 – 108cm
- Pebble gravel with loam and cobbles
- No soil structure
- Stage I + carbonate
- Variable carbonate
- 7.5 YR 7/3 – Pink

Bk3: 108 – 165cm
- Pebble gravel
- No soil structure
- 10 YR 7/4 – very pale brown

USU-3418
Fan unit: Qaf4
OSL age: 74.06 ± 7.45 ka
Sample depth: 1.45 m

Sedimentary Units

Unit 1: 0 – 0.65m
- Pebble gravel with cobble
- Clast supported
- Imbricated clasts
- Coarsining and fining upwards sequences
- Fine silty sand matrix
- Subrounded – subangular clasts

Interpretation: Alluvial fan deposits with some fluvial influence

Unit 2: 0.65 – 1.35m
- Matrix supported
- Pebble gravel with some cobble
- Clasts are slightly imbricated
- Fine silt matrix
- Subrounded clasts
- Overall massive
- Pea gravel pod (10cm thick)
- Basal contact is gradual

Interpretation: Soil developed in gravel with loess with bioturbation

Unit 3: 1.35 – 1.65m
- Matrix supported silt with pebbles
- Some cobbles on the lower portion of the unit
- Clasts are suspended
- Fine silty sand matrix

Interpretation: Siol developed in loessic cap with heavy root bioturbation and cobble lag

Site: BD09
Coordinates: N44.10220 W112.82678
GPS elevation: 1862m

USU-3419
Fan unit: Qaf1
OSL age: 16.01 ± 1.77 ka
Sample depth: 1.35 m

Soil Horizons

A: 0 – 26cm
- Silt loam with pebbles
- Granular
- Mild HCl reaction
- Abundance of roots
- 10 YR 6/3 – Pale brown
- Basal contact defined by decrease loam, increase of class, decrease of roots

ABk1: 26 – 52cm
- Silt loam with increase of pebbles and some cobbles
- Granular
- Moderate HCl reaction
- Roots are present
- Suspended large clasts have carbonate rinds
- 10 YR 6/3 – Pale brown
- Basal contact defined by carbonate rind increase and color change

Bk2: 52 – 78cm
- Pebble gravel with cobbles, few boulders
- No soil structure
- Stage I +
- 10 YR 6/2 – Light brownish gray
- Basal diffuse of carbonate and color change

Bk3: 78 – 110cm
- Pebble cobble gravel with some boulders
- No soil structure
- Rinds are present
- 10 YR 4/3 – Brown

C: 110 – 155cm
- Pebble cobble gravel with boulders
- No soil structure
- 10 YR 5/3 – Brown

Sedimentary Units

Unit 1: 0 – 1.10m
- Bouldery pebble cobble gravel
- Subrounded clasts
- Very variable clasts sizes
- Imbricated clasts
- Stratified in portions

Interpretation: High flow (debris?) alluvial deposit or channel flow

Unit 2: 1.10 – 1.35m
- Matrix supported pebble gravel with cobbles
- Fine silty sand matrix
- Random orientation of clasts
- Some stratification

Interpretation: Soil developed in pebble gravel with root bioturbation

Unit 3: 1.35 – 1.55 m
- Matrix supported, massive, silt with pebbles
- Pebbles are smaller than Unit 2
- Fine silty sand matrix

Interpretation: Soil developed in loessic cap with bioturbation

Site: BD16
Coordinates: N44.10216 W112.82141
GPS elevation: 1871m

Soil Horizons

A: 0 – 12cm
- Silt loam with pebbles
- Granular structure
- Mild HCl reaction
- Bioturbated with roots
- 10 YR 6/5 - Brown

ABk1: 12 – 30cm
- Silt loam with increase of pebbles
- Weakly granular
- Moderate HCl reaction
- Less rocks
- 10 YR 6/4 – Light yellowish brown

Bk2: 30 – 76cm
- Pebble gravel with loam and some cobbles
- No soil structure
- Stage I
- Basal contact defined by lack of carbonate and color

CBk3: 76 – 116cm
- Pebble gravel
- No soil structure
- Slight carbonate coatings
- 10 YR 5/4 – Yellowish brown
- from 116 – 160cm no soil just sand lenses

USU-3420
Fan unit: Qaf2
OSL age: 51.79 ± 5.39 ka
Sample depth: 1.45 m

Sedimentary Units

Unit 1: 0 – 50cm
- Clast supported pebble gravel
- Silty sand lenese
- Lenticular beds of sand
- Pea gravel to fine silty sand
- Imbricated clasts
- Alternating stacks of fine gravel and sand

Interpretation: Quiet small; flow alluvial fan

Unit 2: 0.5- 0.9m
- Pebble gravel with cobbles
- Clast supported
- Lenses of pea gravel
- Fine silty sand matrix
- Imbricated clasts
- Fining upwards sequence overall

Interpretation: Alluvial deposit with fluvial influence

Unit 3: 0.90 – 1.50m
- Pebble gravel with cobbles clasts
- Matrix supported
- Very fine silty matrix
- Some stratigraphy but messy

Interpretation: Soil developed in gravel; bioturbated with roots and loess addition

Unit 4: 1.50 – 1.60m
- Matrix supported massive, silty with pebbles
- Clasts smaller than Unit 3
- Random orientation of clasts
- Subrounded

Interpretation: Soil development in loess cap and bioturbated

Site: BD11
Coordinates: N44.09975 W112.81622
GPS elevation: 1871 m

Soil Horizons

A: 0 16cm
- Silt loam with pebbles
- Granular texture
- Mild HCl reaction
- Bioturbated roots
- 10 YR 5/3 – Brown
- Basal contact defined loss of loam
- Stronger HCl reaction
- Less bioturbation from roots

ABk1: 16 – 32cm
- Silt loam with increase of pebbles from horizon A
- Granular texture
- Mild to moderate HCl reaction
- Less bioturbated than horizon A
- 10 YR 6/3 – Pale brown
- Basal contact with lower horizon defined by increase of HCl reaction, increase in carbonate, and decrease in roots

Bk2: 36 – 78cm
- Pebble gravel with loam
- Moderate HCl
- Very weak granular texture
- Carbonate coatings appear
- Very localized roots
- 10 YR 7/3 – very pale brown
- Basal contact defined

Bk3: 78 – 170cm
- Pebble gravel
- No soil structure
- Stage I carbonate
- Despite being a meter thick; no CBk boundary

USU-3421
Fan unit: Qaf3
OSL age: 69.64 ± 6.04 ka
Sample depth: 1.6 m

Sedimentary Units

Unit 1: 0 – 0.95m
- Pebble gravel with cobbles
- Pea gravel lenticular lenses
- Subangular clasts
- Some stratification
- Coarsening and fining upwards packages that interfinger each other

Interpretation: Alluvial deposit; channel flow into each other or flood sheet packages.

Unit 2: 0.95 – 1.40m
- Matrix supported with pockets of clast supported pebble gravel
- Weakly stratified
- Subrounded – subangular clasts

Interpreation: Soil developed in pebble gravel; bioturbation by roots with channel bed deposits

Unit 3: 1.40 – 1.70m
- Massive matrix supported silt with pebbles
- Pebbles are suspended
- Clasts smaller than Unit 2
- Fine silty sand matrix
- Random orientation of clasts

Interpretation: Soil developed in loessic cap; Bioturbated by roots

Site: BD12
Coordinates: N44.09523 W112.81144
GPS elevation: 1861

Soil Horizons
A: 0 -14cm
Silt loam with pebbles
Granular texture
Larger clasts have carbonate rinds
Mild HCl reaction
roots present
10 YR 5/4 – Yellowish brown
Basal contact defined by increase of clasts, increase of HCl, and decrease of roots
ABk1: 14 – 38cm
Silt loam with increase of pebbles
Weakly granular
Less bioturbated
Moderate HCl reaction
10 YR 6/4 – Light yellowish brown
Basal contact defined by increase HCl decrease of roots, and color change
ABk2: 38 – 74cm
Pebble gravel with very few traces of loam
No soil structure
Very localized roots
Carbonate rinds
Stage II carbonate
10 YR 8/1 – white
Basal contact defined by decrease in carbonate rinds and color change
Bk3: 74 – 114cm
Pebble gravel with cobbles
No soil structure
Carbonate rinds present but less
10 YR 7/3 – Very pale brown
Basal contact defined by increase carbonate

USU-3422
Fan unit: Qaf3
OSL age: 67.34 ± 7.52 ka
Sample depth: 1.45 m

Bk4: 114 – 160cm
Pebble gravel
No soil structure
Increase of rinds from Bk3 but not to Bk2
Groundwater influence?
10 YR 5/3 – Brown

Sedimentary Units
Unit 1: 0 – 0.90 m
Pebble gravel with large cobbles
Clast supported
Moderately sorted
Imbricated clasts
Coarsening and fining upwards sequences
Pea gravel then coarser into cobbles
Interpretation: Alluvial deposit; lower channel fill

Unit 2: 0.9 – 1.45m
Pebble gravel with some cobbles
Overall clast supported but matrix supported towards the top
Moderately sorted
Weakly stratified
Imbrication of clasts
Subrounded clasts
Coarsening and fining upwards sequence
Interpretation: Soil development with pebble gravel with some loess. Weak bioturbation

Unit 3: 1.45 – 1.60m
Massive matrix silt with some pebbles
Larger pebbles and small cobbles
Fine silty sand matrix
Poorly sorted

<u>Interpretation:</u> Soil development in loessic cap with bioturbation

APPENDIX B:

Table 2. Dose Rate Information

Sample num.	USU num.	In-situ H_2O (%)[1]	D_R sub-sample[2]	K (%)[3]	Rb (ppm)[3]	Th (ppm)[3]	U (ppm)[3]	Cosmic (Gy/ka)
BEA_LC_ 101819_01	USU-3211	6.0	F (40%)	1.09±0.03	46.7±1.9	4.7±0.4	4.1±0.3	0.27±0.03
			M (45%)	0.70±0.02	25.7±1.0	2.7±0.2	3.4±0.2	
			C (15%)	0.26±0.01	7.2±0.3	0.7±0.1	1.9±0.1	
BEA_LC_ 101819_02	USU-3212	7.8	F (40%)	1.08±0.03	48.6±1.9	4.5±0.4	4.8±0.3	0.26±0.03
			M (45%)	0.74±0.02	30.1±1.2	2.5±0.2	4.2±0.3	
			C (15%)	0.09±0.01	3.5±0.1	0.4±0.01	0.8±0.1	
N3	USU-3400	-	F (20%)	0.66±0.02	22.4±0.9	1.9±0.2	2.7±0.2	0.27±0.03
			M (40%)	0.31±0.01	11.7±0.5	1.7±0.2	1.9±0.1	
			C (40%)	0.35±0.01	10.3±0.4	1.3±0.2	1.7±0.1	
N2	USU-3401	3.1	F (40%)	0.62±0.02	22.0±0.9	2.3±0.3	2.7±0.2	0.27±0.03
			M (25%)	0.17±0.01	5.4±0.2	0.5±0.1	0.7±0.1	
			C (35%)	0.37±0.01	14.8±0.6	2.0±0.2	2.0±0.1	
N17	USU-3402	-	F (20%)	0.59±0.02	22.6±0.9	2.2±0.4	2.6±0.2	0.26±0.03
			M (25%)	0.19±0.01	6.3±0.3	0.7±0.1	1.9±0.1	
			C (55%)	0.25±0.01	7.3±0.3	0.7±0.1	1.5±0.1	
N1	USU-3403	-	F (25%)	0.48±0.03	20.2±0.8	2.2±0.5	2.2±0.2	0.26±0.03
			M (50%)	0.07±0.01	2.5±0.1	0.2±0.1	1.4±0.1	
			C (25%)	0.19±0.01	6.7±0.3	0.7±0.2	1.6±0.1	
N15	USU-3404	-	F (35%)	0.63±0.02	31.0±1.2	3.0±0.4	2.0±0.1	0.28±0.03
			M (45%)	0.20±0.01	6.4±0.3	0.8±0.1	1.6±0.1	
			C (20%)	0.18±0.01	6.3±0.3	0.6±0.1	1.8±0.1	
N7	USU-3405	-	F (20%)	0.46±0.03	22.8±0.9	2.2±0.5	1.8±0.1	0.27±0.03
			M (40%)	0.06±0.001	2.3±0.1	0.3±0.1	1.1±0.1	
			C (40%)	0.15±0.01	5.7±0.2	0.7±0.2	2.5±0.2	
N6	USU-3406	-	F (25%)	0.44±0.03	19.3±0.8	2.2±0.4	2.0±0.1	0.27±0.03
			M (50%)	0.07±0.001	2.8±0.1	0.3±0.1	1.0±0.1	
			C (25%)	0.24±0.01	11.4±0.5	1.2±0.2	1.4±0.1	
N14	USU-3407	-	F (20%)	0.42±0.03	18.0±0.7	2.0±0.5	1.7±0.1	0.27±0.03
			M (30%)	0.05±0.01	1.6±0.1	0.2±0.1	0.7±0.0	
			C (50%)	0.15±0.01	5.9±0.2	0.7±0.2	2.1±0.1	
N4	USU-3408	-	F (20%)	0.22±0.02	9.7±0.4	1.2±0.4	1.6±0.1	0.27±0.03
			M (45%)	0.05±0.01	1.5±0.1	0.2±0.1	0.7±0.1	
			C (35%)	0.15±0.02	5.7±0.2	0.7±0.2	1.6±0.1	

Sample num.	USU num.	In-situ H_2O (%)[1]	D_R sub-sample[2]	K (%)[3]	Rb (ppm)[3]	Th (ppm)[3]	U (ppm)[3]	Cosmic (Gy/ka)
N5	USU-3409	-	F (20%)	0.33±0.02	14.7±0.6	1.8±0.4	1.8±0.1	0.27±0.03
			M (45%)	0.23±0.01	6.8±0.3	0.9±0.2	1.0±0.1	
			C (35%)	0.09±0.01	3.1±0.1	0.3±0.1	1.8±0.1	
N8	USU-3410	-	F (20%)	0.39±0.03	17.5±0.7	1.9±0.5	1.8±0.1	0.28±0.03
			M (50%)	0.10±0.01	3.2±0.1	0.4±0.1	2.1±0.1	
			C (30%)	0.16±0.01	5.2±0.2	0.6±0.2	2.1±0.1	
N16	USU-3411	4.3	F (25%)	0.40±0.03	18.9±0.8	2.1±0.5	1.8±0.1	0.27±0.03
			M (35%)	0.11±0.01	4.1±0.2	0.5±0.1	2.0±0.1	
			C (40%)	0.11±0.01	3.9±0.2	0.5±0.1	2.3±0.2	
BD1	USU-3412	3.1	F (20%)	0.95±0.04	42.4±1.7	4.3±0.7	3.6±0.3	0.26±0.03
			M (40%)	0.05±0.001	1.9±0.1	0.2±0.03	1.0±0.1	
			C (40%)	0.17±0.01	6.2±0.2	0.7±0.1	1.6±0.1	
BD2	USU-3413	5.4	F (20%)	1.09±0.04	49.6±2.0	4.9±0.7	3.1±0.2	0.26±0.03
			M (60%)	0.10±0.01	4.0±0.2	0.5±0.1	1.4±0.1	
			C (20%)	0.16±0.01	5.9±0.2	0.7±0.1	1.7±0.1	
BD3	USU-3414	2.3	F (20%)	0.59±0.02	26.7±1.1	2.9±0.3	2.3±0.2	0.25±0.03
			M (45%)	0.10±0.01	3.9±0.2	0.4±0.1	1.1±0.1	
			C (35%)	0.68±0.02	21.1±0.8	2.9±0.3	2.5±0.2	
BD5	USU-3415	14.4	F (45%)	0.64±0.02	30.5±1.2	3.8±0.4	2.6±0.2	0.25±0.03
			M (40%)	0.07±0.01	2.5±0.1	0.4±0.1	1.7±0.1	
			C (15%)	0.34±0.01	13.2±0.5	1.4±0.1	2.5±0.2	
BD6	USU-3416	6.3	F (30%)	0.63±0.02	32.3±1.3	3.6±0.4	2.3±0.2	0.25±0.03
			M (70%)	0.19±0.01	7.0±0.3	0.9±0.1	1.6±0.1	
BD7	USU-3417	4.1	F (30%)	0.85±0.03	39.4±1.6	4.5±0.4	3.1±0.2	0.25±0.02
			M (60%)	0.21±0.01	9.3±0.4	1.4±0.1	2.1±0.1	
			C (10%)	0.08±0.01	3.4±0.1	0.5±0.1	1.9±0.1	
BD8	USU-3418	6.9	F (40%)	0.82±0.02	37.6±1.5	4.5±0.4	2.9±0.2	0.25±0.03
			M (40%)	0.30±0.01	12.4±0.5	1.6±0.1	2.2±0.2	
			C (20%)	0.25±0.01	11.1±0.4	1.5±0.1	2.2±0.2	
BD9	USU-3419	2.7	F (35%)	1.24±0.03	52.7±2.1	6.5±0.6	3.3±0.2	0.25±0.03
			M (40%)	0.47±0.01	17.2±0.7	2.7±0.2	2.5±0.2	
			C (25%)	0.30±0.01	8.9±0.4	2.7±0.2	2.1±0.1	
BD16	USU-3420[4]	-	F (40%)	1.00±0.03	46.5±1.9	5.4±0.5	2.8±0.2	0.25±0.02
			M (60%)	0.25±0.01	9.1±0.4	1.4±0.1	1.9±0.1	
			F (70%)	1.24±0.03	56.7±2.3	6.4±0.6	3.0±0.2	
			M (20%)	0.14±0.01	6.0±0.2	0.9±0.1	2.1±0.1	
			C (10%)	0.23±0.01	8.6±0.3	1.1±0.1	1.7±0.1	

Sample num.	USU num.	In-situ H_2O (%)[1]	D_R sub-sample[2]	K (%)[3]	Rb (ppm)[3]	Th (ppm)[3]	U (ppm)[3]	Cosmic (Gy/ka)
			F (25%)	1.14±0.03	51.8±2.1	6.2±0.6	3.2±0.2	
			M (45%)	0.12±0.01	4.3±0.2	0.6±0.1	1.2±0.1	
			C (30%)	0.40±0.01	14.9±0.6	2.2±0.2	2.5±0.2	
BD11	USU-3421	-	F (40%)	1.10±0.03	54.8±2.2	5.4±0.5	1.8±0.1	0.25±0.02
			M (40%)	0.23±0.01	11.2±0.4	1.5±0.1	2.0±0.1	
			C (20%)	0.10±0.01	4.3±0.2	0.7±0.1	2.2±0.2	
BD12_	USU-3422	2.8	F (20%)	0.78±0.03	35.0±1.4	4.0±0.5	2.8±0.2	0.25±0.02
			M (45%)	0.16±0.01	6.4±0.3	0.7±0.1	1.1±0.1	
			C (35%)	0.19±0.01	8.6±0.3	1.1±0.1	1.3±0.1	

[1] Assumed 7.0±2.1% as moisture content over burial history. No field moisture sample was collected where no value is reported.

[2] Dose rate subsamples based on weighted proportions (%) of grain size subsamples: fine-F (<1.7 mm), medium-M (1.7-16 mm), coarse-C (>16 mm), and used with chemistry in beta and gamma dose rate calculation.

[3] Radioelemental concentrations determined using ICP-MS and ICP-AES techniques; dose rate is derived from concentrations by conversion factors from Guérin et al. (2011).

[4] Chemistry incorporated from units above, within, and below D_E sample unit, respectively.

<u>Equivalent dose (D_E) Distributions:</u> Probability density function, radial plot, overdispersion (OD)

USU-3211

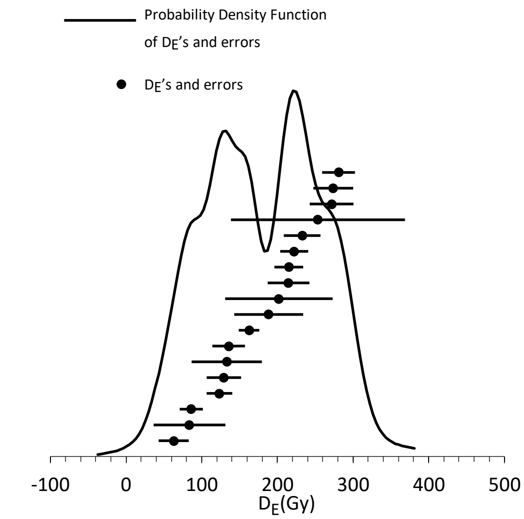

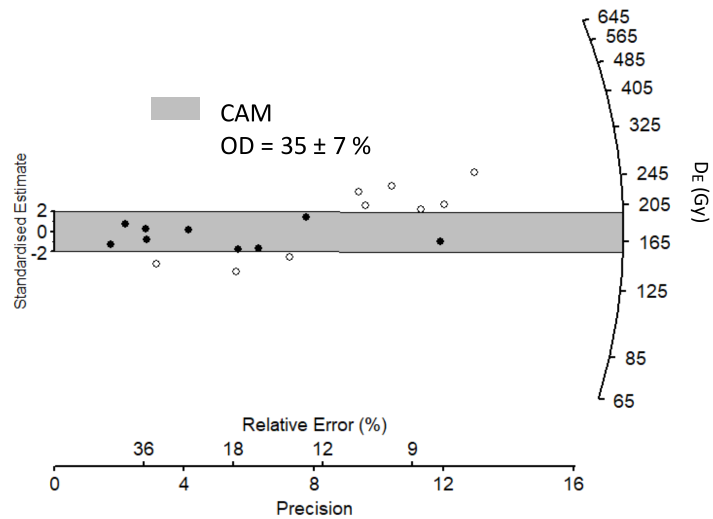

USU-3212

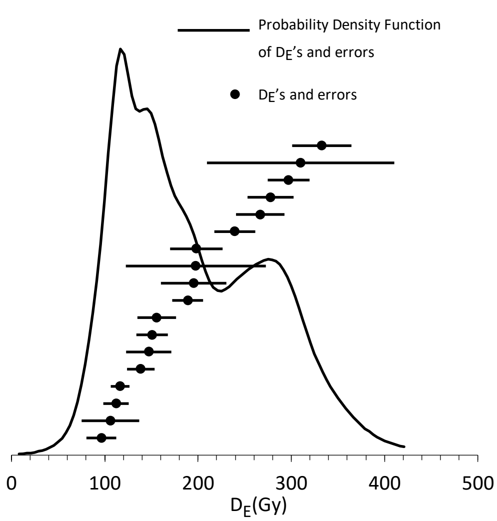

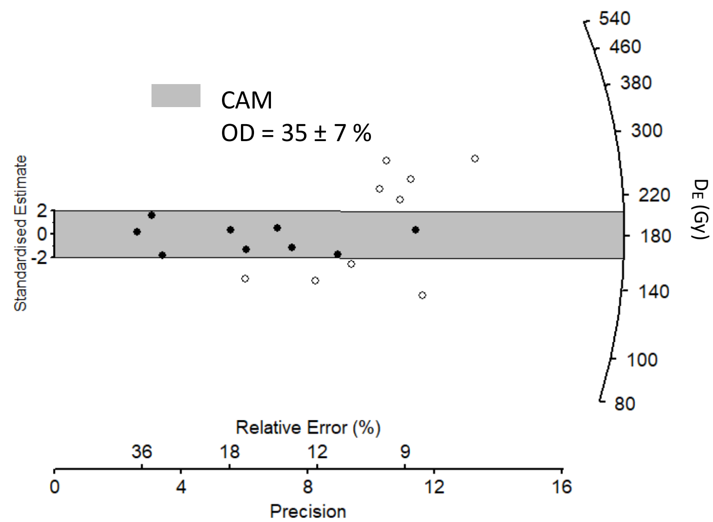

N3, USU-3400

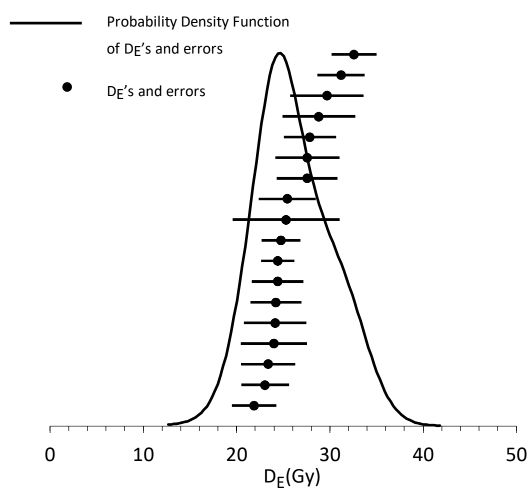

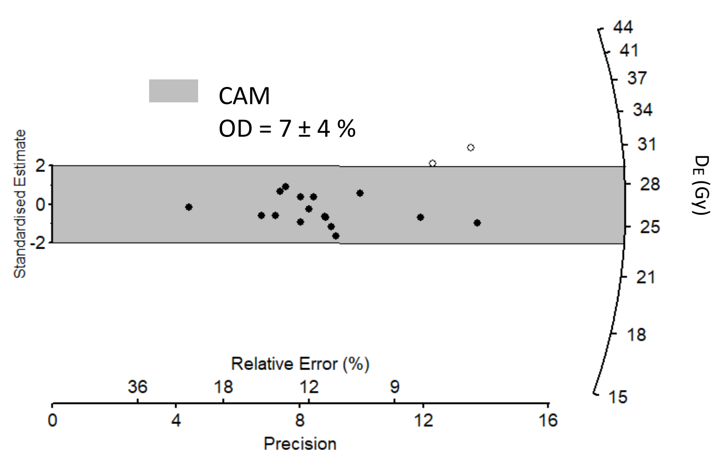

N2, USU-3401

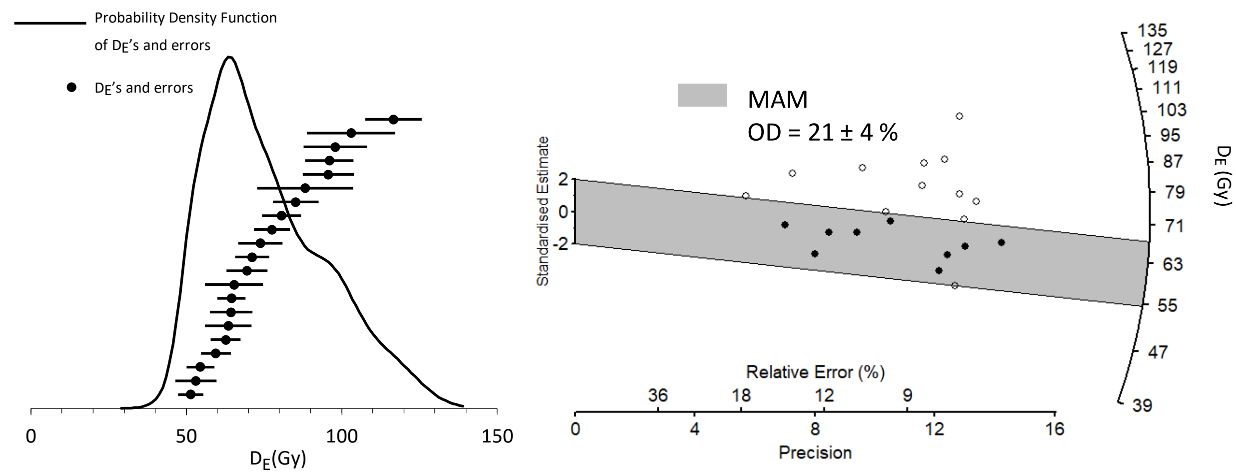

N17, USU-3402

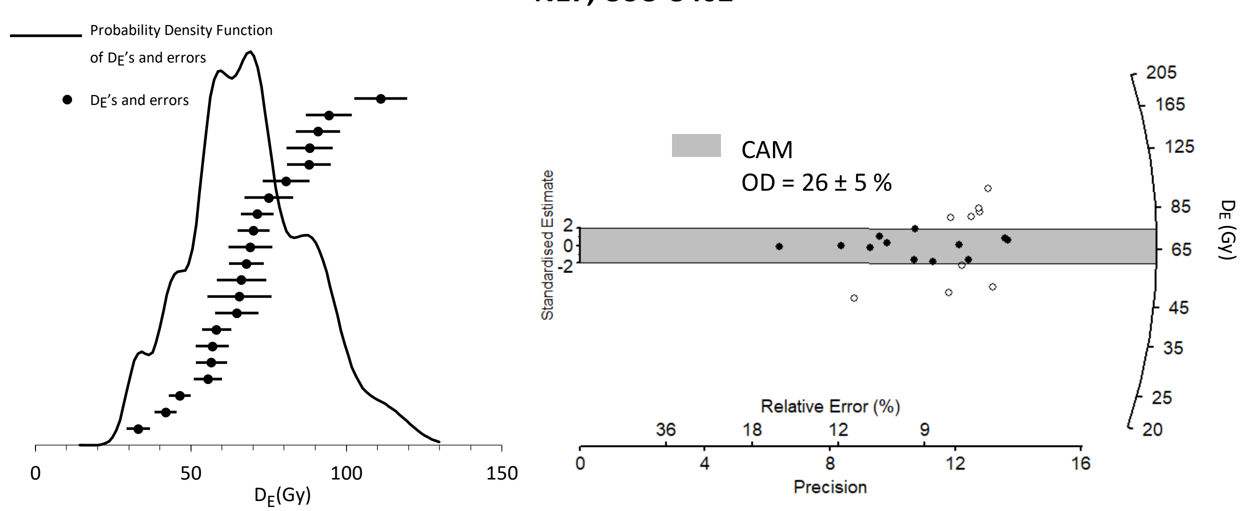

N1, USU-3403

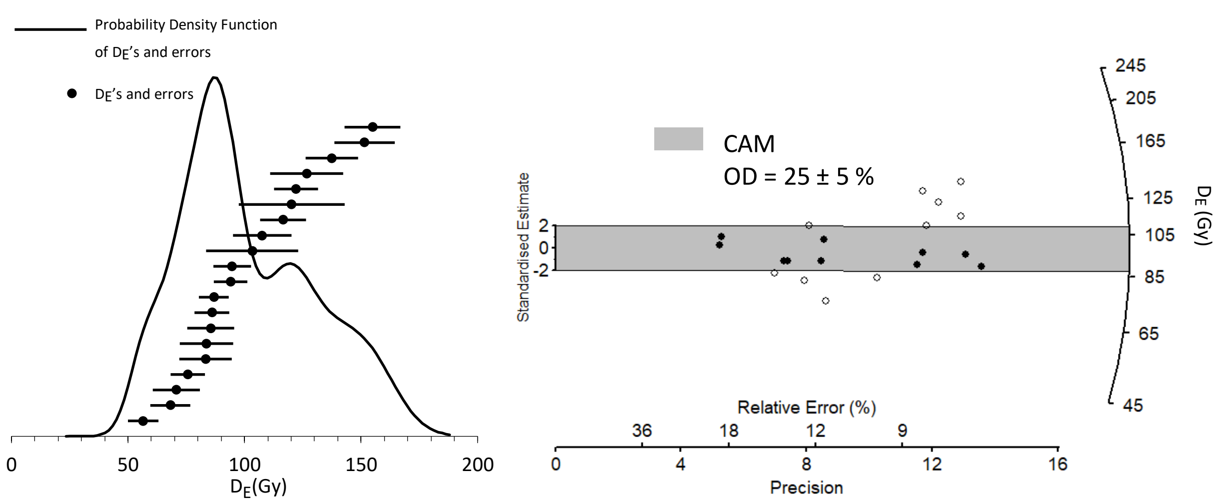

<u>Equivalent dose (D_E) Distributions:</u> Probability density function, radial plot, overdispersion (OD)

N15, USU-3404

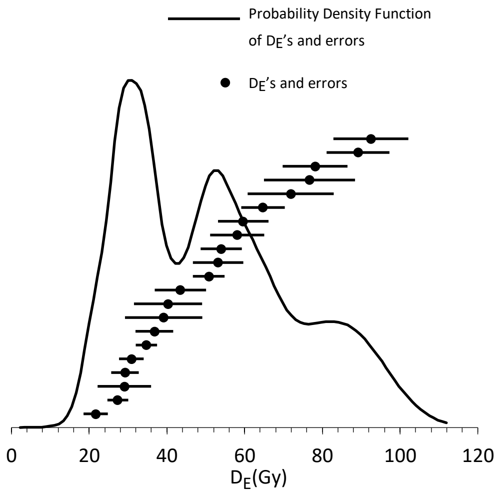

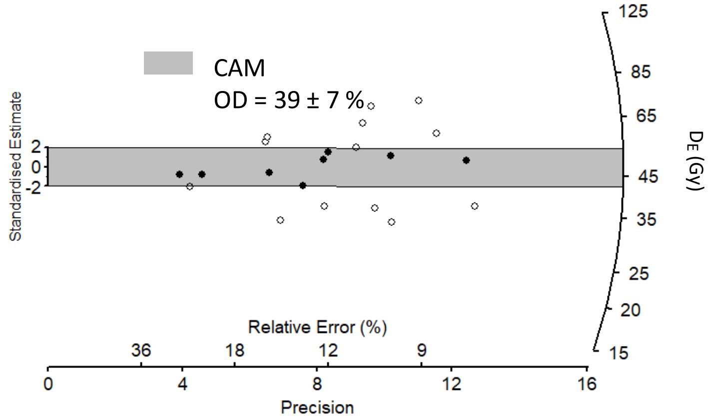

N7, USU-3405

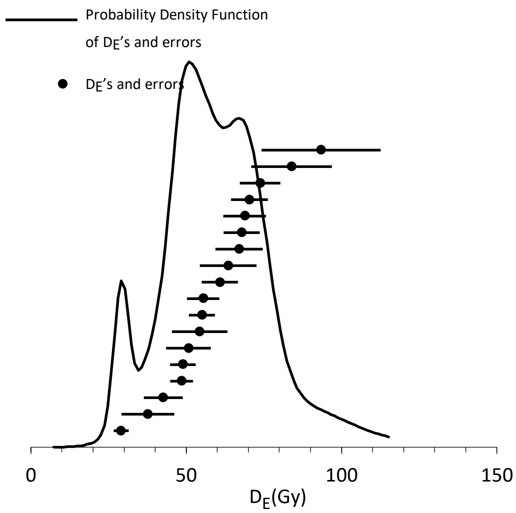

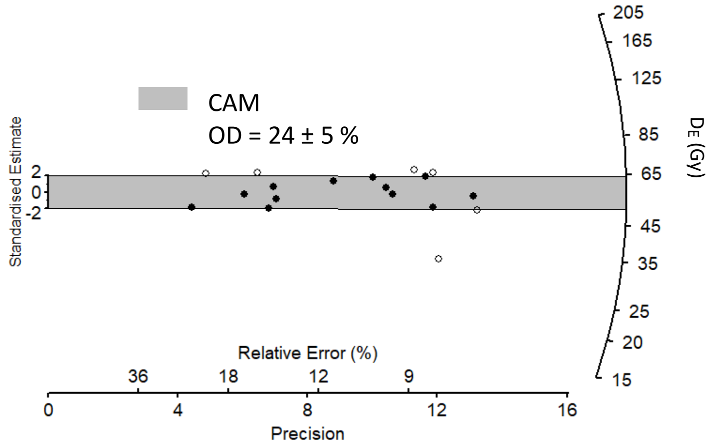

N6, USU-3406

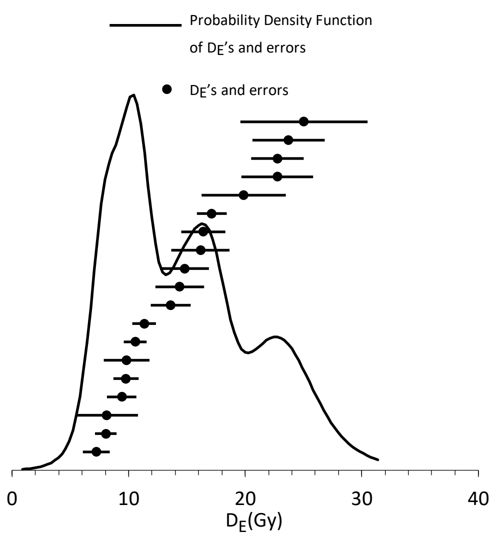

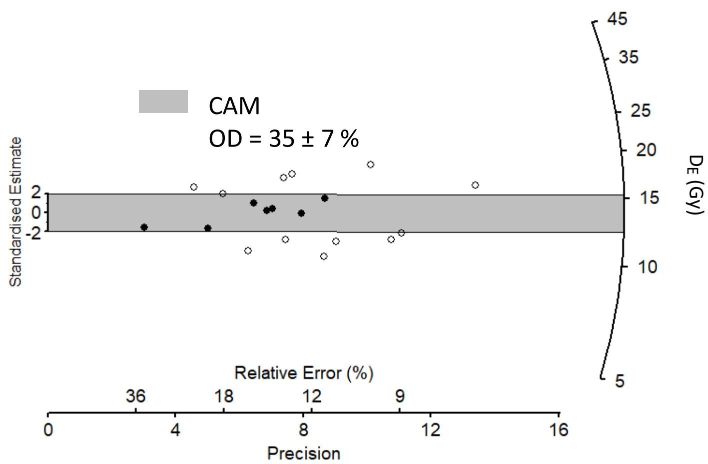

<u>Equivalent dose (D_E) Distributions:</u> Probability density function, radial plot, overdispersion (OD)

N14, USU-3407

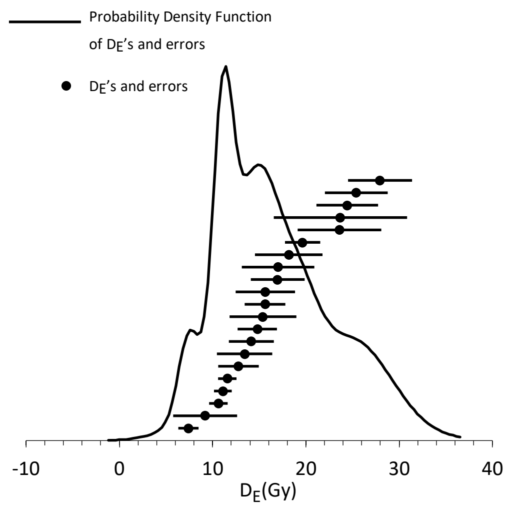

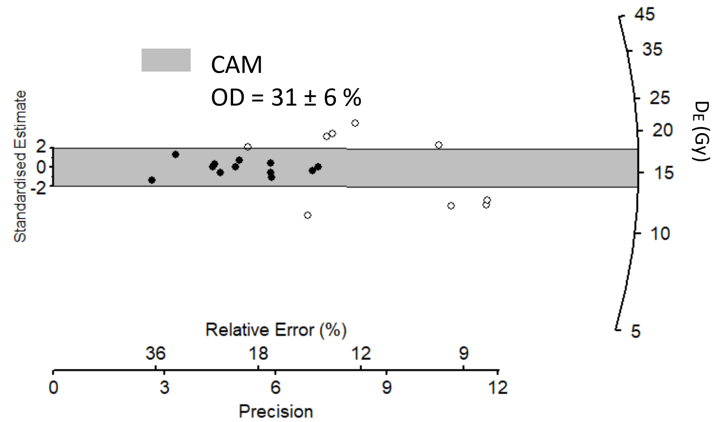

N4, USU-3408

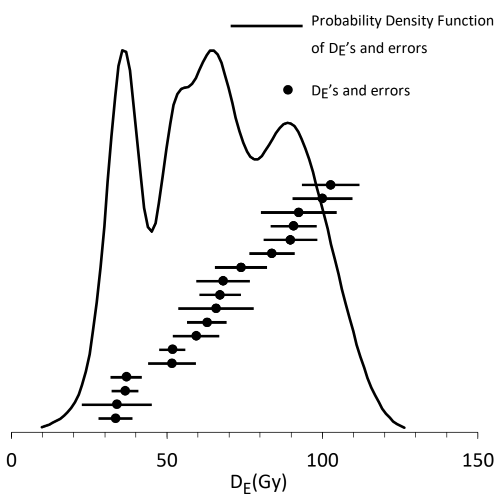

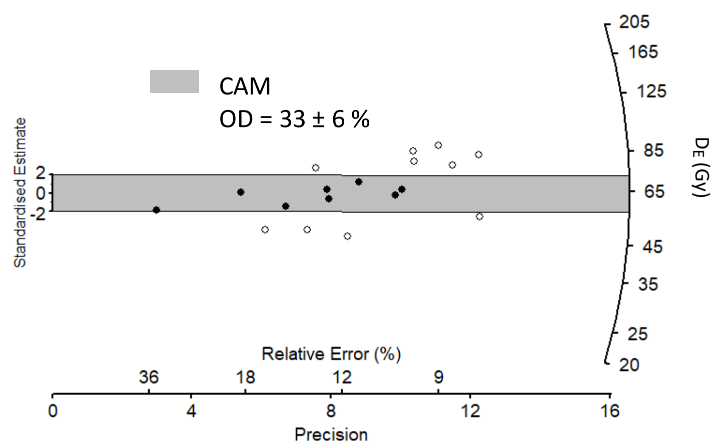

N5, USU-3409

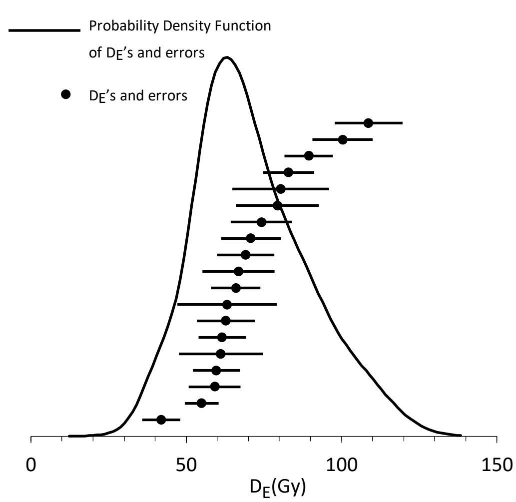

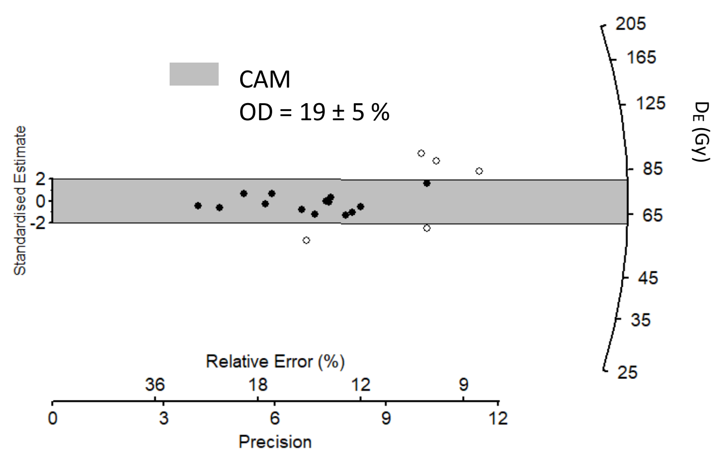

<u>Equivalent dose (D_E) Distributions:</u> Probability density function, radial plot, overdispersion (OD)

N8, USU-3410

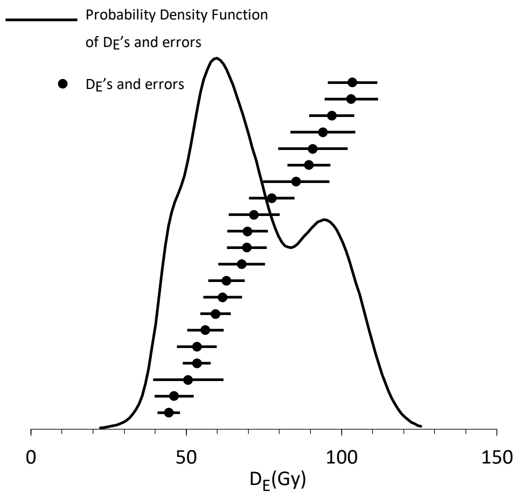

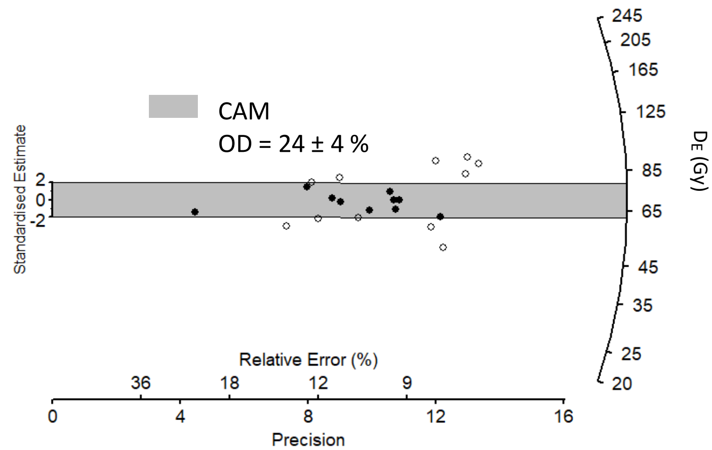

N16, USU-3411

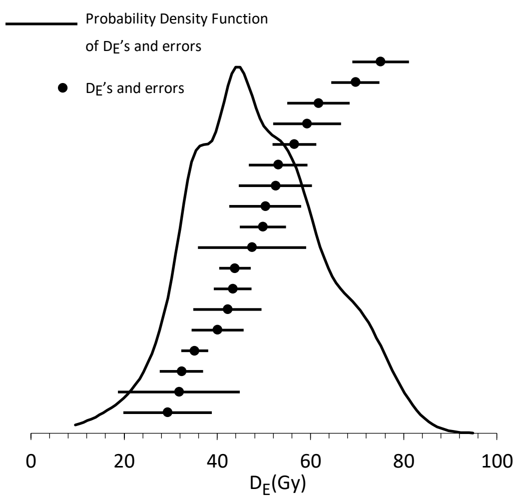

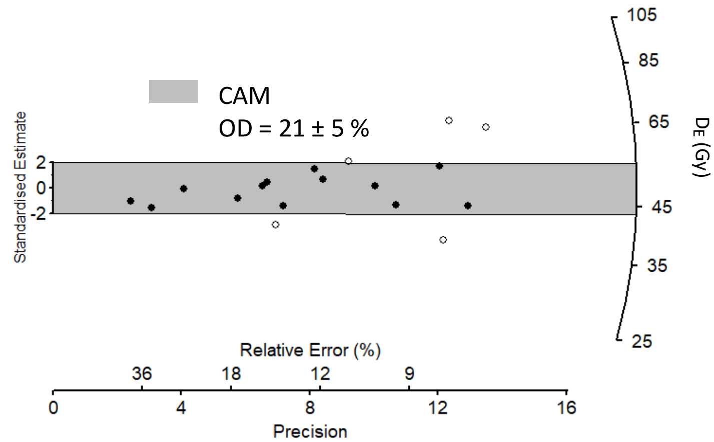

BD1, USU-3412

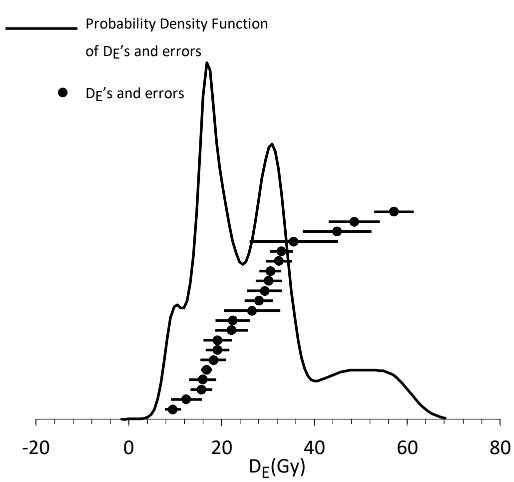

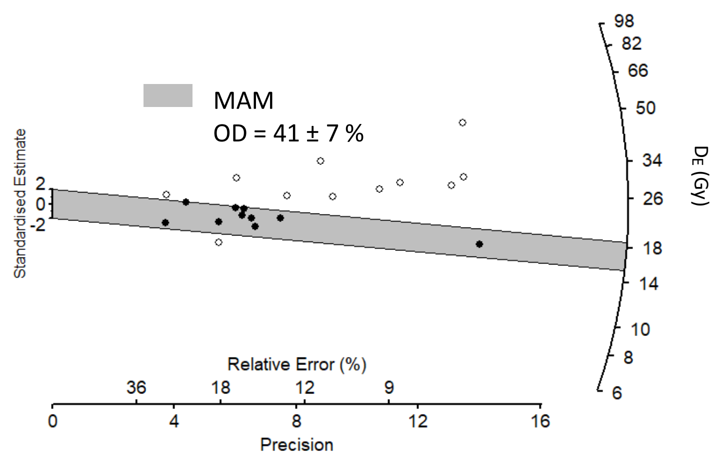

<u>Equivalent dose (D_E) Distributions:</u> Probability density function, radial plot, overdispersion (OD)

BD2, USU-3413

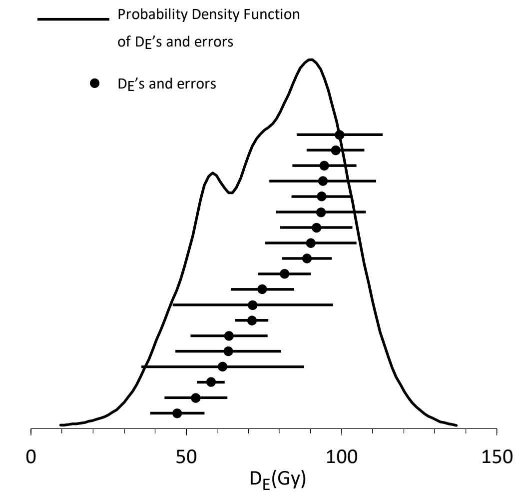

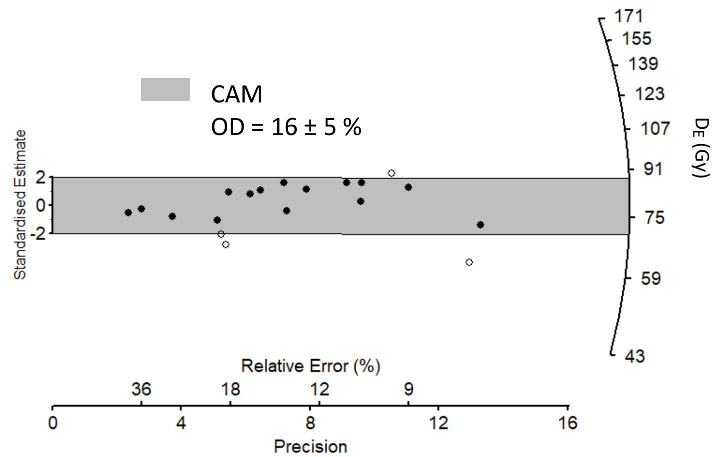

BD3, USU-3414

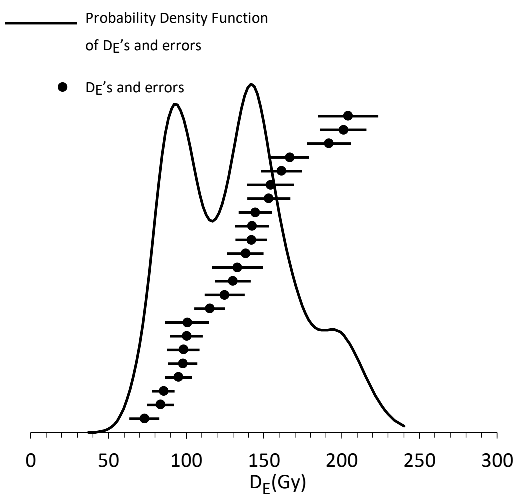

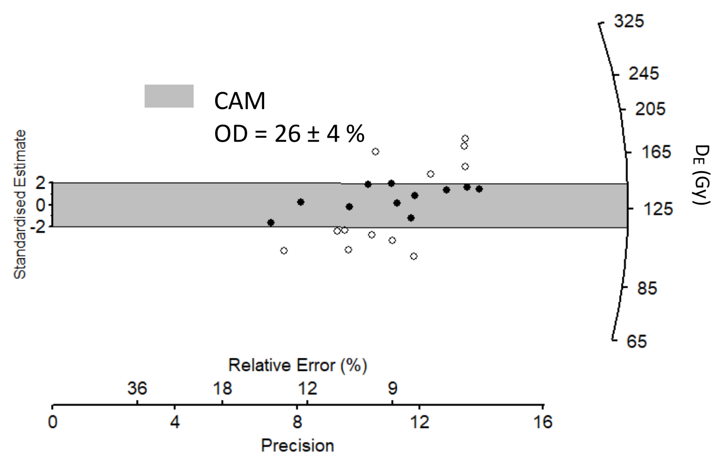

BD5, USU-3415

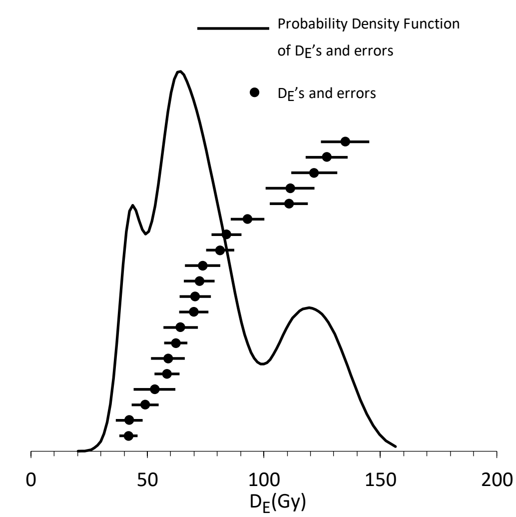

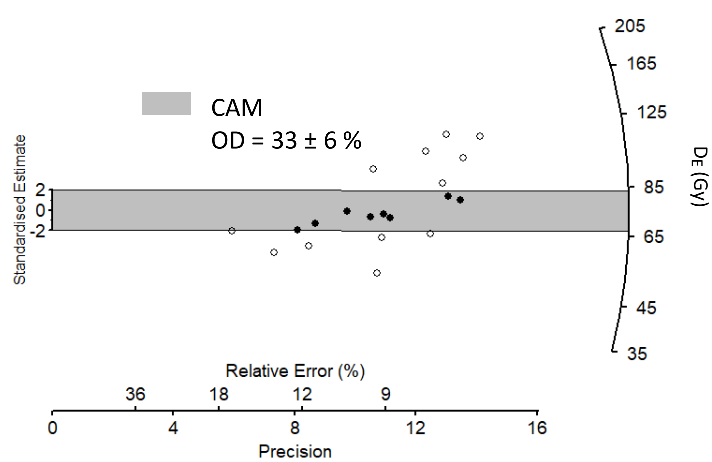

<u>Equivalent dose (D_E) Distributions:</u> Probability density function, radial plot, overdispersion (OD)

BD6, USU-3416

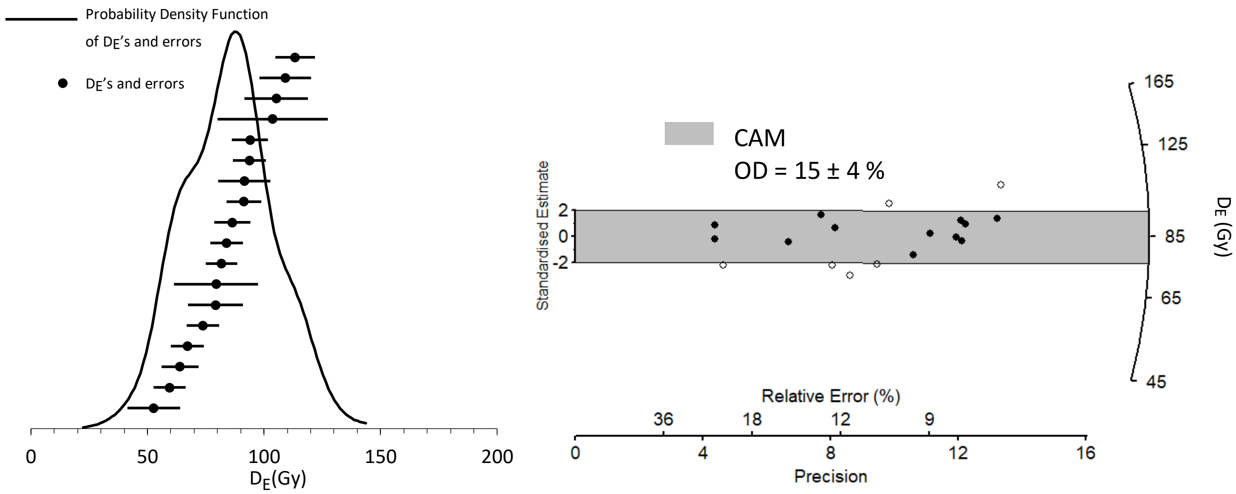

BD7, USU-3417

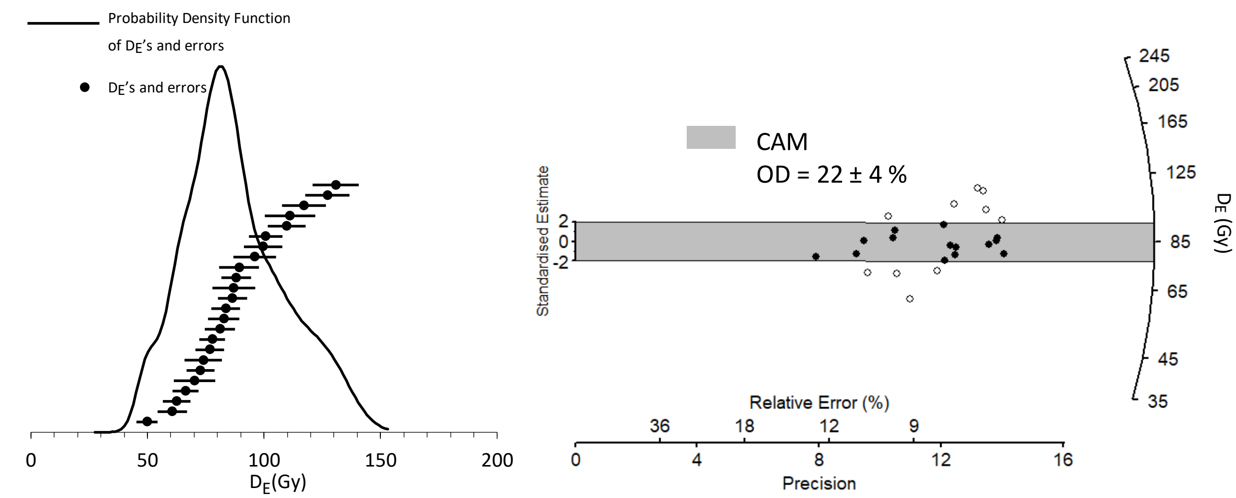

BD8, USU-3418

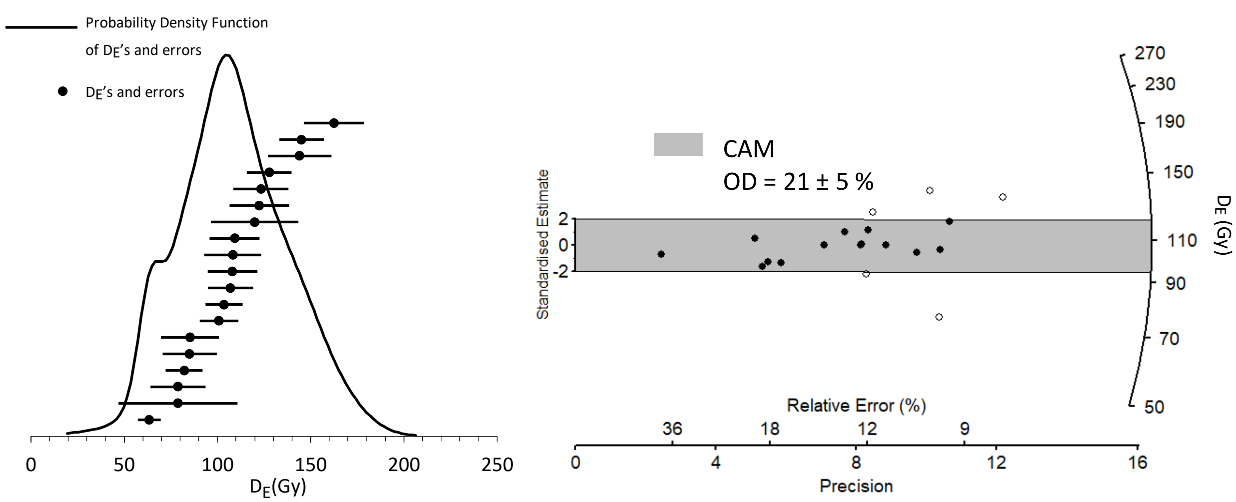

<u>Equivalent dose (D_E) Distributions:</u> Probability density function, radial plot, overdispersion (OD)

BD9, USU-3419

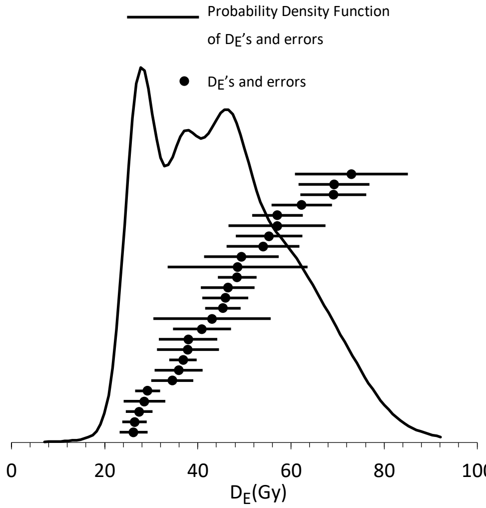

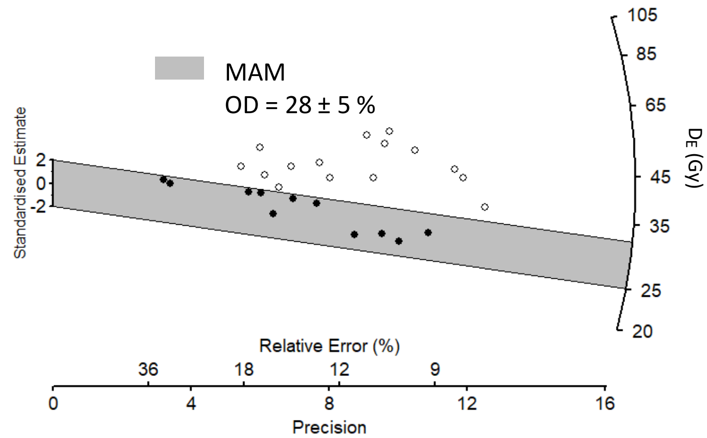

BD16, USU-3420

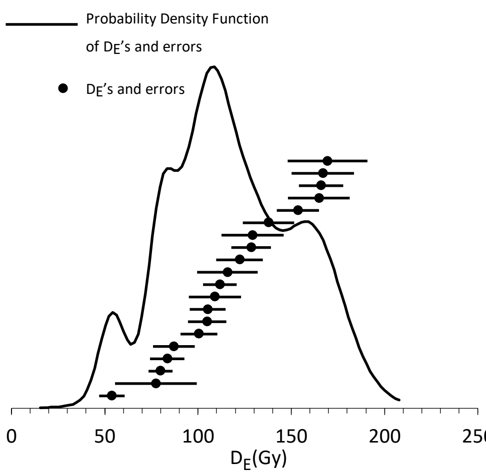

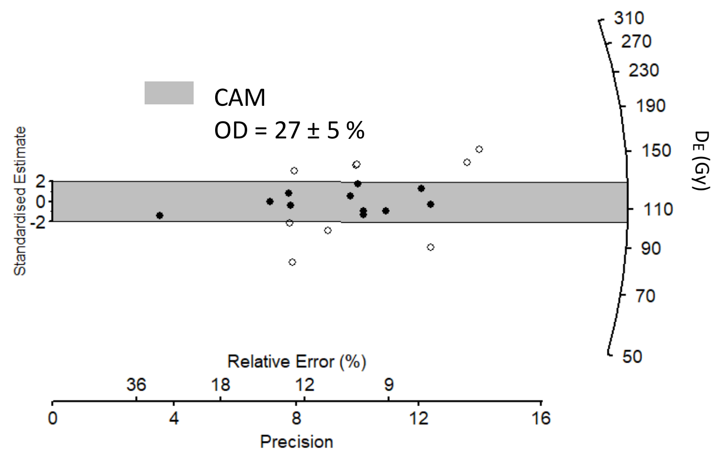

BD11, USU-3421

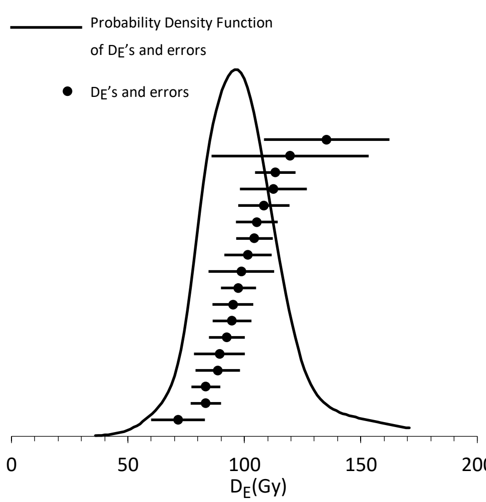

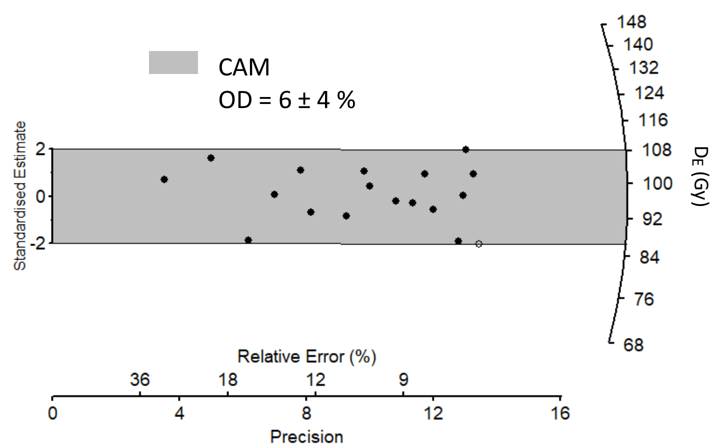

<u>Equivalent dose (D_E) Distributions:</u> Probability density function, radial plot, overdispersion (OD)

BD12, USU-3422

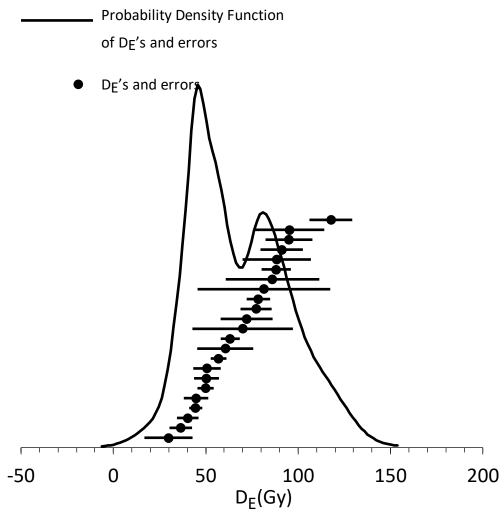

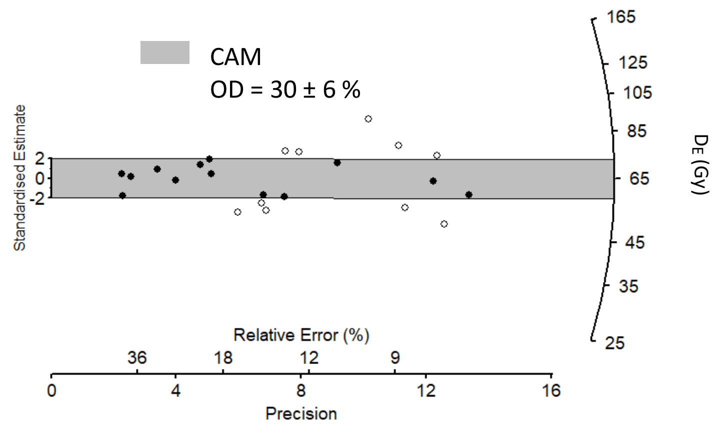

APPENDIX C:

Caliche rind data. Rind thickness was tallied. Raw data shown here.

Nicholia Data

Site	Rind Thickness(x)	Frequency (f)
N7	0.5	0
	1	0
	1.5	1
	2	1
	2.5	1
	3	2
	3.5	0
	4	5
	4.5	2
	5	5
	5.5	1
	6	4
	6.5	0
	7	3
	7.5	4
	8	1
	8.5	4
	9	4
	9.5	5
	10	2
	10.5	1
	11	1
	11.5	0
	12	2
	12.5	1
	13	1

Site	Rind Thickness(x)	Frequency (f)
N15	0.5	1
	1	2
	1.5	1
	2	6
	2.5	3
	3	6
	3.5	5
	4	7
	4.5	4
	5	2
	5.5	3
	6	2
	6.5	1
	7	0
	7.5	2
	8	3
Site	**Rind Thickness(x)**	**Frequency (f)**
N6	0.25	9
	0.5	6
	0.75	9
	1	14
	1.25	7
	1.5	2
	1.75	1
	2	2
Site	**Rind Thickness(x)**	**Frequency (f)**
N4	0.5	0
	1	11
	1.5	15
	2	8
	2.5	2
	3	6
	3.5	3
	4	4
	4.5	0
	5	1
	5.5	0

Site	Rind Thickness(x)	Frequency (f)
N8	0.5	0
	1	1
	1.5	1
	2	3
	2.5	4
	3	2
	3.5	0
	4	1
	4.5	0
	5	3
	5.5	1
	6	5
	6.5	0
	7	6
	7.5	0
	8	5
	8.5	1
	9	4
	9.5	2
	10	4
	10.5	0
	11	3
	11.5	0
	12	0
	12.5	1
	13	2
	13.5	0
	14	1

Site	Rind Thickness(x)	Frequency (f)
N16	0.5	0
	1	2
	1.5	2
	2	7
	2.5	2
	3	4
	3.5	2
	4	6
	4.5	2
	5	6
	5.5	6
	6	5
	6.5	0
	7	2
	7.5	0
	8	4

Site	Rind Thickness(x)	Frequency (f)
N14	0.25	9
	0.5	8
	0.75	6
	1	13
	1.25	8
	1.5	2
	1.75	0
	2	3
	2.25	1

Site	Rind Thickness(x)	Frequency (f)
N5	0.5	0
	1	2
	1.5	0
	2	4
	2.5	1
	3	4
	3.5	1
	4	7
	4.5	1
	5	9
	5.5	1
	6	5
	6.5	1
	7	3
	7.5	1
	8	2
	8.5	0
	9	1
	9.5	1
	10	1
	10.5	0
	11	1
	11.5	1
	12	1
	12.5	0
	13	1

Site	Rind Thickness(x)	Frequency (f)
N3	0.25	15
	0.5	5
	0.75	6
	1	9
	1.25	7
	1.5	1
	1.75	2
	2	2
	2.25	1
	2.5	2
	5	1

Site	Rind Thickness(x)	Frequency (f)
N2	0.5	0
	1	1
	1.5	0
	2	0
	2.5	1
	3	5
	3.5	0
	4	5
	4.5	1
	5	2
	5.5	1
	6	4
	6.5	0
	7	6
	7.5	1
	8	6
	8.5	0
	9	2
	9.5	0
	10	2
	10.5	0
	11	5
		0
	12	3
	12.5	0
	13	2
	13.5	0
	14	2
	14.5	0
	15	1

Site	Rind Thickness(x)	Frequency (f)
N17	0.5	0
	1	0
	1.5	0
	2	0
	2.5	0
	3	0
	3.5	0
	4	1
	4.5	0
	5	1
	5.5	1
	6	2
	6.5	1
	7	4
	7.5	1
	8	9
	8.5	1
	9	7
	9.5	1
	10	4
	10.5	0
	11	2
	11.5	1
	12	4
	12.5	0
	13	1
	13.5	1
	14	3
	14.5	0
	15	2
	15.5	0
	16	0
	16.5	0
	17	1
	17.5	0
	18	1
	21.5	1

Blue Dome Caliche

Site	Rind Thickness(x)	Frequency(f)
BD5	0.5	5
	1	3
	1.5	1
	2	2
	2.5	2
	3	2
	3.5	0
	4	1
	4.5	0
	5	4
	5.5	1
	6	6
	6.5	0
	7	7
	7.5	0
	8	5
	8.5	0
	9	3
	9.5	1
	10	2
	10.5	0
	11	3
	11.5	0
	12	1
	19	1

Site	Rind Thickness(x)	Frequency(f)
BD6	0.25	6
	0.5	6
	0.75	2
	1	13
	1.25	5
	1.5	2
	1.75	0
	2	5
	2.25	0
	2.5	1
	2.75	0
	3	4
	3.25	0
	3.5	1
	3.75	0
	4	2
	4.25	0
	4.5	0
	4.75	0
	5	3

Site	Rind Thickness(x)	Frequency(f)
BD7	0.25	12
	0.5	11
	0.75	4
	1	10
	1.25	3
	1.5	2
	1.75	0
	2	4
	2.25	0
	2.5	1
	2.75	0
	3	2
	3.25	0
	3.5	0
	3.75	0
	4	1

Site	Rind Thickness(x)	Frequency(f)
BD8	0.25	6
	0.5	2
	0.75	0
	1	7
	1.25	0
	1.5	3
	1.75	0
	2	10
	2.25	0
	2.5	1
	2.75	0
	3	3
	3.25	0
	3.5	3
	3.75	0
	4	3
	4.25	0
	4.5	2
	4.75	0
	5	4
	5.25	0
	5.5	1
	5.75	0
	6	3
	6.25	0
	6.5	1
	6.75	0
	7	1

Site	Rind Thickness(x)	Frequency(f)
BD2	0.5	4
	1	5
	1.5	1
	2	5
	2.5	3
	3	4
	3.5	0
	4	7
	4.5	0
	5	6
	5.5	0
	6	5
	6.5	0
	7	4
	7.5	0
	8	2
	8.5	1
	9	1
	9.5	0

Site	Rind Thickness(x)	Frequency(f)
BD3	0.5	0
	1	4
	1.5	2
	2	6
	2.5	0
	3	7
	3.5	2
	4	2
	4.5	0
	5	5
	5.5	0
	6	5
	6.5	1
	7	7
	7.5	0
	8	3
	8.5	0
	9	0
	9.5	1
	10	1
	10.5	0
	11	1
	11.5	0
	12	1
	12.5	0
	13	2
Site	**Rind Thickness(x)**	**Frequency(f)**
BD9	0.25	6
	0.5	11
	0.75	3
	1	8
	1.25	5
	1.5	2
	1.75	0
	2	7
	2.25	0
	2.5	2
	2.75	0
	3	3
	3.25	0
	3.5	1
	3.75	0
	4	2

Site	Rind Thickness(x)	Frequency(f)
BD16	0.25	19
	0.5	9
	0.75	6
	1	7
	1.25	5
	1.5	3
	1.75	0
	2	0
	2.25	0
	2.5	0
	2.75	0
	3	1
Site	**Rind Thickness(x)**	**Frequency(f)**
BD11	0.25	9
	0.5	9
	0.75	8
	1	8
	1.25	6
	1.5	5
	1.75	0
	2	2
	2.25	0
	2.5	0
	2.75	0
	3	2
	6	1

Site	Rind Thickness(x)	Frequency(f)
BD12	0.5	8
	1	5
	1.5	5
	2	1
	2.5	5
	3	2
	3.5	1
	4	3
	4.5	1
	5	5
	5.5	1
	6	6
	6.5	2
	7	3
	7.5	1
	8	2

Site	Rind Thickness(x)	Frequency(f)
BD1	0.25	21
	0.5	11
	0.75	9
	1	7
	1.25	1
	1.5	0
	1.75	0
	2	1
	2.25	0
	2.5	0
	2.75	0
	3	0

APPENDIX D:
Long Canyon Trinity F90: Processing Report

Survey Data

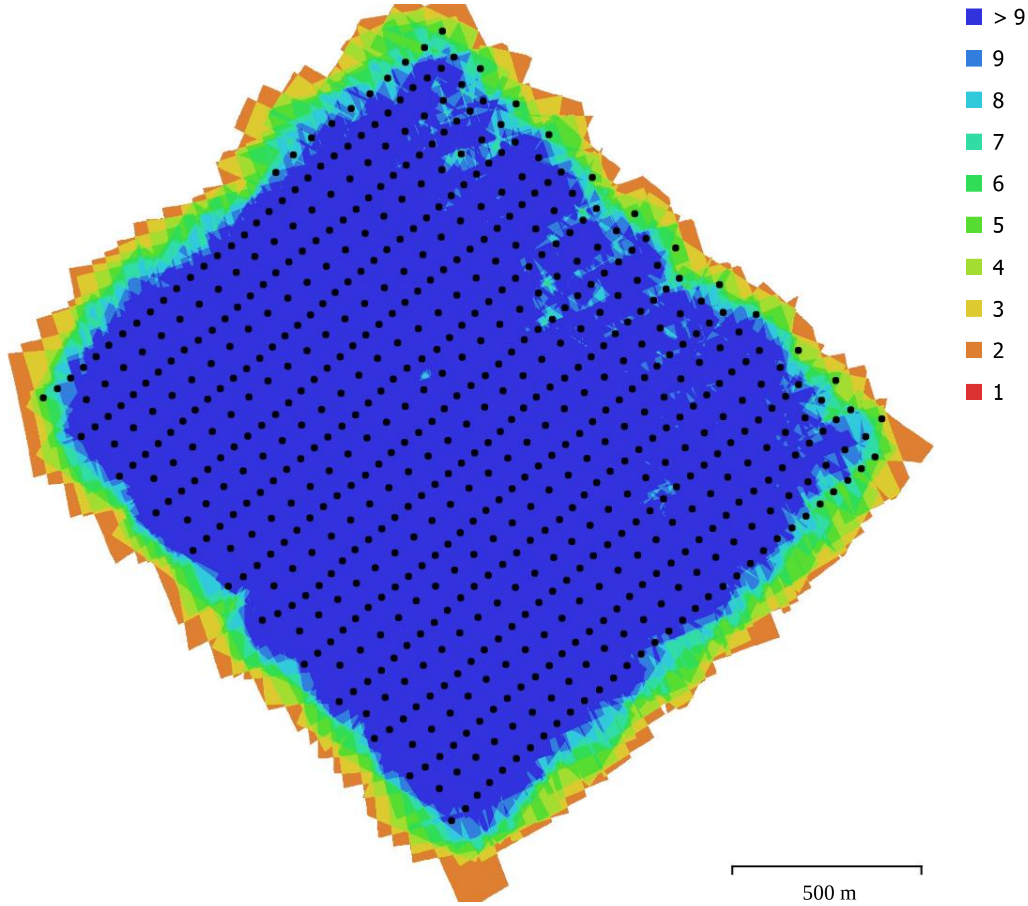

Fig. 1. Camera locations and image overlap.

Number of images:	647	Camera stations:	647
Flying altitude:	284 m	Tie points:	4,753,128
Ground resolution:	3.59 cm/pix	Projections:	20,626,778
Coverage area:	3.06 km²	Reprojection error:	0.273 pix

Camera Model	Resolution	Focal Length	Pixel Size	Precalibrated
DSC-RX1RM2 (35mm)	7952 x 5304	35 mm	4.53 x 4.53 μm	No

Table 1. Cameras.

Camera Calibration

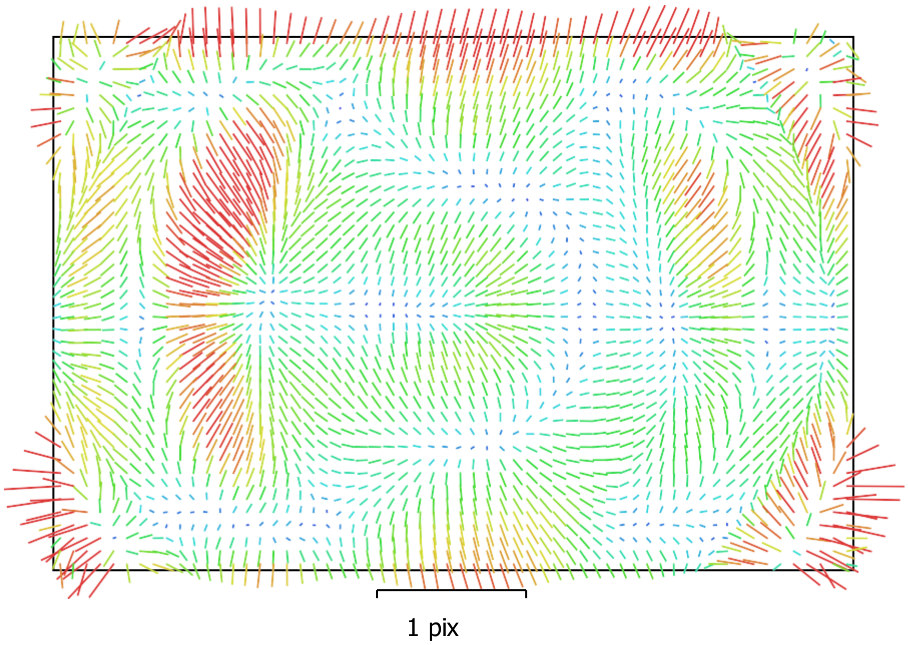

Fig. 2. Image residuals for DSC-RX1RM2 (35mm).

DSC-RX1RM2 (35mm)

647 images

Type	Resolution	Focal Length	Pixel Size
Frame	**7952 x 5304**	**35 mm**	**4.53 x 4.53 μm**

	Value	Error	F	Cx	Cy	B1	B2	K1	K2	K3	K4	P1	P2
F	**7535.69**	0.026	1.00	0.04	0.04	-0.04	0.01	-0.12	0.18	-0.25	0.32	-0.13	0.01
Cx	**-4.88834**	0.0053		1.00	-0.02	-0.46	0.18	-0.02	0.00	-0.00	0.00	0.08	-0.01
Cy	**-3.49205**	0.005			1.00	-0.21	-0.50	0.00	-0.00	0.00	0.00	-0.02	-0.20
B1	**0.751236**	0.00082				1.00	0.00	0.03	-0.01	0.00	0.00	0.21	0.09
B2	**0.442452**	0.00083					1.00	-0.01	0.00	-0.00	0.00	-0.07	0.28
K1	**-0.126596**	7.6e-06						1.00	-0.96	0.91	-0.85	0.00	0.02
K2	**0.673143**	8.1e-05							1.00	-0.98	0.95	-0.01	-0.01
K3	**-3.21394**	0.00034								1.00	-0.99	0.03	0.01
K4	**4.67845**	0.00049									1.00	-0.04	-0.00
P1	**1.45126e-05**	1.2e-07										1.00	-0.01
P2	**0.000198647**	9.6e-08											1.00

Table 2. Calibration coefficients and correlation matrix.

Camera Locations

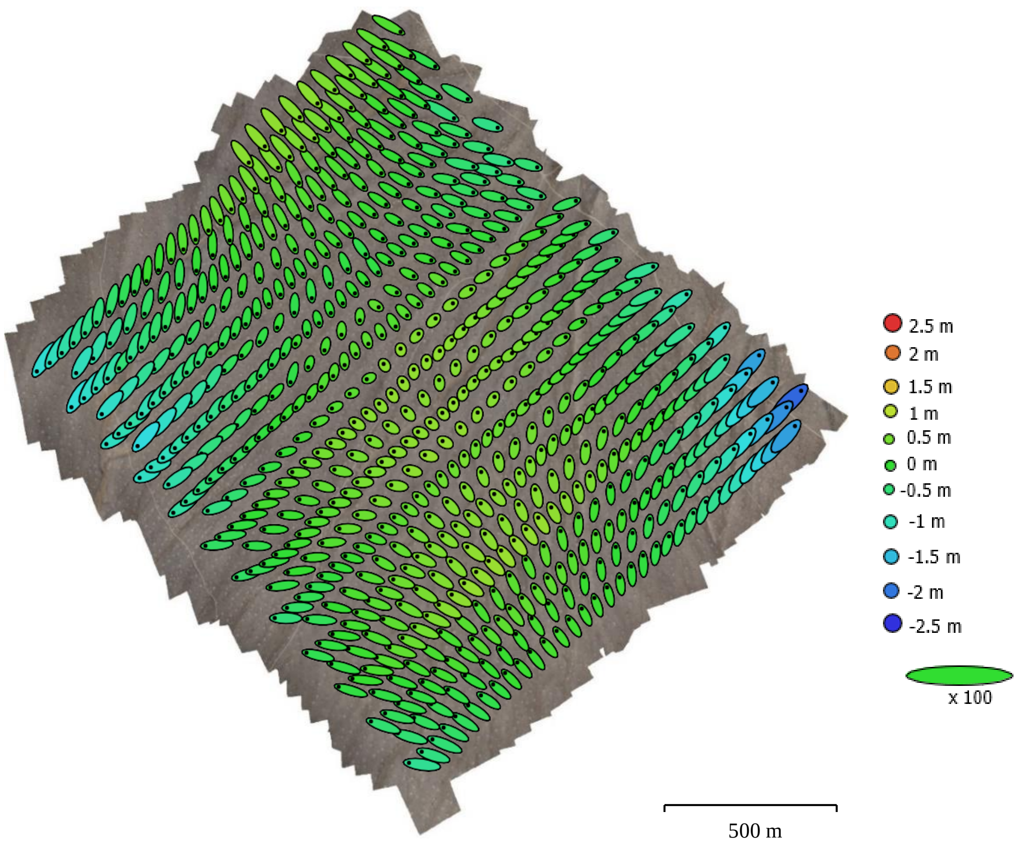

Fig. 3. Camera locations and error estimates.

Z error is represented by ellipse color. X,Y errors are represented by ellipse shape.

Estimated camera locations are marked with a black dot.

X error (cm)	Y error (cm)	Z error (cm)	XY error (cm)	Total error (cm)
38.1259	34.027	48.4639	51.1021	70.4285

Table 3. Average camera location error.X - Longitude, Y - Latitude, Z - Altitude.

Digital Elevation Model

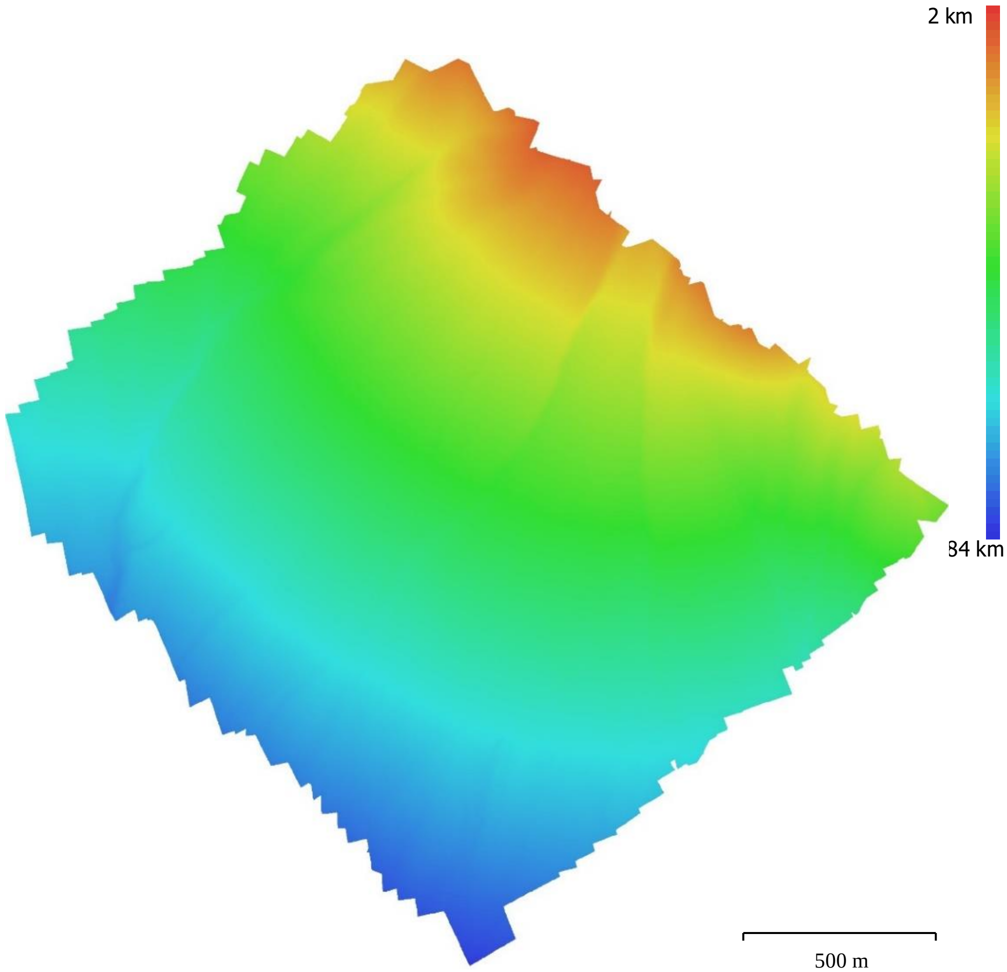

Fig. 4. Reconstructed digital elevation model.

Resolution:	7.18 cm/pix
Point density:	194 points/m^2

Processing Parameters

General	
Cameras	647
Aligned cameras	647
Coordinate system	WGS 84 (EPSG::4326)
Rotation angles	Yaw, Pitch, Roll
Point Cloud	
Points	4,753,128 of 5,176,740
RMS reprojection error	0.125299 (0.272856 pix)
Max reprojection error	1.29739 (7.18953 pix)
Mean key point size	2.2067 pix
Point colors	3 bands, uint8
Key points	No
Average tie point multiplicity	4.63914
Alignment parameters	
Accuracy	Highest
Generic preselection	Yes
Reference preselection	No
Key point limit	75,000
Tie point limit	0
Guided image matching	No
Adaptive camera model fitting	No
Matching time	25 minutes 31 seconds
Matching memory usage	9.05 GB
Alignment time	25 minutes 36 seconds
Alignment memory usage	2.30 GB
Optimization parameters	
Parameters	f, b1, b2, cx, cy, k1-k4, p1, p2
Adaptive camera model fitting	No
Optimization time	1 minutes 30 seconds
Software version	1.6.4.10928
File size	490.14 MB
Depth Maps	
Count	647
Depth maps generation parameters	
Quality	High
Filtering mode	Aggressive
Processing time	4 hours 53 minutes
Memory usage	6.64 GB
Software version	1.6.4.10928
File size	5.42 GB
Dense Point Cloud	
Points	595,523,940
Point colors	3 bands, uint8
Depth maps generation parameters	
Quality	High
Filtering mode	Aggressive
Processing time	4 hours 53 minutes

Memory usage	6.64 GB
Dense cloud generation parameters	
Processing time	3 hours 4 minutes
Memory usage	18.56 GB
Software version	1.6.4.10928
File size	7.62 GB
DEM	
Size	45,778 x 44,561
Coordinate system	WGS 84 (EPSG::4326)
Reconstruction parameters	
Source data	Dense cloud
Interpolation	Enabled
Processing time	7 minutes 19 seconds
Memory usage	198.95 MB
Software version	1.6.4.10928
File size	1.79 GB
Orthomosaic	
Size	68,222 x 65,610
Coordinate system	WGS 84 (EPSG::4326)
Colors	3 bands, uint8
Reconstruction parameters	
Blending mode	Mosaic
Surface	DEM
Enable hole filling	Yes
Processing time	40 minutes 23 seconds
Memory usage	7.58 GB
Software version	1.6.4.10928
File size	41.88 GB
System	
Software name	Agisoft Metashape Professional
Software version	1 7.0 build 11736
OS	Windows 64 bit
RAM	31.85 GB
CPU	Intel(R) Core(TM) i7-6700 CPU @ 3.40GHz
GPU(s)	GeForce GTX 950

Bare Canyon Phantom Pro V4: Processing Report

Survey Data

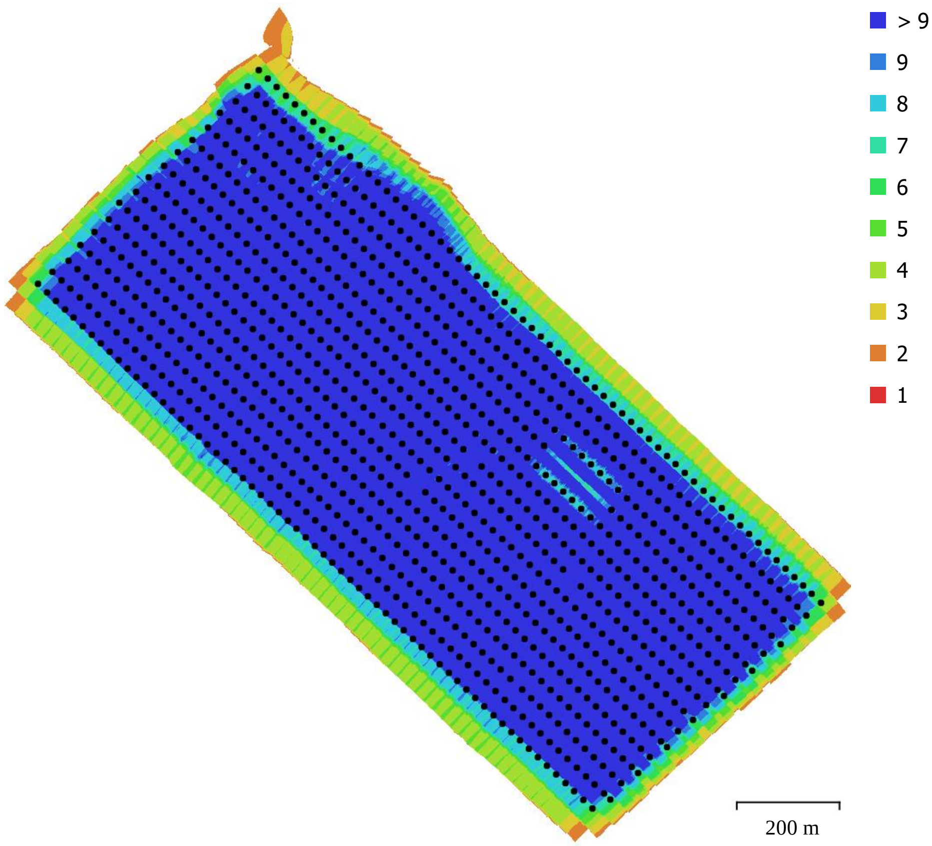

Fig. 1. Camera locations and image overlap.

Number of images:	1,059	Camera stations:	1,059
Flying altitude:	102 m	Tie points:	1,225,553
Ground resolution:	2.53 cm/pix	Projections:	6,536,855
Coverage area:	1.17 km²	Reprojection error:	0.425 pix

Camera Model	Resolution	Focal Length	Pixel Size	Precalibrated
FC6310 (8.8mm)	5472 x 3648	8.8 mm	2.41 x 2.41 μm	No

Table 1. Cameras.

Camera Calibration

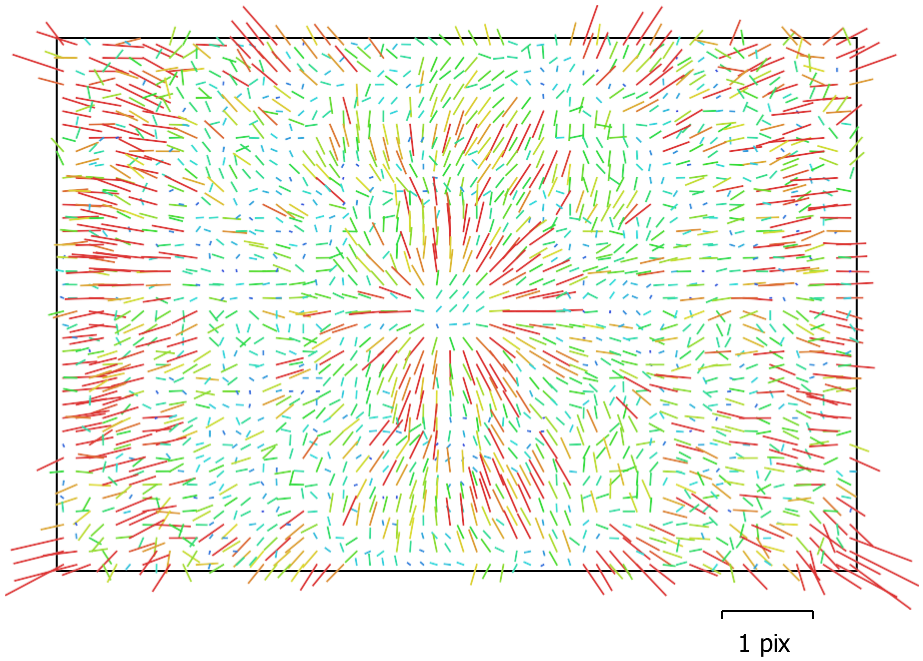

Fig. 2. Image residuals for FC6310 (8.8mm).

FC6310 (8.8mm)

1059 images

Type	Resolution	Focal Length	Pixel Size
Frame	**5472 x 3648**	**8.8 mm**	**2.41 x 2.41 µm**

F:	3686.92		
Cx:	2.48273	B1:	0
Cy:	6.15131	B2:	0
K1:	0.00923047	P1:	-0.0003011
K2:	-0.01491	P2:	-0.00125589
K3:	0.0140457	P3:	0
K4:	0	P4:	0

Camera Locations

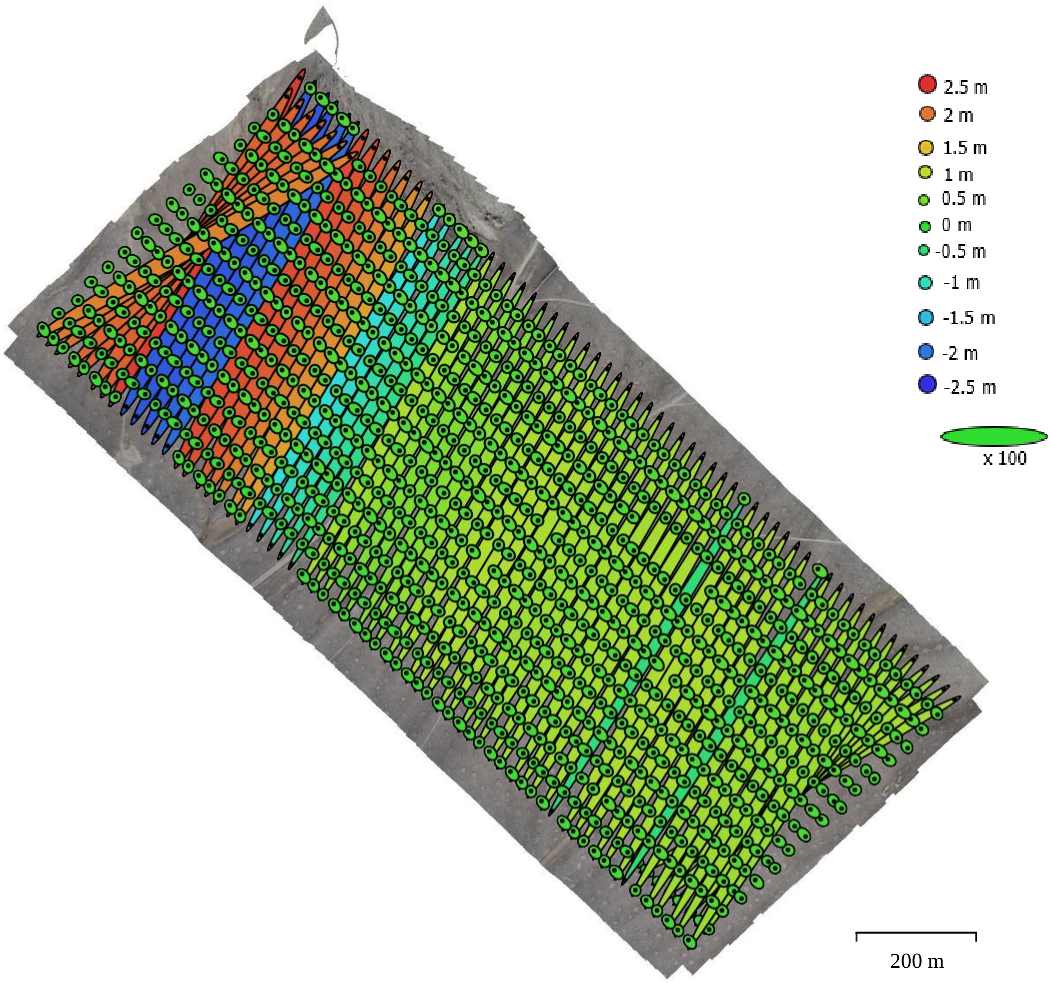

Fig. 3. Camera locations and error estimates.

Z error is represented by ellipse color. X,Y errors are represented by ellipse shape.

Estimated camera locations are marked with a black dot.

X error (m)	Y error (m)	Z error (m)	XY error (m)	Total error (m)
86.8981	129.534	22.192	155.982	157.552

Table 2. Average camera location error.X - Longitude, Y - Latitude, Z - Altitude.

Ground Control Points

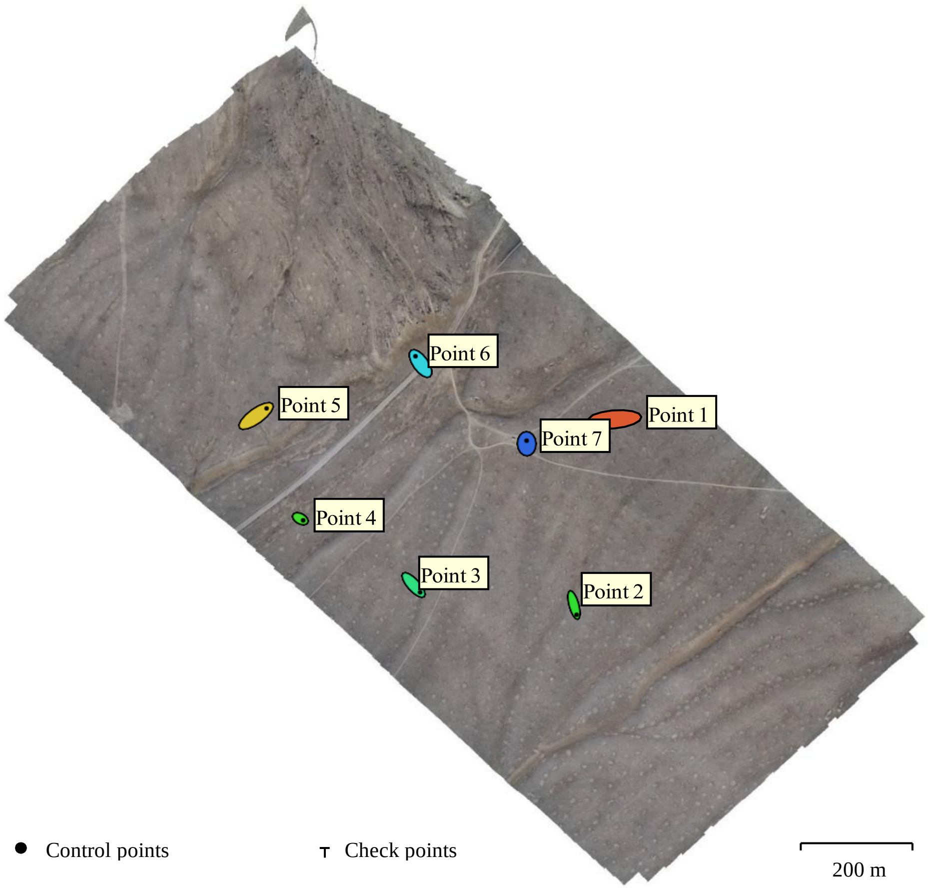

Fig. 4. Control points.

Z error is represented by ellipse color. X,Y errors are represented by ellipse shape.

Estimated GCP locations are marked with a dot or crossing.

Count	X error (cm)	Y error (cm)	Z error (cm)	XY error (cm)	Total (cm)
7	2.09806	1.51195	1.38639	2.58609	2.93427

Table 3. Control points RMSE. X - Longitude, Y - Latitude, Z - Altitude.

Label	**X error (cm)**	**Y error (cm)**	**Z error (cm)**	**Total (cm)**	**Image (pix)**
Point 1	-4.48405	-0.426133	2.20272	5.014	1.410 (11)
Point 2	0.628843	-2.33915	-0.0076813	2.42221	0.855 (9)
Point 3	1.51591	-1.78712	-0.583723	2.41506	1.203 (6)
Point 4	0.661013	-0.372899	0.126666	0.769439	0.487 (5)
Point 5	2.49142	1.84066	1.42177	3.40832	1.203 (9)
Point 6	-1.1697	1.75665	-1.33796	2.49883	1.048 (14)
Point 7	-0.0265728	0.736253	-2.10573	2.23089	2.366 (8)
Total	**2.09806**	**1.51195**	**1.38639**	**2.93427**	**1.341**

Table 4. Control points. X - Longitude, Y - Latitude, Z - Altitude.

Digital Elevation Model

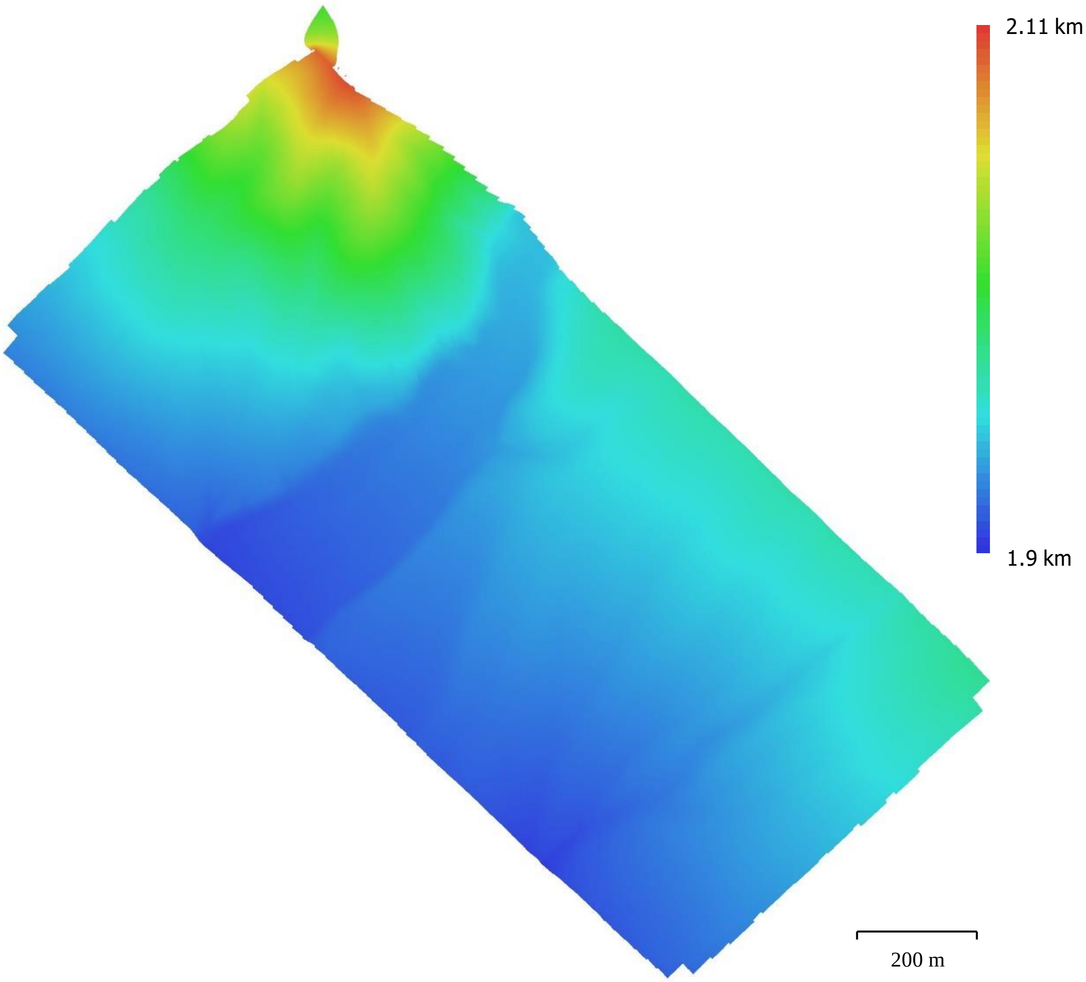

Fig. 5. Reconstructed digital elevation model.

Resolution:	5.07 cm/pix
Point density:	390 points/m²

Processing Parameters

General	
Cameras	1059
Aligned cameras	1059
Markers	7
Coordinate system	WGS 84 (EPSG::4326)
Rotation angles	Yaw, Pitch, Roll
Point Cloud	
Points	1,225,553 of 1,261,361
RMS reprojection error	0.206441 (0.425264 pix)
Max reprojection error	0.619041 (18.0468 pix)
Mean key point size	2.11556 pix
Point colors	3 bands, uint8
Key points	No
Average tie point multiplicity	5.40338
Alignment parameters	
Accuracy	Highest
Generic preselection	Yes
Reference preselection	Source
Key point limit	40,000
Tie point limit	6,000
Guided image matching	No
Adaptive camera model fitting	No
Matching time	20 minutes 25 seconds
Matching memory usage	888.41 MB
Alignment time	13 minutes 41 seconds
Alignment memory usage	657.91 MB Software
version	1.6.4.10928
File size	135.80 MB
Depth Maps	
Count	1059
Depth maps generation parameters	
Quality	High
Filtering mode	Aggressive
Processing time	8 hours 9 minutes
Memory usage	2.13 GB
Software version	1.6.4.10928
File size	5.30 GB
Dense Point Cloud	
Points	470,800,313
Point colors	3 bands, uint8
Depth maps generation parameters	
Quality	High
Filtering mode	Aggressive
Processing time	8 hours 9 minutes
Memory usage	2.13 GB
Dense cloud generation parameters	

Processing time	3 hours 25 minutes
Memory usage	7.96 GB
Software version	1.6.4.10928
File size	6.66 GB
DEM	
Size	46,453 x 46,277
Coordinate system	WGS 84 (EPSG::4326)
Reconstruction parameters	
Source data	Dense cloud
Interpolation	Enabled
Processing time	12 minutes 28 seconds
Memory usage	372.03 MB
Software version	1.7.0.11736
File size	1.42 GB
Orthomosaic	
Size	65,095 x 64,302
Coordinate system	WGS 84 (EPSG::4326)
Colors	3 bands, uint8
Reconstruction parameters	
Blending mode	Mosaic
Surface	DEM
Enable hole filling	Yes
Enable ghosting filter	No
Processing time	55 minutes 6 seconds
Memory usage	2.82 GB
Software version	1.7.0.11736
File size	28.84 GB
System	
Software name	Agisoft Metashape Professional
Software version	1 7.0 build 11736
OS	Windows 64 bit
RAM	31.85 GB
CPU	Intel(R) Core(TM) i7-6700 CPU @ 3.40GHz
GPU(s)	GeForce GTX 950